Fakultät für Physik und
Astronomie
Universität Heidelberg

Diploma Thesis
in Physics
submitted by
Peter Schichtel
born in Heidelberg, Germany
2011

Jets in LHC searches

Peter Schichtel

Institut für theoretische Physik
Universität Heidelberg

This Diploma Thesis has been carried out by
Peter Schichtel
at the
Institut für Theoretische Physik
under supervision of
Tilman Plehn
in 2011

Abstract

One of the main physics search goals at the LHC is to detect a viable dark matter candidate. As dark matter is at most weakly interacting, missing energy is a striking but not sufficient signature. To dig out the signature of a dark matter candidate we have to distinguish it from other physics processes generating missing energy like weak boson production. In LHC events we are also confronted with a large number of particles in the final state which come along as a collimated spray, the so called jets. Standard Model backgrounds as well as possible new physics signals are accompanied by those jets at the LHC. Thus it is important to understand the structure and behavior of multi-jet observables if we are to identify new physics signals. We study the characteristics of the exclusive number of jets observable for various Standard Model backgrounds and observe a unique scaling behavior the so called staircase scaling. We establish a link to the inclusive definition and show that the theoretical uncertainties are well under control. In the photon plus jets channel we then study the kinematic properties of different scaling types. We use this knowledge to control the uncertainties of an other multi-jet observable, the effective mass. With these two multi-jet observables we set up an inclusive search strategy in the jets plus missing energy channel which enables us to automatically focus on the phase space regions showing the largest deviation from the Standard Model background only hypothesis.

Zusammenfassung

Eines der Hauptziele des LHC ist die Entdeckung eines geeigneten Dark Matter Kandidaten. Da Dark Matter höchstens schwach interagiert, ist Missing Energy ein wichtiges, aber nicht hinreichendes Signal zur Entdeckung. Um einen Dark Matter Kandidaten zu entdecken müssen wir sie von anderen Prozessen, die Missing Energy erzeugen, wie Weak Boson Produktion unterscheiden. Des Weiteren sind wir am LHC mit einer großen Zahl stabiler Teilchen, die als kollimierter Strahl, den so genannten Jets, auftreten, im Entzustand konfrontiert. Sowohl Standard Model als auch neue Physik Prozesse treten am LHC mit diesen Jets auf. Daher ist es wichtig die Struktur und das Verhalten von Multijet Observablen zu verstehen, wenn wir Aussagen über neue Physik am LHC treffen wollen. Wir studieren die exklusive Anzahl an Jets für verschiedene Standard Model Untergründe und beobachten ein einzigartiges Skalierungsverhalten das Staircase Scaling. Wir leiten eine Verbindung zur inklusiven Definition her und zeigen, dass die theoretischen Unsicherheiten klein sind. Im Photonen plus Jets Kanal untersuchen wir dann die kinematischen Eigenschaften verschiedener Skalierungstypen. Wir benutzen dieses Wissen um die Unsicherheiten einer weiteren Multijet Observablen, der effektiven Masse, zu bestimmen. Mit diesen beiden Observablen erstellen wir eine inklusive Suchstrategie im Jets plus Missing Energy Kanal, die es uns ermöglicht automatisch auf die Phasenraumregionen zu fokusieren, die die größte Abweichung von der Standard Model Nullhypothese zeigen.

Contents

Chapter 1
Introduction

The LHC is up running and the whole world is exited about its discoveries[1]. Many physicists expect new phenomena to occur at the weak scale the LHC is probing. And there are good reasons for that. Although the Standard Model of particle physics is a well established framework describing until now all observations in particle physics to a very high precision, it is also clear that it is not the fundamental theory describing nature. This becomes evident when we take a step back and focus not only on the picture describing small scale physics, but take a look at the framework describing large scale physics, cosmology. On a large scale the only important interaction in space is gravitation, an interaction not even implemented in the Standard Model. Through analyzing the cosmic micro wave background radiation we are able to measure the energy content of the universe [1]. Only 4.6% of our universe are made of matter described by the Standard Model. Another 23% are made of cold dark matter and 72% are made of a kind of dark energy. But there are also issues within the standard model. It is not able to explain the amount of CP-asymmetry permitting in the first place our existence [2] and suffers an ultra violet sensitivity in the corrections of the Higgs propagator known as fine-tuning problem [3]. Over the last decades many theories and models like SUSY, EXTRA DIMENSIONS, LITTLE HIGGS or TECHNICOLOR have been developed to solve one or several of those issues [3–6]. Many of these theories predict a viable dark matter candidate in the reach of the LHC. Thus one of the main goals of the LHC searches is to find this dark matter candidate and measure its properties [7].

Missing transverse energy is a general signature for dark matter related new physics at hadron colliders [8]. It has a long history at the Tevatron and to date gives the strongest bounds on squark and gluino masses in supersymmetric extensions of the Standard Model. At the LHC the first new exclusion limits for squarks and gluinos have recently appeared, in the CMSSM toy model as well as in a more general setup [9–11]. All of these analysis are based on jets plus missing energy including a lepton veto which constitutes the most generic search strategy for strongly interacting new particles decaying into a weakly or super-weakly interacting dark matter candidate [8, 12].

While the first results are based on very inclusive cuts, following the ATLAS [13] and CMS [14] documentations we expect more specific analysis to appear soon. The reason is that in their current form the analysis can and should be optimized for specific new physics mass spectra. More specialized analysis for jets plus missing energy rely on a missing transverse momentum cut and on a certain number of staggered jet transverse momentum cuts [13, 14]. Unfortunately, they are therefore hard to adapt to modified mass spectra and by definition show a poor performance for not optimized model parameters. In addition, they are counting experiments in certain phase-space regions, which means that for any additional information on the physics behind an anomaly we have to wait for a dedicated analysis. If we want to use more general strategies with less constraining cuts we have to face enormous QCD backgrounds at the LHC . Understanding the QCD backgrounds puts us in a situation where we do not need to figure out the special phase space region in which the signal contributes most and where we do not have to face the sculpting of our signal due to specialized cut scenarios.

One possibility to understand Standard Model backgrounds at the LHC is the so called staircase scaling feature of QCD [15] which is established in data for $W^{\pm}, Z$+jets and QCD jets. The theoretical foundation of staircase scaling is not fully understood. Nonetheless, there is no doubt that this feature exists in data [16], which is, on the other hand, well reproduced by state of the art Monte Carlo codes, which include matching procedures based on the CKKW [17, 18] or MLM [19] schemes. Staircase scaling heavily contrasts to a Poissonian distribution of the number of radiated photons in QED, which is a well known result for the re summation of p_T-ordered photon emission

[1] As this thesis is finished first hints for an excess which could be the Higgs are around!

with a well defined probabilistic interpretation [20]. By construction, Poisson-like jet multiplicities are present for QCD in the abelian limit, where the gluon self interaction is turned off.

Although not obvious at first sight the photon plus jets channel is very promising to study staircase as well as Poisson like scaling properties. It comes with a relatively large cross section predestinated to be tested with early LHC data.

Therefore this thesis is outlined as follows. First we recapitulate in chapter 2 our current understanding of QCD and what we know about how jets[2] emerge in QCD events. We then give a short motivation and introduction into supersymmetry as one possible new physics model delivering a viable dark matter candidate. In the following chapter 3 we explore in more detail the staircase scaling feature of QCD jet radiation in various SM backgrounds as well as the from QED well known Poisson scaling in the photons plus jets laboratory. Comparing the different kinematic configurations for the two cases enables us to understand better in which situations we can expect staircase scaling. In chapter 4 we use this knowledge to set up an analysis strategy in the missing energy plus jets channel. We use the staircase scaling properties of QCD and apply as inclusive cuts as possible thus enabling us to use a log-likelihood computation to scan a large phase space region automatically providing us with possible information about the mass scale and the color structure of the new physics.

The work [15, 21] presented in this thesis was done together with Christoph Englert, Tilman Plehn and Steffen Schuman.

[2]Note that we use the term jet and final state parton synonymously as the jet algorithms described in 2.1 relates those concepts closely.

Chapter 2

Basic Concepts

The Standard Model of particle physics (SM) is a very successful framework describing many observations with a high precision, see for example the electroweak precision data [23]. All SM particles shown in figure 2.1 except for the Higgs boson have been observed[1]. Moreover no additional elementary particles have been observed until now.

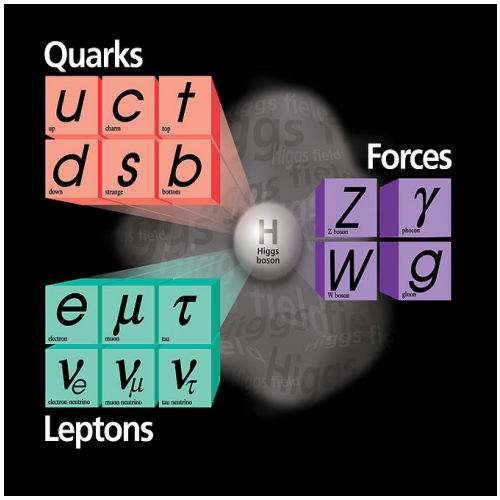

Figure 2.1: Particles and force carriers in the standard model in their mass eigen states, figure taken from [22].

The particles in the SM are characterized by there transformation properties under Lorentz transformations. The Higgs is a scalar while all the other force carriers are vectors. Those particles obey Bose-Einstein statistics and are thus called bosons. All other particles are described by spinors. They obey Fermi-Dirac statistics and are called fermions. Lorentzsymmetry is not the only symmetry respected by the particles of the SM. The whole gauge symmetry group of the SM is $SU(3)_C \times SU(2)_L \times U(1)_Y$. C denotes color. This part is described by Quantum Chromo Dynamics (QCD) which will be studied in more detail trough the next section. The field content of the SM is massless which causes it to be chiral. This means the spinors have an irreducible representation denoted by so called WEYL spinors. Those spinors come along as left and right handed. Only left handed spinors can take part in the weak interactions whose symmetry thus has the subscript L. The hypercharge carried by the particles is described by the symmetry denoted with Y and is closely linked to the electric charge of the particles via $Q_{\text{electric}} = L + Y/2$ where L and Y are the quantum numbers[2] shown in the rows of table 2.1. The latter two are closely connected and referred to as electroweak symmetry. The Higgs mechanism incorporated in the SM breaks this symmetry and thus gives rise to the particle masses. Although we know that neutrinos must have a mass from neutrino oscillation experiments [24][3] they are massless in the SM even after symmetry breaking thus only their left handed versions exist.

Here we cannot study all the features arising from those symmetry properties. We are mostly interested in multi-jet observables and their structure as well as the behavior of colored particles.

[1] Although the first promising statistical deviations, indicating the existence of a Higgs, have been shown on conferences while this thesis is written. The future will show if they are significant.

[2] The weak charge is mostly referred to as I_3 denoting the weak isospin as the concept of weak symmetry was first studied in the connection between protons and neutrons and is described by two spin like degrees of freedom.

[3] This is one hint to physics beyond the SM but is not addressed in this thesis.

	$SU(3)_C$	$SU(2)_L$	$U(1)_Y$
L	1	2	$-1/2$
e_R	1	1	-1
Q	3	2	$1/6$
u_R	3	1	$2/3$
d_R	3	1	$-1/3$

Table 2.1: Quantum numbers for the fermions. Left handed leptons and quarks are combined to doublets due to their symmetry properties with respect to the $SU(2)_L$ symmetry and denoted by L respectively by Q which are not the same as the Q used for the electric charge or the L used for the weak charge. This scheme also applies for the other generations shown in figure 2.1.

Note that though a jet is a collimated spray of color neutral hadrons we use this term also for colored SM particles. A connection between both is given by the jet algorithms in the next section. In the first two parts of section 2.1 we recapitulate the basics of QCD and how to compute *inclusive* observables as a first step to connect theory predictions to observables at a hadron collider. However, the structure of a single event can only be understood in *exclusive* observables. We also use *exclusive* observables through out the following chapters in this thesis. Therefore we show in section 2.1.3 how we can turn inclusive computations into exclusive ones and how to proper simulate QCD events and their structure. There are many good text books, e.g [20], [25] and [26], which give a thorough and much deeper introduction into QCD than can be done here. Also the literature contains many works of how to simulate an exclusive final state correctly, like [17–19], which give much more computational details than can be stated here. A complete overview of jet algorithms is given in [27]. A brief introduction in all three topics can be found in [28]. In the second section of the chapter we shortly introduce supersymmetry (SUSY) as an additional symmetry possibly realized in nature and what kind of signatures we can expect from this new physics concept at the LHC . A much deeper and more complete introduction can be found in [3]. We close this chapter with some remarks how to find evidence for a new physics idea like SUSY at the LHC.

2.1 From QCD to event simulation

2.1.1 The QCD Lagrangian and Feynman rules

Quantum Chromo Dynamics is the gauge theory of colored quarks and gluons. Originally motivated by a $SU(3)$ flavor symmetry the need for an additional degree of freedom arouse to satisfy the request of having anti-symmetrized wave functions for baryons and mesons [25]. Color turned out to fill this need. The gauge group of color is $SU(3)_C$. The quarks transform under the fundamental of the group giving rise to three quark colors respectively anti-colors for the anti-quarks. The gluons as gauge bosons of the theory transform under the adjoined representation giving rise to eight gluon charges. Being charged enables the gluons to interact with each other. An effect directly emerging from the fact that a SU(3) gauge theory is non-abelian. It is this non-abilianity which makes QCD so interesting and its phenomenology so rich. Here we like to exploit this symmetry to built a SU(3) invariant Lagrangian from which we can deduce the structure of the Feynman rules of QCD [26] which are a tool to compute physical observables from theoretical models.

To built a proper quantum theory we need to write down a gauge invariant Lagrangian for our fields. First we study the symmetry properties of $SU(3)_C$ to deduce the invariant terms[4] going into the Lagrangian. The group members of any SU(N) can be expressed with $N^2 - 1$ real parameters

[4]We consider only terms with mass dimension four or less as we have to make sure our Lagrangian is renormalizable.

θ_a

$$U(\theta) = exp(i\theta_a T^a)$$
$$U^\dagger U = 1, \tag{2.1}$$

where the T^a are the generators for the fundamental representation of SU(N) obeying

$$[T^a, T^b] = if^{abc}T_c \tag{2.2}$$

and f^{abc} are the so called structure constants. Group theory gives us several constraints [26] on those quantities like the Jacobi identity

$$f^{abe}f^{ecd} + f^{aed}f^{cbe} + f^{ace}f^{dbe} = 0. \tag{2.3}$$

These, equations (2.1) to (2.3), are the properties we use to check for gauge invariance. We start with the free case which is given by Dirac's equation. The Lagrangian for a free quark reads

$$\mathcal{L}_{\text{quark}} = \bar{q}(i\not{\partial} - m)q, \tag{2.4}$$

where q and $\bar{q}$ denote the spinors for the quarks respectively the anti-quarks and m is the mass. This is clearly invariant under $q' = Uq$. If we want to promote the symmetry to a local symmetry $U \to U(x)$ to get a local gauge theory for quantization we need to replace ∂ by the covariant derivative

$$D^\mu = \partial^\mu + ig_s A^\mu \quad \text{with} \quad A^\mu = A^\mu_a T^a, \tag{2.5}$$

where we introduce $N_c^2 - 1$ real valued gauge fields A^μ_a [26]. The Lorentz indices we contract with the metric denoted by $\eta_{\mu\nu}$. This way we can ensure that

$$D^\mu(A')q'(x) = U(x)D^\mu(A)q(x) \tag{2.6}$$

if and only if the gauge fields A^μ transform as

$$A'^\mu = U(x)A^\mu U(x)^{-1} + \frac{i}{g_s}\left[\partial^\mu U(x)\right]U(x)^{-1}. \tag{2.7}$$

At this point we also have to think about gauge invariant terms involving the gauge fields. In particular there is only one further gauge invariant term we can add to the Lagrangian[5], the field strength tensor

$$F^{\mu\nu} = \frac{-i}{g_s}\left[D^\mu, D^\nu\right] \qquad F^{\mu\nu} \to U(x)F^{\mu\nu}U(x)^{-1}. \tag{2.8}$$

From this we construct the gauge invariant term

$$\mathcal{L}_{\text{gauge}} = -\frac{1}{2}\text{Tr}\left\{F_{\mu\nu}F^{\mu\nu}\right\}. \tag{2.9}$$

The classical locally gauge invariant QCD Lagrangian with gluons, n_f quarks and their interactions then reads

$$\mathcal{L}_{\text{QCD}} = \sum_{n_f} \bar{q}(i\not{D} - m)q \; - \; \frac{1}{2}\text{Tr}\left\{F_{\mu\nu}F^{\mu\nu}\right\}. \tag{2.10}$$

However this Lagrangian is not sufficient to formulate the full quantum theory. Indeed the propagator for the gluon is not well defined [20]. To solve this problem we have to add gauge fixing and ghost terms:

$$\mathcal{L}_{\text{fix}} = -\frac{1}{2\xi}\left(\partial_\mu A^{a\mu}\right)\left(\partial_\nu A^{a\nu}\right)$$
$$\mathcal{L}_{\text{ghost}} = \partial_\mu \eta^{a\dagger}\left(\partial^\mu \delta^{ab} + g_s f_{abc}A^{c\mu}\right)\eta^b. \tag{2.11}$$

[5]There is also another invariant term built from the dual field strength tensor. It is proportional to a parameter θ and leads to non perturbative effects violating parity (P) and charge conjugation (C) symmetry, which are known to be respected by QCD [26]. From experiments we know that this parameter θ has to be very small and through out this thesis we consider it to be zero. This is also referred to as the strong CP problem.

In particular the gauge fixing and ghost terms are needed to remove a divergence in the path integral due to the infinite number of equal gauge field configurations. Here we show the Lagrangian in covariant gauge $\partial_\mu A^{a\mu} = 0$. Putting all the pieces together the full QCD Lagrangian for n_f flavors reads

$$\begin{aligned}\mathcal{L}_{\text{QCD}} = &\sum_{n_f} \bar{q}(i\not{D} - m)q \\ &- \frac{1}{2}\left[\left(\partial_\mu A^a_\nu - \partial_\nu A^a_\mu\right)\left(\partial^\mu A^{a\nu} - \partial^\nu A^{a\mu}\right) + \frac{1}{\xi}\left(\partial^\mu A^a_\mu\right)\left(\partial^\nu A^a_\nu\right)\right] \\ &+ \left(\partial^\mu \eta^{a\dagger}\right)\left(\partial_\mu \eta^a\right) - g_s T^a \bar{q} \not{A}^a q + g_s f_{abc}\left(\partial_\mu \eta^{a\dagger}\right)\eta^b A^{c\mu} \\ &+ g_s f_{abc}\left(\partial_\mu A^a_\nu\right) A^{b\mu} A^{c\nu} - \frac{g_s^2}{4} f_{abc} f_{ade} A^{b\mu} A^{c\nu} A^d_\mu A^e_\nu. \end{aligned} \tag{2.12}$$

From this form we can deduce the existing Feynman diagrams and their structure. The first three terms give rise to quark, gluon and ghost propagators. Note the complicated form of the gluon propagator due to gauge fixing. The next two terms describe the gluon quark and the gluon ghost vertices while the last terms give rise to the gluon self couplings namely the triple and quartic gluon vertices, see fig. 2.2 and fig. 2.3, coming from the commutator structure of SU(3).

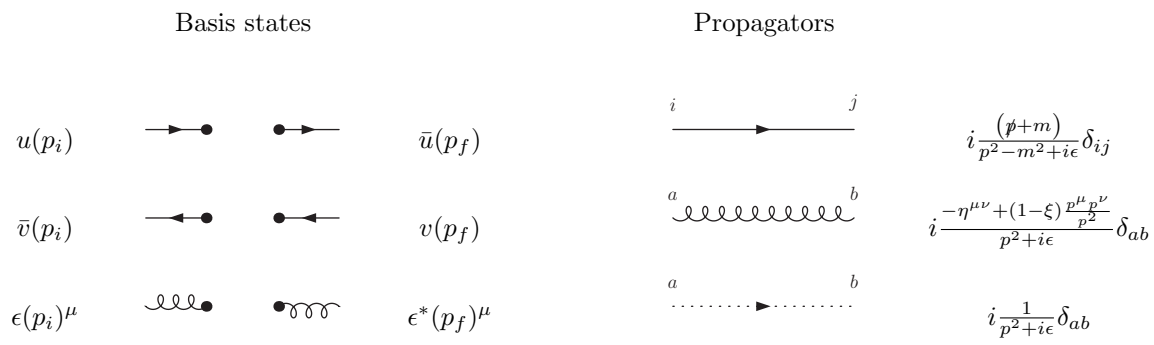

Figure 2.2: The Feynman rules of QCD [26]. The basis states for fermions are represented by spinors while for gluons they are described by their polarization vectors. As ghosts are scalars they have unit base states. The complicated form of the gluon propagator results from the gauge fixing.

We have to mention some additional rules which are not obvious from the figures[6]:

- Closed loops of fermions or ghosts get an additional minus sign because they are anti commuting.
- Closed loops with bosons get an additional symmetry factor of 1/2 to take into account their interchangeability.

The Feynman rules are the first step to link theoretical ideas as gauge symmetries to computations. They use the idea of computing physical quantities to arbitrary precision through a perturbative series in the coupling constant. With the Feynman rules we can compute amplitudes for the processes of interest. Together with the phase space we can compute cross sections σ respectively the rates of reactions through $\dot{N} = \mathcal{L}\sigma$ where the experimental properties are encrypted in the luminosity $\mathcal{L}$. In an experiment we are not able to directly prepare quarks or gluons as initial states as we find in nature only bound, color neutral QCD objects, the hadrons. But together with the Feynman rules for QED [20] we are able to compute elementary processes at colliders, e.g. $e^+e^- \to q\bar{q}$, see figure 2.4 for a pictorial illustration. We are also not able to detect partons but again only hadrons. However, the computed rate is still correct as long as we add up all detected hadrons. If we want to compute observables at a hadron collider we need to find a description for the proton as the initial state we actually can prepare and how to link it to the basic objects of our theory the quarks and gluons or shortly partons for which we can compute scattering amplitudes.

[6] Although it seems that we insert these factors by hand they in fact drop out of a correct quantization via the path integral formalism occurring there as power in the Jacobian determinant reflecting the bosonic (commutators) respectively fermionic (anti-commutators) nature of the involved fields.

Quark gluon vertex

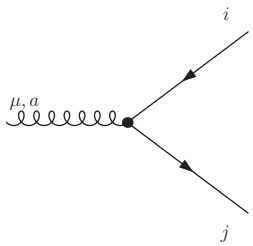

$$ig_s T^a_{ij}\gamma^\mu$$

Ghost gluon vertex

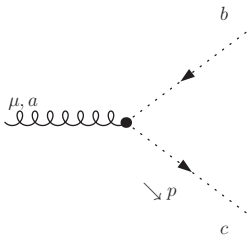

$$-g_s f_{abc} p_\mu$$

Triple gluon vertex

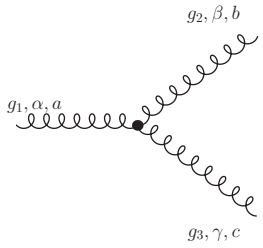

$$\begin{aligned} +g_s f_{abc}[&+ \eta_{\alpha\beta}(g_1 - g_2)_\gamma \\ &+ \eta_{\beta\gamma}(g_2 - g_3)_\alpha \\ &+ \eta_{\gamma\alpha}(g_3 - g_1)_\beta] \end{aligned}$$

Quartic gluon vertex

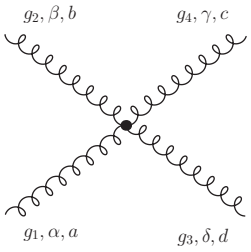

$$\begin{aligned} ig_s^2[&+ f_{abe}f_{cde}(\eta_{\alpha\gamma}\eta_{\beta\delta} - \eta_{\alpha\delta}\eta_{\beta\gamma}) \\ &+ f_{ace}f_{dbe}(\eta_{\alpha\delta}\eta_{\beta\gamma} - \eta_{\alpha\beta}\eta_{\gamma\delta}) \\ &+ f_{ade}f_{bce}(\eta_{\alpha\beta}\eta_{\gamma\delta} - \eta_{\alpha\gamma}\eta_{\beta\delta})] \end{aligned}$$

Figure 2.3: The Feynman rules of QCD [26]. Note that for the vertices all momenta are outgoing and thus sum to zero. The gluon self interaction is a direct result of the commutator structure of SU(3).

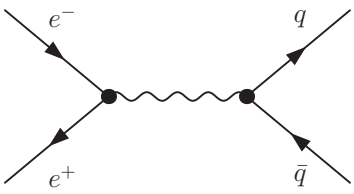

Figure 2.4: Feynman graph for electron positron scattering to quarks. With the spinor technique from [20] we are able to compute the total cross section for this process and thus the expected rate at a e^+e^- collider.

2.1.2 Parton splitting and the DGLAP equation

We can also compute the amplitudes for parton parton scattering as is done in appendix A. But we would get no complete description of the collider phenomenology because in nature we only can observe color singlets like hadrons. While the potential energy between electrical charged objects

heads for zero if they are apart, the potential energy between color charged objects grows linear. This is another consequence of the gluon self interaction. For hadron collider phenomenology it means we have to find a connection between partons which are the fundamental objects of our theory and hadrons which are the objects we can collide and observe in detectors. For the final state we do not have to worry to much. What ever happens to the final state partons does not matter if we integrate over all final state hadron configurations. This is a fully *inclusive* result. For the initial states the computation is not that easy. If we are to collide for example protons as is done at the LHC we need to know which partons we can expect to participate in the interaction and how their weights are distributed among one another.

The proper quantity to describe partons in a proton are the parton density functions (pdf's or $f_i(x, \mu_f)$). They describe the probability to find a parton i carrying the momentum fraction x of the proton. μ_F is an unphysical artifact of the derivation of the DGLAP equation we deal with in this section which describes the evolution of the parton density functions if probed at different scales and could be a typical scale of the process of interest, e.g. m_Z for Z^0 production. The general formula for any process P accompanied by any number of final state partons X would be the master equation

$$\sigma(h_1 h_2 \to P + X) = \sum_{\mathrm{i,j}} \int dx_1 dx_2 f_i(x_1, \mu_F) f_j(x_2, \mu_F) \sigma_{(\mathrm{ij}\to\mathrm{P})}(x_1, x_2, \mu_F), \tag{2.13}$$

where i and j denote the partons in the hadrons h_1 respectively h_2 and x the energy fraction of the proton the parton is carrying. It is energetically very easy for partons to radiate other partons thus filling the proton with many interacting objects. The pdf's describe how these objects are distributed with respect to the momentum fraction of the proton they carry. The DGLAP equation on the other hand guides their evolution to different scales by incorporating how partons split. To understand how the DGLAP equation influences the parton densities we need to understand this splitting property of the partons.

For that reason we study how a parton can split from a core process with given multiplicity n, thus giving us a process with multiplicity $n+1$. Understanding this splitting leads to an evolution equation for the pdf's and thus a description of the proton as well as an algorithm to simulate events with an unknown number of additional final state partons.

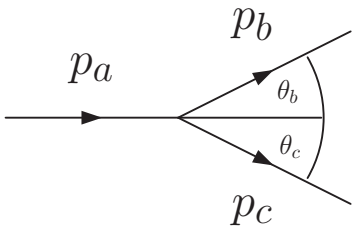

Figure 2.5: Splitting of a parton a in partons b and c and kinematic configuration with the four vectors p and the branching angles θ.

We start with the $n+1$ particle phase space as it is the same for all possible parton branching. In this computation we use the energy fraction

$$z = \frac{|E_b|}{|E_a|} = 1 - \frac{|E_c|}{|E_a|} \tag{2.14}$$

to describe kinematics, see [25]. z is also closely linked to the infrared divergence of QCD as we shall see in equation (2.31). We can transform the $n+1$ particle phase space according to

$$d\Phi_{n+1} = d\Phi_n \frac{dp_{c,3} dp_T^2 d\phi}{2(2\pi)^3 |E_c|} \frac{1}{z}. \tag{2.15}$$

To simplify this expression we work in the so called Sudakov decomposition [28] where the energy fraction enters as a variable again

$$-p_a = p_b + p_c = (-zp_a + \beta n + p_T) + (-(1-z)p_a - \beta n - p_T) \tag{2.16}$$

and we define a four vector n which describes the decay plane as well as a free parameter β. Forcing the outgoing parton c to be on shell we can use this decomposition to write the phase space as

$$d\Phi_{n+1} = d\Phi_n \frac{dz dp_a^2 d\phi}{4(2\pi)^3} = d\Phi_n \frac{dz dp_a^2}{4(2\pi)^2} \tag{2.17}$$

where in the last step we assume spherical symmetry. For the cross section this means we can write

$$d\sigma_{n+1} = \frac{2g_s^2}{p_a^2} \hat{P}(z) \overline{|M_n|^2} d\Phi_n \frac{dp_a^2 dz}{4(2\pi)^2}. \tag{2.18}$$

Here we assume that we can factorize the matrix element with appropriate splitting kernels

$$\overline{|M_{n+1}|^2} = \frac{2g_s^2}{p_a^2} \hat{P}(z) \overline{|M_n|^2}. \tag{2.19}$$

This factorization holds exactly in the collinear or soft limit. In terms of cross sections we get the common form

$$\sigma_{n+1} = \int \sigma_n \frac{dp_a^2}{p_a^2} dz \frac{\alpha_s}{2\pi} \hat{P}(z). \tag{2.20}$$

In this form we can see that we can built the n particle cross section through successive radiation of partons starting at a hard core process, which will cross our path again once we study the parton shower approach.

Let us now construct the appropriate splitting kernels for the factorization using the Feynman rules from figure 2.3. As can be seen in figure 2.5 this involves a propagator for parton a which is $\propto 1/p_a^2$. If we express this in terms of the energy fraction and the Mandelstam variable t, we find

$$t = p_a^2 = 2E_b E_c (1 - cos\theta) \approx z(1-z) E_a^2 \theta^2. \tag{2.21}$$

From this we can deduce that the matrix element is enhanced in the collinear limit region. We also observe that z is indeed linked to the divergence of QCD. Thus we focus our examination on the collinear region and neglect higher terms in θ. On the other hand we can express θ as

$$\theta = \frac{1}{E_a} \sqrt{\frac{t}{z(1-z)}} = \frac{\theta_b}{1-z} = \frac{\theta_c}{z}. \tag{2.22}$$

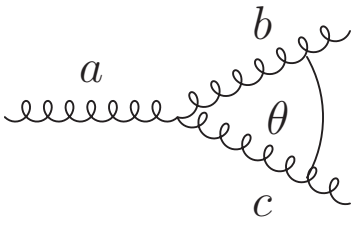

Figure 2.6: Gluon splitting described by the triple gluon vertex. For small θ the splitting is enhanced

We consider the pure gluon case which involves not only the above mentioned propagator but also the triple gluon vertex, see fig. 2.3. Contracting it with the polarization vectors for the gluons we get

$$V_{ggg} = g_s f_{abc} \epsilon_a^\alpha \epsilon_b^\beta \epsilon_c^\gamma [\eta_{\alpha\beta}(p_a - p_b)_\gamma + \eta_{\beta\gamma}(p_b - p_c)_\alpha + \eta_{\gamma\alpha}(p_c - p_a)]. \tag{2.23}$$

Since the three gluons are nearly on their mass-shell we can assume that their polarization vectors are transverse [25] $\epsilon_i p_i = 0$, so we can write

$$V_{ggg} = -2g_s f_{abc}[(\epsilon_a\epsilon_b)(\epsilon_c p_b) - (\epsilon_b\epsilon_c)(\epsilon_a p_b) - (\epsilon_c\epsilon_a)(\epsilon_b p_c)] \tag{2.24}$$

As basis we choose polarizations normal to the branching plane ϵ^{out} and parallel to the branching plane ϵ^{in}, so that

$$\begin{aligned} \epsilon_i^{in}\epsilon_j^{in} &= \epsilon_i^{out}\epsilon_j^{out} = -1 \\ \epsilon_i^{in}\epsilon_j^{out} &= \epsilon_i^{out} p_j \quad = 0. \end{aligned} \tag{2.25}$$

As we are working in the collinear region we can expand in θ

$$\begin{aligned} \epsilon_a^{in} p_b &\approx -z(1-z)E_a\theta = -\sqrt{tz(1-z)} \\ \epsilon_b^{in} p_c &\approx (1-z)E_a\theta \quad\quad = \sqrt{\frac{t(1-z)}{z}} \\ \epsilon_c^{in} p_b &\approx -zE_a\theta \quad\quad\quad = -\sqrt{\frac{tz}{(1-z)}} \end{aligned} \tag{2.26}$$

using equation (2.22) for the last equality. Merging all the parts we get an expression for the matrix element of the splitting

$$M_{\text{split}} = \frac{2ig_s}{t} f_{abc}[(\epsilon_a\epsilon_b)(\epsilon_c p_b) - (\epsilon_b\epsilon_c)(\epsilon_a p_b) - (\epsilon_c\epsilon_a)(\epsilon_b p_c)]. \tag{2.27}$$

Now we have to square this expression and incorporate the right averaging factors for the colors and polarizations [28]

$$\overline{|M_{\text{split}}|^2} = \frac{2g_s^2}{t^2}\frac{1}{N_c^2-1}\frac{1}{N_a}\left[\sum_{3 \text{ terms}} \pm f_{abc}(\epsilon_i\epsilon_j)(\epsilon_k p_{(l\neq k)})\right]^2, \tag{2.28}$$

where i, j, k, l denote the combinations from equation (2.27). Note that while f_{abc} is totally anti-symmetric the terms in the sum are symmetric with respect to two of the indices. This means that all interference terms in the sum vanish and the squared sum becomes a sum of squares.

$$\overline{|M_{\text{split}}|^2} = \frac{2g_s^2}{t}\frac{f_{abc}f_{abc}}{N_c^2-1}\frac{1}{N_a}\left[\sum \frac{(\epsilon_i\epsilon_j)^2(\epsilon_k p_{(l\neq k)})^2}{t}\right]. \tag{2.29}$$

For the sum we use equation (2.25) and (2.26) and get

$$\overline{|M_{\text{split}}|^2} = \frac{4g_s^2}{t} C_A \left[\frac{1-z}{z} + \frac{z}{1-z} + z(1-z)\right] = \frac{4g_s^2}{t} C_A \hat{P}_{gg}(z) \tag{2.30}$$

where $\hat{P}_{gg}(z)$ is the so called unregularized gluon splitting kernel.

The computation for the other splitting kernels is very similar, but includes the spinors for the quarks. Working out all the combinations for the gluon polarizations and the quark helicities we get for all the splitting kernels [28]:

$$\begin{aligned} \hat{P}_{\text{gg}}(z) &= C_A\left[\frac{1-z}{z} + \frac{z}{1-z} + z(1-z)\right] \\ \hat{P}_{\text{qg}}(z) &= T_R\left[z^2 + (1-z)^2\right] \\ \hat{P}_{\text{qq}}(z) &= C_F\frac{1+z^2}{1-z} \\ \hat{P}_{\text{gq}}(z) &= C_F\frac{1+(1-z)^2}{z}. \end{aligned} \tag{2.31}$$

These quantities are divergent for $z \to 0$ and $z \to 1$. This reflects the infrared divergence of QCD and shows us also that these splitting kernels are not yet the right quantities to describe the proton. z denotes the energy fraction, so integrating over z would mean to ask how large is the probability to find any splitting with any energy fraction. For the splitting kernels in this form the answer would not be finite while we expect a finite result for a probabilistic picture.

Nevertheless we can use the parton splitting from equation (2.31) to describe incoming partons in the proton. Note that while the factorization is a collinear approximation it is well suited to describe the partons in an incoming proton. The proton is a bound object so its constituents have all nearly the same direction of movement giving them parallel trajectories. If a collinear splitting occurs the trajectories will still be parallel. If the splitting is not collinear it can not be hard enough for the parton to leave the proton as protons are stable objects[7] [30]. In that case the splitting is soft and again well described by our approximation. Again we consider the pure gluon case. To find an appropriate description of the proton we have to consider multiple branching as the proton is a dynamical object. In figure 2.7 we look at a gluon line successively radiating gluons. In this

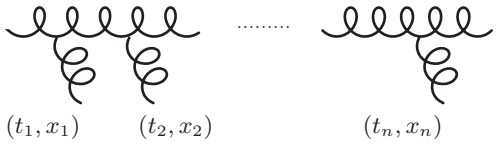

Figure 2.7: Successive radiation of gluons changing carried energy fraction and virtuality.

process starting at some energy fraction x_1 and some virtuality $|t_1|$ the energy fraction decreases so that $x_j > x_{j+1}$ while the virtuality increases due to recoil $|t_j| < |t_{j+1}|$. The distribution of the partons at some energy fraction x and virtuality t is encoded in the parton distribution function $f(x,t)$. Looking at the (x,t) plane in figure 2.8 and the flow of branching we can establish an evolution equation for the parton densities. To achieve this we study a small square $(\delta x, \delta t)$ of the

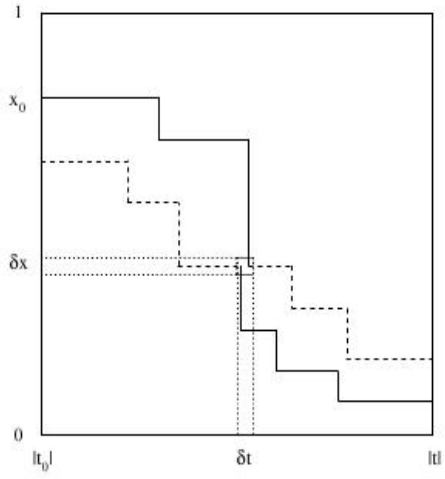

Figure 2.8: (x,t) plane and possible flow of the parton densities, taken from [28]

(x,t) plane and the flow of partons into the square and out of it, which is proportional to δt

$$\delta f_{\text{in}}(-t) = \delta t \left(\frac{\alpha_s \hat{P}}{2\pi t} \otimes f \right)(x, -t)$$
$$\delta f_{\text{out}}(-t) = \delta t \int_0^1 dy \frac{\alpha_S \hat{P}(y)}{2\pi t} f(x, -t). \tag{2.32}$$

[7] Although there is some discussion about proton decay [31], they have been stable the last 13 billion years.

For the incoming flow we use a convolution, defined as

$$(f \otimes g)(x) = \int_0^1 dx_1 dx_2 f(x_1) g(x_2) \delta(x - x_1 x_2) = \int_0^1 \frac{dx_1}{x_1} f(x_1) g\left(\frac{x}{x_1}\right), \tag{2.33}$$

because we do not know from which starting position the parton comes, while we use an integral for the outgoing flow, because we have to integrate over the possible final states. Combining those to a net flow we get

$$\begin{aligned} \delta f(x,-t) &= \frac{\delta t}{t}\left[\int_0^1 \frac{dz}{z}\frac{\alpha_s}{2\pi}\hat{P}(z) f\left(\frac{x}{z},-t\right) - \int_0^1 dy \frac{\alpha_s}{2\pi}\hat{P}(y) f(x,-t)\right] \\ &= \frac{\delta t}{t}\int_x^1 \frac{dz}{z}\frac{\alpha_s}{2\pi}\hat{P}(z)_+ f\left(\frac{x}{z},-t\right). \end{aligned} \tag{2.34}$$

Here we introduce the plus subtraction scheme

$$F(z)_+ = F(z) - \delta(1-z)\int_0^1 dy F(y), \tag{2.35}$$

which renders the per se unregularized splitting kernels finite. Note that this comes along on its own and is not introduced by hand as we treat the incoming and outgoing flux coherently. Furthermore we switch the integration boundary from 0 to x, because $x < z \leq 1$. To get an evolution equation in the pure gluonic picture we have to compute the plus subscription for the gluon splitting kernel. For a correct description of the proton we would have to include the splitting from and to quarks as well, but instead we only compute the gluonic part, as we have done for the parton branching before, and state the other contributions after wards. We start with the outgoing flux and try to find the parts which are proportional to $\delta(1-z)$:

$$\begin{aligned} -\int_0^1 dy \frac{\alpha_S}{2\pi}\hat{P}_{\mathrm{gg}}(y) &= -\frac{\alpha_S}{2\pi} C_A \int_0^1 dy \left[\frac{2y}{1-y} + y(1-y)\right] \\ &= \frac{\alpha_s}{2\pi} C_A \left[\frac{11}{6} - \delta(1-z) 2 \int_0^1 dy \frac{z}{1-y}\right]. \end{aligned} \tag{2.36}$$

Putting this together with our gluon splitting kernel we find

$$P_{\mathrm{gg}}(z) = 2C_A\left[\frac{z}{(1-z)_+} + \frac{1-z}{z} + z(1-z)\right] + \frac{11}{6}C_A\delta(1-z). \tag{2.37}$$

Note that this is indeed finite, because $0 \leq x < z \leq 1$. Including n_f quarks we get [25, 28]

$$\begin{aligned} P_{\mathrm{gg}}(z) &= 2C_A\ \left[\frac{z}{(1-z)_+} + \frac{1-z}{z} + z(1-z)\right] + \frac{11}{6}C_A\ \delta(1-z) + \frac{3}{2} n_f T_R \delta(1-z) \\ P_{\mathrm{qg}}(z) &= T_R\ \left[z^2 + (1-z)^2\right] \\ P_{\mathrm{gq}}(z) &= C_F\ \frac{1+(1-z)^2}{z} \\ P_{\mathrm{qq}}(z) &= C_F\ \left[\frac{1+z^2}{(1-z)_+} + \frac{3}{2}\delta(1-z)\right]. \end{aligned} \tag{2.38}$$

These are now the right objects to describe what happens in the proton. With these regularized splitting kernels we can write down the DGLAP equation from its proto form of equation (2.34) for the whole parton content of the proton as

$$\frac{df_i(x,\mu_F)}{d\ \log \mu_F^2} = \frac{\alpha_S}{2\pi}\sum_j (P_{\mathrm{ij}} \otimes f_j)(x,\mu_F). \tag{2.39}$$

Note the missing hat on the splitting kernels. This means we really have a finite description. To get to this standard form we have to do some identification of scales. First we identify the virtuality with the factorizations scale $-t = \mu_F$. This scale is connected to our derivation of the splitting kernels for describing the collinear divergences. But similar to QED we also have to take care of the renormalization scale μ_R connected to the ultraviolet divergences from loops. This scale enters

our formula via α_s, which is due to the running of the coupling a function of μ_R. We also identify those two scales with each other, $\mu_R = \mu_F$.

The DGLAP equation gives us not an explicit solution for the parton densities, but is an evolution equation. With the DGLAP equation we evolve the parton densities to the scale μ_F and fold them into the cross section. Thus we get a fully *inclusive* result taking the structure of the proton at the scale of the process of interest and the evolution of the partons into account. A large set of pdf's can be found at [29]. At this stage we are able to do phenomenology at a hadron collider, predicting cross sections and their higher order corrections. We could study particle production processes like Higgs production [32] or even do cross section predictions for new physics models [33]. Stating this computation to be inclusive means that all possible additional final state partons X from equation (2.13) are integrated over by means of the pdf's. However, this means not that we can only compute $2 \to 2$ processes. If we, for example, like to study a $2 \to 4$ process in perturbative QCD, we had to take into account all the events with at *least* four jets but ignoring anything else. We are also able to compute higher order corrections to processes thus using the perturbative character of the Feynman rules to get more precise rate predictions.

2.1.3 Parton Shower and Matrix Element Merging

The prescription of QCD we have recapitulated so far is a fully *inclusive* one described by the master equation (2.13). It predicts the correct rates at hadron colliders, but is blind to the actual structure of jets in a single event. To simulate proton collisions at the LHC we need an *exclusive* description of QCD together with a probabilistic interpretation for the actual simulation. Note also that the multi-jet observables we study in the next chapters are defined to be *exclusive* through out this thesis. They are interesting as many new physic models also predict a rich jet structure. Therefore we line out how to get *exclusive* predictions and how to implement them in an algorithm, known as CKKW algorithm [18], to get a literally pictorial simulation of QCD events.

In a first step we study how we compute exclusive quantities from inclusive ones. The quantity we need to study is the so called Sudakov form factor [18, 28]

$$\Delta_i(t, t_0) = exp\left(-\sum_j \int_{t_0}^{t} \frac{dt'}{t'} \int_0^1 dy \frac{\alpha_s}{2\pi} \hat{P}_{ij}(y)\right). \tag{2.40}$$

At this stage t and t_0 as well as t_{hard} and t_{match}, we will encounter later on, are just integration boundaries. Their physical meaning gets clarified later. The Sudakov form factor is found in the DGLAP equation if we re write it in terms of unregularized splitting kernels [28]. Note first that

$$\frac{1}{\Delta_i(t, t_0)} \frac{d\Delta_i(t, t_0)}{dt} = -\sum_j \int_{t_0}^{t} \frac{dt'}{t'} \int_0^1 dy \frac{\alpha_s}{2\pi} \hat{P}_{ij}(y) \tag{2.41}$$

for the derivative of the Sudakov form factor. This gives us the possibility to re write the derivative of the parton density as

$$\frac{df_i(x,t)}{dt} = \frac{1}{t} \sum_j \int_0^1 \frac{dz}{z} \frac{\alpha_s}{2\pi} \hat{P}_{ij}(z) f_j\left(\frac{x}{z}, t\right) + \frac{f_i(x,t)}{\Delta_i(t)} \frac{d\Delta_i(t)}{dt}, \tag{2.42}$$

where $\Delta_i(t)$ is just a short notion for $\Delta_i(t, t_0)$. If we now consider the quantity f_i/Δ_i [18] we find that it satisfies the DGLAP equation with unregularized splitting kernels

$$\begin{aligned} \frac{d}{dt}\frac{f_i(x,t)}{\Delta_i(t)} &= \frac{1}{\Delta_i(t)} \frac{df_i(x,t)}{dt} - \frac{f_i(x,t)}{\Delta_i^2(t)} \frac{d\Delta_i(t)}{dt} \\ &= \frac{1}{\Delta_i(t)} \frac{1}{t} \sum_j \int_0^{1-\epsilon} \frac{dz}{z} \frac{\alpha_s}{2\pi} \hat{P}_{ij}(z) f_j\left(\frac{x}{z}, t\right), \end{aligned} \tag{2.43}$$

where we modified the upper integration bound to keep the integral finite following the argumentation from [25]. To understand how this rewriting of the DGLAP equation helps us to generate

exclusive quantities we integrate it over appropriate values of t and introduce $\Delta(t,t') = \frac{\Delta_i(t)}{\Delta_i(t')}$ [28]

$$\begin{aligned}
\frac{f_i(x,t)}{\Delta_i(t)} - \frac{f_i(x,t_0)}{\Delta_i(t_0)} &= \int_{t_0}^{t} \frac{dt'}{t'} \sum_j \int_0^{1-\epsilon} \frac{dz}{z} \frac{\alpha_s}{2\pi} \hat{P}_{ij}(z) \frac{f_j\left(\frac{x}{z},t'\right)}{\Delta_i(t')} \\
f_i(x,t) &= \frac{\Delta_i(t)}{\Delta_i(t_0)} f_i(x,t_0) + \int_{t_0}^{t} \frac{dt'}{t'} \frac{\Delta_i(t)}{\Delta_i(t')} \sum_j \int_0^{1-\epsilon} \frac{dz}{z} \frac{\alpha_s}{2\pi} \hat{P}_{ij}(z) f_j\left(\frac{x}{z},t'\right) \\
&\equiv \Delta(t,t_0) f_i(x,t_0) + \int_{t_0}^{t} \frac{dt'}{t'} \Delta(t,t') \sum_j \int_0^{1-\epsilon} \frac{dz}{z} \frac{\alpha_s}{2\pi} \hat{P}_{ij}(z) f_j\left(\frac{x}{z},t'\right). \qquad (2.44)
\end{aligned}$$

Rewriting the integrated DGLAP equation in this form has the following advantage: we are able to assign a probabilistic interpretation to the Sudakov form factor. Note that the Sudakov is multiplied to f_i without any additional change. While the second term encodes the evolution of partons through the splitting kernels. To fully use the Sudakov in a probabilistic way two further steps are required. First the term in the exponent can be integrated out in the leading logarithm approximation [18, 28] to yield the integrated splitting functions

$$\begin{aligned}
\Gamma_q(t_{\text{hard}},t) &= \frac{C_F}{\pi} \frac{\alpha_s(t)}{t} \left(\frac{1}{2} log \frac{t_{\text{hard}}}{t} - \frac{3}{4}\right) \\
\Gamma_g(t_{\text{hard}},t) &= \frac{C_A}{\pi} \frac{\alpha_s(t)}{t} \left(\frac{1}{2} log \frac{t_{\text{hard}}}{t} - \frac{11}{12}\right) \\
\Gamma_f(t) &= \frac{n_f}{6\pi} \frac{\alpha_s(t)}{t}, \qquad (2.45)
\end{aligned}$$

where q denotes the emission of a gluon from a quark, g the splitting of one gluon into two and f the splitting of a gluon into two quarks. In this formulation the Sudakov form factors now read

$$\begin{aligned}
\Delta_q(t_{\text{hard}},t_{\text{match}}) &= exp\left(-\int_{t_{\text{hard}}}^{t_{\text{match}}} dt\ \Gamma_q(t_{\text{hard}},t)\right) \\
\Delta_g(t_{\text{hard}},t_{\text{match}}) &= exp\left(-\int_{t_{\text{hard}}}^{t_{\text{match}}} dt\ [\Gamma_g(t_{\text{hard}},t) + \Gamma_f(t)]\right). \qquad (2.46)
\end{aligned}$$

Second think of a Poisson distribution[8] for the number of observations

$$P(n,\lambda) = \frac{\lambda^n}{n!} exp(-\lambda), \qquad (2.47)$$

then the probability to observe nothing is

$$P(0,\lambda) = exp(-\lambda). \qquad (2.48)$$

This together with the last line of equation (2.44) is the foundation of our interpretation of the Sudakov form factor as *non-splitting* probability. The first part of the last line of (2.44) reads nothing happened to the pdf while the second part, also involving a Sudakov, but only up to the scale t', reads at least one splitting has occurred. Consider now some simple $2 \to 2$ process for example electron positron scattering to quarks. To get the *exclusive* two jet rate we just multiply each quark line with a Sudakov factor [18]. In this case the only way to get a three jet configuration is the emission of an additional gluon. Equation (2.45) gives us the correct factor to insert: $\Gamma_q \Delta_g$. As the emission can have any value of energy fraction we also have to include an

[8] A Poisson distribution is for example found for the re summation of infrared divergent soft and collinear photon emission [20].

additional integration. The exclusive n_{jet} fractions for electron positron scattering are then [18]

$$\begin{aligned}
R_2(Q_1,Q) &= [\Delta_q(Q_1,Q)]^2 \\
R_3(Q_1,Q) &= 2[\Delta_q(Q_1,Q)]^2 \int_{Q_1}^{Q} dq\ \Gamma(q,Q)\Delta_g(Q_1,q) \\
R_4(Q_1,Q) &= 2[\Delta_q(Q_1,Q)]^2 \\
&\quad \left(\int_{Q_1}^{Q} dq\ \Gamma(q,Q)\Delta_g(Q_1,q) \int_{Q^1}^{Q} dq' \Gamma_q(q',Q)\Delta(Q_1,q') \right. \\
&\quad + \int_{Q_1}^{Q} dq\ \Gamma(q,Q)\Delta_g(Q_1,q) \int_{Q_1}^{q} dq' \Gamma_g(q',q)\Delta_g(Q_1,q') \\
&\quad \left. + \int_{Q_1}^{Q} dq\ \Gamma(q,Q)\Delta_g(Q_1,q) \int_{Q_1}^{q} dq' \Gamma_f(q')\Delta_f(Q_1,q') \right)
\end{aligned} \tag{2.49}$$

and so on for higher multiplicities. There are few things to note about this formula. First we changed the variables from virtuality t to the for this case more suitable c.o.m energy Q as we choose electron positron scattering as an example for simplicity. q denotes the energy of the emitted parton and is integrated over. Q_1 corresponds to the integration boundary t_{match} or t_0 above. The physical meaning behind these integration boundaries are the different energy scales in QCD processes. The scattering takes place at a high scale, e.g. the c.o.m. energy Q corresponding to the variable t_{hard}, and is described by perturbative QCD while the hadrons we observe are low energy objects which form around the scale Q_1. To quantify Q_1 we need a resolution measure counting partons to separated jets. The appropriate measure is a so called k_T-resolution [18]

$$y_{\text{ini}} = \frac{Q_1^2}{Q^2}. \tag{2.50}$$

We will meet the k_T measure and its relation to jets, see also [27], in the last part of this section again. The probabilistic evolution of partons is called *Parton Shower* (PS). For a coherent PS description of QCD events at a hadron collider we need to address two further points: initial partonic states and the probabilistic distributions which generate exclusive events in a Monte Carlo code. This is done by assigning branching probabilities through Sudakov factors [17, 25] and solving those with flat random numbers to generate exclusive final state partons [28]. The no-branching probabilities P for forward (F) and backward[9] (B) shower evolution read [25]

$$\begin{aligned}
P^{(\text{F})}_{\text{no},i}(t_1,t_2) &= \frac{\Delta_i(t_1,t_0)}{\Delta_i(t_2,t_0)} \\
&\text{and} \\
P^{(\text{B})}_{\text{no},i}(t_1,t_2,x) &= \frac{\Delta_i(t_1,t_0) f_i(x,t_2)}{\Delta_i(t_2,t_0) f_i(x,t_1)}.
\end{aligned} \tag{2.51}$$

The ratios of parton density functions makes sure the pdf's are taken at the right scale. The kinematics, e.g four vectors, are then computed as follows. Going from a given starting point (x_1,t_1) to the next point (x_2,t_2) gives us two constraints, namely the virtuality which has to fulfill $|t_2| > |t_1|$ and the energy fraction with $x_2 < x_1$. Those we get through flat random numbers (r_t, r_x) according to the equations [28][10]

$$P_{\text{no},i}(t_1,t_2) = r_t \qquad \frac{\int_0^{x_2/x_1} dy \frac{\alpha_s}{2\pi}\hat{P}(y)}{\int_0^1 dy \frac{\alpha_s}{2\pi}\hat{P}(y)} = r_x \qquad \text{with } r \in [0,1]. \tag{2.52}$$

Having the outgoing parton on mass shell fixes the third condition. For the fourth we use the fact that the splitting kernels are invariant under transformations in the azimuthal angle Φ, so we generate it randomly in $[0, 2\pi]$ [28]. At this point we have a coherent and probabilistic description of the PS which is implemented in state of the art Monte Carlo codes [34]. However, due to

[9] This gives us the possibility to evolve initial state partons.

[10] Getting $t_2 < t_0$ corresponds then to no branching at all.

the factorization in the derivation of the splitting kernels the PS does not take interferences into account.

Alternatively we might use exact Matrix Elements (ME). We still need the Sudakov form factors to render the results exclusive. However, in equation (2.49) the factors of Γ need to be interchanged by the appropriate ME [18]. The advantage is that these take all interference effects into account. The disadvantage is that their number and complexity increase fast with their perturbative order[11] and the number of involved partons. For infrared parton configurations the ME are divergent introducing a lower cut off similar to the resolution idea of equation (2.50). Furthermore the passage to hadrons invokes free scale dependent parameters which would require re tuning of parameters for every c.o.m [18]. The partons in the ME all carry color. For hadronization the need to be grouped to color neutral objects. This clearly limits the applicability of ME. On the other hand we know that the splitting kernels in the PS are only valid in the infrared regime and that they do not take interference effects into account. To gain more insight we compare the emission of an additional gluon in electron positron scattering in figure 2.9.iate ME [18]. The advantage is that these take all interference effects into account. The disadvantage is that their number and complexity increase fast with their perturbative order[12] and the number of involved partons. For infrared parton configurations the ME are divergent introducing a lower cut off similar to the resolution idea of equation (2.50). Furthermore the passage to hadrons invokes free scale dependent parameters which would require re tuning of parameters for every c.o.m [18]. The partons in the ME all carry color. For hadronization the need to be grouped to color neutral objects. This clearly limits the applicability of ME. On the other hand we know that the splitting kernels in the PS are only valid in the infrared regime and that they do not take interference effects into account. To gain more insight we compare the emission of an additional gluon in electron positron scattering in figure 2.9. The plot on the right side tells us that the impact of the interference terms is large

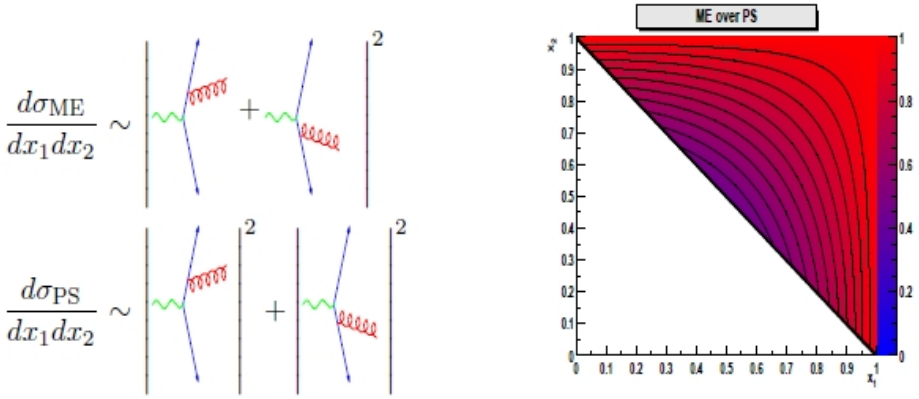

Figure 2.9: Pictorial representation of contributions to single gluon emission in $e + e- \to q\bar{q}g$ as given by the ME and the PS. As indicated, the PS does not take into account the interference contributions present in the ME. This leads to the ratio ME/PS as depicted in the contour plot. At the soft and collinear boundaries of the phase space in the $x_1 - x_2$ plane (where x_i corresponds to the energy fraction of the quark and antiquark) the PS correctly reproduces the ME, whereas in the region of hard gluon emission the PS omits the (destructive) interference contribution, taken from [18].

for hard emissions at large angles. While the edges of phase space are well described by the PS. For an accurate description of QCD events over the full phase space we need to merge ME with PS to generate n_{jet} exclusive events. There are different schemes to merge ME with the PS. Here we describe the CKKW scheme [17, 18, 28] in the following, another possibility would be the MLM scheme [19].

We describe the CKKW scheme [17, 18] as it is implemented in the Monte Carlo framework of SHERPA [34] as this is the software we use for all SM computations. First of all for the hadron collider case the k_T measure is slightly different from that for the e^+e^- collider used for the simple

[11] For the algorithms and techniques presented here we focus solely on LO ME.
[12] For the algorithms and techniques presented here we focus solely on LO ME.

examples above [34]:

$$Q_{ij}^2 = 2 \min\left(m_{T,i}^2, m_{T,j}^2\right) \frac{cosh(y_i - y_j) - cos(\Phi_i - \Phi_j)}{D^2}, \tag{2.53}$$

where D is a parameter of the jet algorithm of order one [34, 35] and m_T, y and Φ are transverse mass, rapidity and azimuthal angle. The main idea of the CKKW scheme is to separate the phase space in one part filled by ME calculations while the rest is filled by the PS [18, 34]. The two domains are divided by a cut value defined by the k_T measure $Q_{\text{cut}} > Q_{ij}$ [17, 18, 34] also called jet criterion. This differs from the usual k_T measure from [27] in that the transverse mass instead of the transverse momentum or energy is used[13]. The process then follows this sequence [34]:

1. The exact ME σ_k are calculated under the condition that the partons fulfill the jet criterion $Q_{\text{cut}} < Q_{ij}$. In addition the transverse momentum has to be larger than Q_{cut} which also sets the factorization (pdf's) and renormalization (α_S) scales in this first step. In the case where virtuality is chosen as variable this sets the matching scale t_{match}.

2. A process of fixed parton multiplicity is chosen with probability $\sigma_k / \sum_l \sigma_l$ fixing also the distribution of the particle momenta.

3. The parton configuration of the ME is clustered backwards with the jet criterion of equation (2.53) to obtain a shower history of the ME [17]. This is needed to set a starting scale for the PS. Also for each clustered parton Q_{ij} yields a value used for α_s at this node to reweight the ME. The clustering is stopped if a $2 \to 2$ or core process is reached. This process , also called hard process, sets the upper integration limit t_{hard}. This shower history is a pseudo shower configuration off which the event's evolution is properly continued by the PS.

4. The reweighting proceeds with the correct Sudakov factors from equation (2.46) according to the clustered shower history. Internal particle lines are reweighted with ratios of Sudakovs according to equation (2.51). Ensuring no at Q_{cut} resolvable branching occurred. Here Q_{cut} corresponds to t_{match} respectively t_0 or Q_0 in the formulas above[14].

5. The ME defines the hard parton emissions. In principle there could have been soft emissions on the internal lines of the ME before the emission of the hard external parton. But these soft emissions are coherent additional soft emissions of the cascade of partons yet to be produced by the parton shower. This means they rely on the color information of the hard parton but should not be generated before it and thus steal some of its energy fraction. Therefore a truncated shower is employed generating coherent soft emission [17, 36].

6. With the reweighted ME the PS is started at the scale determined by the shower history of step three. For the PS implemented in SHERPA the invariant mass of the mother particle gives the corresponding scale. If a splitting above the matching (t_{match}) respectively the cutting (Q_{cut}) scale is generated the hole event is vetoed to avoid double counting as this is already taken into account by the ME.

There are two further remarks necessary. To simulate a correct final state a hadronization model has to be added. Therefore the correct color configuration needs to be known. This is achieved by using color-flow decompositions of QCD amplitudes [17, 37]. Second the computation of ME is only practical up to a certain number of final state partons N. To fill the whole phase space correctly there is no PS veto for the highest multiplicity ME. In figure 2.10 a pictorial output of a SHERPA event is displayed. There one can observe how the PS evolves the partons from the core process.

[13] In [18] the measure also differs between final state partons and initial state partons. However the implementation in SHERPA [34] first uses only one kind of measure. Later in development a more abstract criterion is proposed [17].

[14] t_0 is used to denote the general stop of the PS at which non perturbative effects start to play an important role. As the merging uses the ME in one phase space domain we have to change t_0 or Q_0 to t_{match} or Q_{cut} in the formulas denoting the a priori arbitrary matching scale.

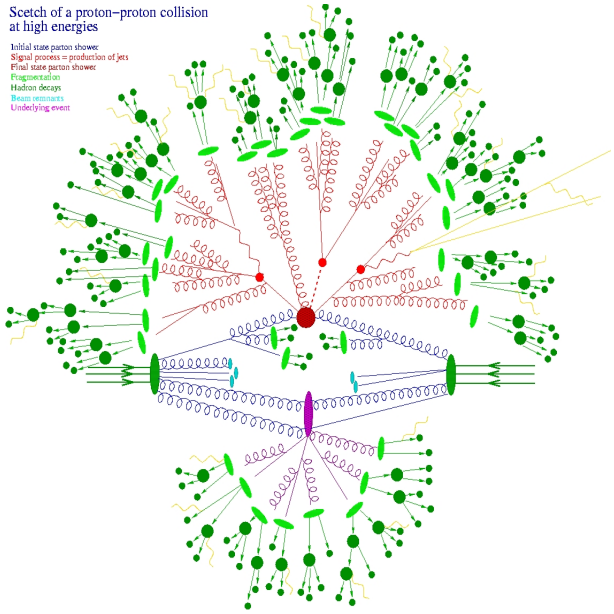

Figure 2.10: Pictorial display of a SHERPA event. The different colors denote different phases during event generation. The algorithm described in the text is responsible for the generation of the blue and the red parts. Other parts, for example the hadronization, are generated by non perturbative models. The decay of hadrons is computed with their measured branching ratios, taken from [38].

2.1.4 Connecting perturbative predictions with detectable observables

In principle we have everything to simulate an event at the LHC and compute the basic behavior of physical observables. Through the Feynman rules we can compute the perturbative SM or new physics processes we are interested in. Then we can decide if we wish to compute inclusive quantities including their higher order corrections or if we compute exclusive quantities staying on tree level but therefore getting information about the event topology. But there are still some issues we have to take care of. First we have to mention some further steps to a realistic simulation of an actual event in the detector. Then we have to find a way back to connect the measurable quantities in a detector to our theoretical concepts.

Hadronization and Detector simulation

Although we developed a picture how to describe perturbative QCD accurately this is not the most realistic picture. It enables us to compute observables and their distribution and is thus useful in understanding the concepts of nature, but still lacks the ability to tell us the particles and signatures we would observe in an actual experiment. Due to confinement we are not able to detect partons, but only color neutral hadrons. This fact of nature forced us to introduce the pdf's to describe the incoming partons correctly inside the protons we collide. But of course the same argument is true for the final state particles in the detector. After simulating an event on parton level we have to add an additional step which describes the transition from partons to hadrons. This can not be done by perturbative calculations and thus has to rely on so called hadronization models. Subsequent to the hadronization we have to decay the now physical particles according to their branching ratios as only few hadrons live long enough to be detected. A general overview can be found in [39].

This last step brings us to detectable stable particles. A further step would be a detector simulation, e.g. [42]. This is very important if we actually try to understand the signatures we observe and how they are connected to the physical process we are interested in. In such a simulation we would compute the respond and interaction of the different detector components to the particles we produce in our Monte Carlo simulation. Thus tracking down how the geometry and material of the detector influences the event signatures.

Jet algorithms

On detector level we measure energy deposits in the calorimeter cells over the whole spatial detector range. To assign them to well defined localized objects jet algorithms are applied. The idea of jet algorithms is that partons cause a collinear spray of hadrons. Thus we have to assign criteria to all the hadrons telling us if we should count them into a single jet. Doing so we also have to take care of the infrared divergence of QCD as we want the objects created by the jet algorithm to be not sensitive to this divergence to enable us to compare different algorithms as well as different experiments with different resolution and energy thresholds.

One approach to merge particles into jets are the so called cone algorithms. The basic idea is to collect all particles in some range of a hard particle giving the preferred direction of the cone. Thus those algorithms work with a seed given by the hardest particle. Unfortunately the do not fulfill the requirement of being infrared safe [35]. This requirement is important as we want the structure of the event to be independent of soft and collinear radiation we always expect at a hadron collider on an unpredictable footing. By infrared safe we mean that the algorithm should not only cancel infrared divergences but also be stable against addition of any soft or collinear particles. In figure 2.11 we show how the infrared properties of QCD can spoil the jet reconstruction.

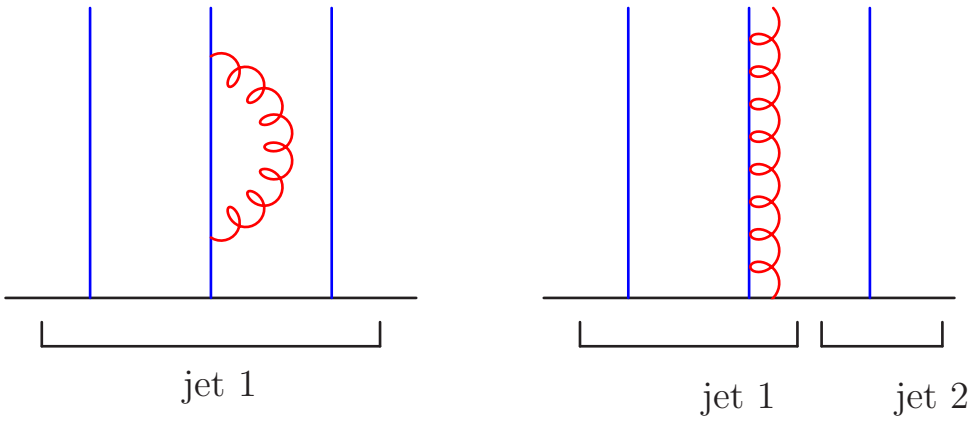

Figure 2.11: In perturbative calculations the loop divergence cancels with the infrared divergence yielding finite cross section predictions. Using a cone algorithm with a seed spoils this cancellation as processes which should be dealt with together get grouped into different jets.

There exists a cone approach for jet finding using no seeds which does not face the problem of being infrared unsafe. The so called SISCone [27] algorithm which is a seedless cone algorithm. It finds all stable cones without using a seed. If we now add a soft particle the number of hard cones will not change. Thus the set of hard cones is infrared safe. However, this algorithm faces computational problems like computing time and memory use [27].

Instead of using cones which are motivated by the idea that jets are a collimated spray of particles originating from one mother particle, e.g. a parton, sequential recombination algorithms use the branching picture we have developed to describe the parton shower. They recombine two objects on base of a distance measure. There are different infrared save jet algorithms, mainly the Cambridge Aachen(C/A), k_T and ANTI-k_T algorithm, using this technique. They differ basically

in the criterion applied as a distance measure between two reconstructed particles i and j:

$$\begin{aligned}
&k_T && y_{ij} = \frac{\Delta R_{ij}}{D}\min(p_{T,i}, p_{T,j}) && y_{iB} = p_{T,i} \\
&\text{C/A} && y_{ij} = \frac{\Delta R_{ij}}{D} && y_{iB} = 1 \\
&\text{anti-}k_T && y_{ij} = \frac{\Delta R_{ij}}{D}\min(p_{T,i}^{-1}, p_{T,j}^{-1}) && y_{iB} = p_{T,i}^{-1} \\
&\text{with} && \Delta R_{ij} = \sqrt{\Delta\eta_{ij}^2 + \Delta\Phi_{ij}^2}, && (2.54)
\end{aligned}$$

where η denotes the pseudo rapidity and Φ the azimuthal angle. These jet algorithms are indeed infrared safe. If we add a collinear branching this just gets recombined to the original particle.

A very detailed description of the here mentioned and other algorithms is given in [27]. Here we only show their general concept, following [28]. We assign all four vectors of our particles to so called proto-jets.

- For all combinations of two proto-jets in the event find the minimum $y^{\min} = \min(y_{ij}, y_{iB})$
- if $y^{\min} = y_{ij} < y_{\text{cut}}$ merge proto-jets i and j and add their momenta, go back to (1)
- if $y^{\min} = y_{iB} < y_{\text{cut}}$ remove proto-jet i, call it beam radiation, go back to (1)
- if $y^{\min} > y_{\text{cut}}$ keep all proto-jets, done

There is one subtlety connected with the merging of the four momenta. Usually we would set the invariant mass of our new proto-jet object to zero, inspired by the idea that we are looking for mass-less partons. We can also choose to keep all masses thus getting a jet mass [28].

Those well defined objects are the key to relate our perturbative QCD partons which are not detectable to measurable physical quantities. Therefore we take the following point of view. From section 2.1 we know that parton branching in the collinear regime is enhanced. Thus many QCD objects will propagate collimated around a vector approximately given by our perturbatively simulated partons. These then hadronize to form color singlets. The hadrons inherit the direction and collimation of the partons they combine to color singlets. In that way they deposit a large and localized amount of energy in the calorimeter as well as they produce collimated tracks in the detector. So in this sense we take the jets to be the objects carrying the information from our perturbative QCD partons.

2.1.5 Tools

As we are interested in the principal behavior of jets and the structure of multi-jet observables, we limit ourselves to simulate the events only on parton level. A full detector simulation needs a dedicated understanding of the detector itself and accurate data input to be reliably and is thus beyond our reach. Here we like to summarize the tools we use with respect to the considerations of the previous sections to achieve the results in the following chapters.

- To simulate all relevant standard model processes we use the SHERPA frame work [34]. It implements an improved CKKW approach [17] and efficiently computes high multiplicity matrix elements, thus supporting our aim to understand jets and their structure over the entire phase space region.
- As we use some SUSY benchmark points [47] as an example to see how the jet structure of new physics might differ from that of the standard model we need to reliably simulate their decay toward standard model particles. Given the right branching ratios the HERWIG++ [43] code automatically decays heavy particles and showers them consistently due to their color charge.
- Both simulation tools are able to generate the commonly used HEPMC [44] event record. The reconstruction of the jets is then done with the FASTJET [45] package providing us with several infrared save jet algorithms.

2.2 SUSY and Dark Matter

Although the SM describes many experiments very well, there are severe open issues not tackled down by the SM. From cosmological observations [1] we know that only 4.6% of the universe are made up from matter described by the SM. As is shown in figure 2.12 23% are made of Dark Matter and 72% consist of Dark Energy. This is a clear sign that there must be physics beyond the SM.

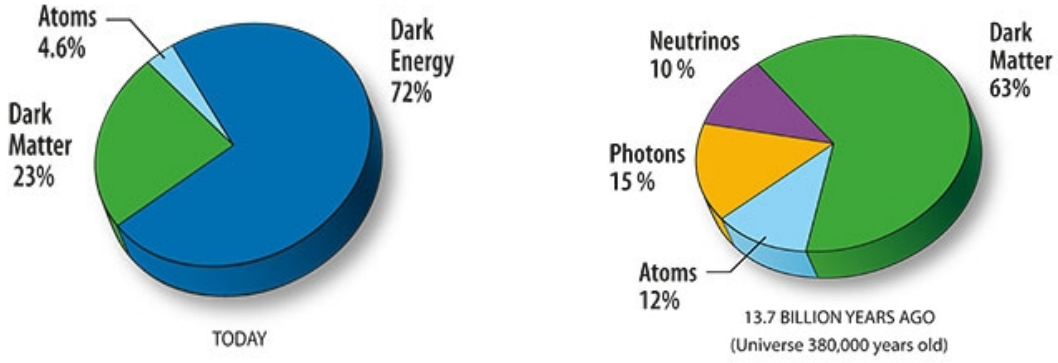

Figure 2.12: Energy content of the universe today and close to the BIG BANG. Most of the matter is not described by the SM , figure taken from [40].

Not only has the SM no dark matter candidate, there are also questions within the computational framework of the SM. If we compute the loop corrections to the Higgs propagator, see figure 2.13, we encounter quadratically divergent integrals dependent on the masses of the particles running in the loop. As these loops compute the correction for the Higgs mass the values of the masses must be fine tuned to achieve a reasonable mass correction.

As a solution to these severe problems supersymmetry (SUSY) is proposed [3]. The key idea of SUSY is to relate fermions and bosons through introduction of a new symmetry[15] assigning each boson a new fermionic partner as well as each fermion a new bosonic partner with the same quantum numbers[16]. Through the additional minus sign between fermion and boson loops the divergences are canceled, see figure 2.13. The SM itself can not be super symmetric, as for example the super partner of the photon would be a massless fermion of the SM. But even the lightest fermions, the neutrinos, are known to have some mass. Thus we have to assign each SM field

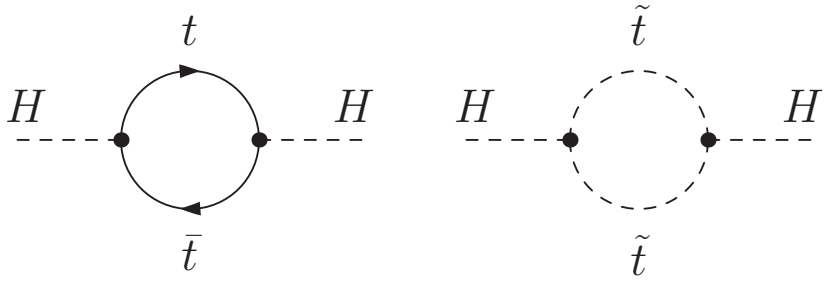

Figure 2.13: Quadratically divergent loop integral for the Higgs propagator due to a top loop and cancellation due to its SUSY partner $\tilde{t}$.

[15] Due to group theory reasons this symmetry needs fermionic operators. As algebras with fermionic operators are called "super" the symmetry described by those operators is called "super" symmetry.

[16] The scalar partners of the fermions are denoted with an s in front, e.g stop for the top quark partner, while the fermionic partners of the bosons get an into at their end denoting the partner of a gluon as gluino.

a supersymmetric partner merging them into a supermultiplet, in this way at least doubling the particle content as is shown in table 2.2 and 2.3 .

Names		Spin 0	Spin 1/2	$SU(3)_C,\ SU(2)_L,\ U(1)_Y$
squarks, quarks	Q	$(\tilde{u}_L\ \tilde{d}_L)$	$(u_L\ d_L)$	$(3,\ 2,\ \frac{1}{6})$
($\times$3 families)	$\bar{u}$	$\tilde{u}_R^*$	$u_R^\dagger$	$(\bar{3},\ 1,\ -\frac{2}{3})$
	$\bar{d}$	$\tilde{d}_R^*$	$d_R^\dagger$	$(\bar{3},\ 1,\ \frac{1}{3})$
sleptons, leptons	L	$(\tilde{\nu}\ \tilde{e}_L)$	$(\nu\ e_L)$	$(1,\ 2,\ -\frac{1}{2})$
($\times$3 families)	$\bar{e}$	$\tilde{e}_R^*$	$e_R^\dagger$	(1, 1, 1)
Higgs, higgsinos	H_u	$(H_u^+\ H_u^0)$	$(\tilde{H}_u^+\ \tilde{H}_u^0)$	$(1,\ 2,\ +\frac{1}{2})$
	H_d	$(H_d^0\ H_d^-)$	$(\tilde{H}_d^0\ \tilde{H}_d^-)$	$(1,\ 2,\ -\frac{1}{2})$

Table 2.2: Chiral supermultiplets and their charges under the SM gauge groups. The spin 0 fields are complex scalars and the spin 1/2 fields are left handed, two component WEYL fermions. The SUSY partners of the SM fields have the same quantum numbers except for their spin. Note that for electroweak symmetry breaking to work in the frame work of SUSY additional Higgs bosons are needed, taken from [3].

Names	Spin 1/2	Spin 1	$SU(3)_C,\ SU(2)_L,\ U(1)_Y)$
gluino, gluon	$\tilde{g}$	g	$(8,\ 1,\ 0)$
winos, W bosons	$\tilde{W}^\pm\ \tilde{W}^0$	$W^\pm\ W^0$	$(1,\ 3,\ 0)$
bino, B boson	$\tilde{B}^0$	B^0	$(1,\ 1,\ 0)$

Table 2.3: Gauge supermultiplets and their SM charges. The spin 1/2 fields are left handed, two component WEYL fermions and the spin 1 fields are real vector bosons, taken from [3].

We also can deduce that the particles emerging from SUSY have to be heavy. Were they light the particles and there interactions would have been observed by accelerator experiments for example at the Tevatron. One key motivation for SUSY is to cancel quadratic loop divergences by introducing particles with the *same* quantum numbers to avoid fine tuning. Having different masses spoils this cancellation. But we do not need this cancellation to be absolutely exact. The corrections to the Higgs mass just do not have to become too large. So different masses are OK as long as they are not too heavy compared to the masses in the SM. This makes SUSY a testable theory at the LHC. The heaviest SM particle is the top quark with a mass of around 170 GeV, so SUSY masses around the TeV scale are just the hierarchy we can allow for our particles nicely testable at LHC energies of 7 TeV respectively 14 TeV. The SUSY particles having different masses than the SM particles means also that SUSY can not be an exact symmetry at the weak scale. To describe this property we need to introduce symmetry breaking terms in our Lagrangian. These terms are explicitly not supersymmetric and introduce a high number of new free parameters. Thus if we only impose a broken supersymmetry we could not do many phenomenological predictions as we do not know the exact parameter point if SUSY is really a description of nature.

There is one prediction we can make for such a general ansatz as we have outlined until now. If we would just introduce super partners for the SM particles we would encounter a severe problem: proton decay. For example the diagram in figure 2.14 would decay the proton to a pion and a positron instantaneously. If SUSY is in any kind a description of nature we have to forbid such interactions. So called R or matter parity does the job. All SM particles are charged with $+1$ and all super partners with -1. At each vertex the R parity has to be conserved thus allowing interactions with two super partners and one SM particle, but never the other way around. In addition R parity forces the lightest SUSY particle to be stable (LSP). From the fact that we have not yet observed a charged stable SUSY particle we can deduce that this particle has to be neutral and can only interact weakly, therefore often called weakly interacting massive particle (WIMP). Such a WIMP is a perfect dark matter candidate. As it is weakly interacting the cross

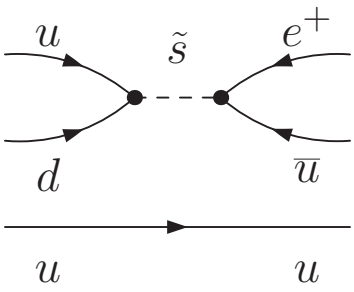

Figure 2.14: Interaction with a SUSY particle leading to proton decay $p \to \pi^0 + e^+$.

section for the direct production is not very high at the LHC. Here again R parity is of great help. For all the other supersymmetric particles exists only the possibility to decay to an other SUSY particle and a SM particle[17] to conserve R parity in the decay process. The heavier a particle is relative to the other SUSY particles the more possibilities are open for its decay. But in the end all the decay processes stop at the LSP. In figure 2.15 we show a typical decay chain for squark pair production. As squarks are colored particles they have a much larger production rate at the LHC than direct LSP production. Thus we can get observable rates for the WIMP dark matter candidate in SUSY although it is weakly interacting.

Asking only for a minimal set of requirements, namely broken SUSY with R parity, to have concordance with very basic observations, namely no light SUSY partners and stable protons, we can deduce the most generic signature for a SUSY event: missing energy from the LSP escaping the detector accompanied by decay jets plus the estimation that SUSY as a solution to the mentioned problems should be in the reach of the LHC.

The MSSM

One particular interesting model which then fulfills the requirements to be an extension of the SM is the so called Minimal Supersymmetric Standard Model (MSSM). It is minimal in the sense of the added extra particle content, but introduces many new parameters (124 in total) due to the implementation of SUSY breaking [3]. We impose the SUSY condition for the field content of the Lagrangian. But as we still have to full fill all the mechanisms imposed in the SM we have to work out the actual mass eigenstates of the theory. As is familiar from the weak gauge bosons these are a mixture of the gauge eigen states and listed in table 2.4.

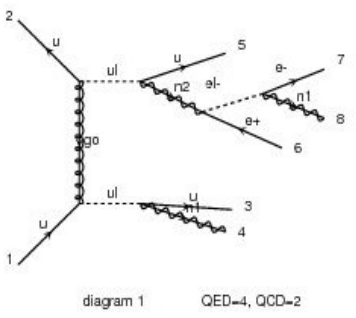

Figure 2.15: Decay chain for sparticles to neutralino with decay jets, generated with MADGRAPH [46].

[17] As the SUSY particles have the same quantum numbers as the SM particles they also share the same interactions allowing them to decays.

Names	Spin	P_R	Gauge Eigenstates	Mass Eigenstates
Higgs bosons	0	+1	$H_u^0\ H_d^0\ H_u^+\ H_d^-$	$h^0\ H^0\ A^0\ H^\pm$
squarks	0	−1	$\tilde{u}_L\ \tilde{u}_R\ \tilde{d}_L\ \tilde{d}_R$	(same)
			$\tilde{s}_L\ \tilde{u}_R\ \tilde{d}_L\ \tilde{d}_R$	(same)
			$\tilde{t}_L\ \tilde{u}_R\ \tilde{d}_L\ \tilde{d}_R$	$\tilde{t}_1\ \tilde{t}_2\ \tilde{b}_1\ \tilde{b}_2$
sleptons	0	−1	$\tilde{e}_L\ \tilde{e}_R\ \tilde{\nu}_e$	(same)
			$\tilde{\mu}_L\ \tilde{\mu}_R\ \tilde{\nu}_\mu$	(same)
			$\tilde{\tau}_L\ \tilde{\tau}_R\ \tilde{\nu}_\tau$	$\tilde{\tau}_1\ \tilde{\tau}_2\ \tilde{\nu}_\tau$
neutralinos	1/2	−1	$\tilde{B}^0\ \tilde{W}^0\ \tilde{H}_u^0\ \tilde{H}_d^0$	$\tilde{N}_1\ \tilde{N}_2\ \tilde{N}_3\ \tilde{N}_4$
charginos	1/2	−1	$\tilde{W}^\pm\ \tilde{H}_u^+\ \tilde{H}_d^-$	$\tilde{C}_1^\pm\ \tilde{C}_2^\pm$
gluino	1/2	−1	$\tilde{g}$	(same)
goldstino	1/2	−1	$\tilde{G}$	(same)
(gravitino)	3/2			

Table 2.4: Sparticle content of the MSSM . The mass eigenstates arise due to a mixing of the gauge eigenstates. Thus providing us through N_1 with dark matter candidate, taken from [3].

Until now we have not addressed what we mean by SUSY to be broken at the weak scale. We just imposed it as a condition to meet the requirement of heavy SUSY particles. To be more than an effective Lagrangian with the right particle content SUSY must be an exact symmetry at some higher scale, usually referred to as GUT scale[18], as the electroweak symmetry is before breaking at the weak scale. The breaking mechanism for the SM is the Higgs mechanism giving rise to the different masses in the SM. Indeed there are also dynamical breaking mechanisms for SUSY. In the mSUGRA (minimal super gravity) frame work SUSY breaking is mediated by gravity [3]. That reduces the number of parameters to five as shown in table 2.5. These five high scale parameters are than evolved by a renormalization group equation (RGE), similar, but more complex, to the equation for the running coupling in the SM. In figure 2.16 we show the evolution of different SUSY parameters if we impose typical mSUGRA motivated boundary conditions.

$m_{1/2}$	Gluino mass
m_0	Scalar mass
A_0	Soft breaking trilinear coupling constant
$\tan\beta$	Ratio of the two Higgs VEV's
$\text{sign}(\mu)$	Sign of the higgsino mass parameter

Table 2.5: mSUGRA parameters at the GUT scale. The notion gluino mass for $m_{1/2}$ may be miss leading. It is meant that this parameter drives mainly the evolution of the gluino mass. This table is not to be taken as a one to one correspondence but rather to outline the influence of the parameter choice on the spectrum.

The parameter space of mSUGRA is still five dimensional and thus very large. For better comparison and easier handling so called snowmass benchmark points have been introduced [47] to collect typical parts of the SUSY parameter space and their spectra. In figure 2.17 we show two possible choices known as SPS1a and SPS4 benchmark points. The specific parameter values are shown in table 2.6. These choices show how rich and different the collider signatures for

[18] GUT is a short form of grand unified theory. Those theories aim at unifying all forces in nature, something not achieved by the SM. However, the SM contains through its RGE for the running couplings a hint at which scale this theory should life. It is clearly higher than the electroweak scale of the SM $O(TeV)$, but should still be much smaller than the Planck scale of $O(10^{16}TeV)$.

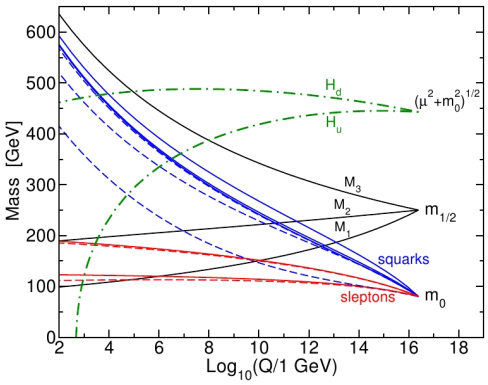

Figure 2.16: RGE flow to the weak scale. Each sparticle has its own running mass equation, thus giving rise to a phenomenological rich sparticle spectrum starting from only five parameters. Here we see the actual evolution of the masses due to mSUGRA inspired boundary conditions, taken from [3].

Parameter	SPS1a	SPS4
$m_{1/2}$	$250GeV$	$300GeV$
m_0	$100GeV$	$400GeV$
A_0	$-100GeV$	0
$\tan\beta$	10	50
sign(μ)	+	+

Table 2.6: Specific parameter choice in the mSUGRA parameter space for the SPS1a and SPS4 benchmark as introduced in [47].

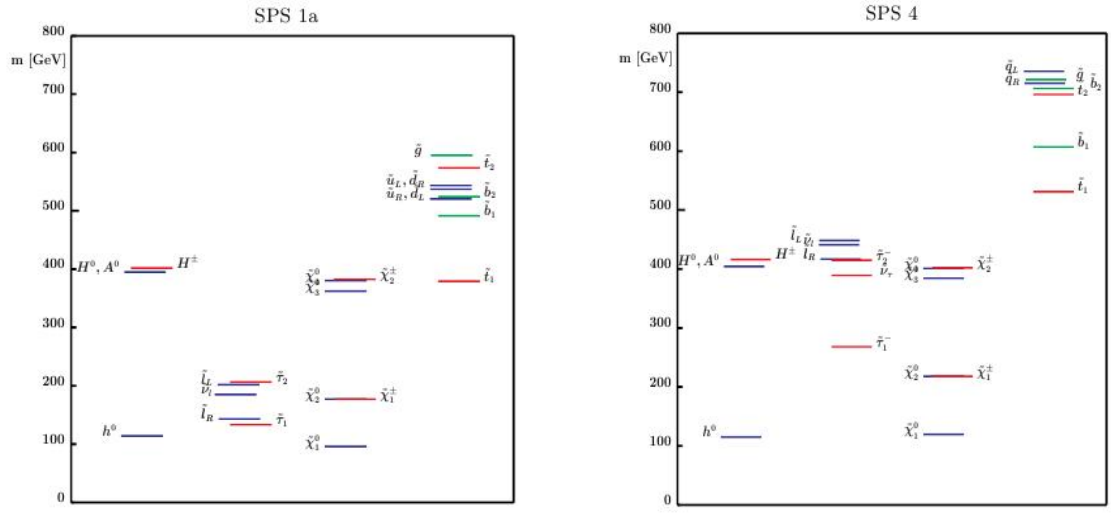

Figure 2.17: Particle spectrum of the SPS1a and SPS4 benchmark points. Note the inversion in the mass relations between gluinos and squarks as well as the shift for the sleptons, taken from [47]

SUSY can still be although we narrowed the parameter space to five parameters by making explicit assumption on the SUSY breaking mechanism. For example by going from the SPS1a choice to SPS4 we flip the mass hierarchy of the squarks with respect to the gluinos. Thus getting different decay structures for those two choices. As the parameter space is very large there are many ways how SUSY could be realized[19]. This makes it difficult to use spectrum specific search strategies to search for SUSY signals. A point we address in the next section and in chapter 4 in more detail.

[19] Also mSUGRA is not the only way to impose dynamical symmetry breaking.

2.3 Why to consider backgrounds

With the material of the previous sections we could develop a strategy to search for a SUSY signal at the LHC. One search strategy which we like to refer to as spectrum specific strategy would take a certain set of parameters of the new physics model one has in mind. This could be for example the SPS1a benchmark point for the MSSM introduced in the previous section. We then take a set of observables whose distributions are sensitive to the new physics we are searching for. On these observables we define a set of cuts, for example on the p_T of certain jets, and tune these cuts to suppress the SM backgrounds without killing our signal. The quantity of interest in such a strategy is the ratio of expected signal over expected background S/B. If we can tune our cuts maximizing this quantity we can claim discovery if our statistics are high enough to make sure that the excess we observe is unlikely to come from a fluctuation of the background.

This point is also a problem of this ansatz. If we suppress the background very strong small fluctuations can have a huge impact on S/B. Furthermore by choosing very restrictive cuts to enhance S/B we also force the signal as well as the background events to lie in very specific phase space regions. This may lead to sculpting of the signal and background distributions. But there is also another point related to the idea of a new physics search. In principle we do know nothing about the phenomena which might or might not occur at the LHC. Thus we can by no means rely on the parameter point we chose for the spectrum specific strategy. Even if we are using the correct physics model in general we miss the correct parameter point. But this spoils our cut optimization to enhance S/B. Thus a spectrum specific search only can be one step in the line of analysis toward a more dedicated understanding of the new physics.

We propose an inclusive analysis as possible starting point of such a line. The set up of such an strategy should have very generic cuts based only on the main features of the new physics we have in mind. For SUSY this would be the missing energy plus jets signature we motivated in section 2.2. Such an analysis strategy should provide us also with some generic information about the new physics thus preparing the ground for more dedicated analysis. Once we only impose generic cuts we have to face huge backgrounds dominating our samples. If we want to make any statement about new physics we have to reliably predict these backgrounds with simulation tools. That we are able to do so we show in the following chapter 3 about staircase scaling a feature observed in many SM processes at the LHC. Then we use this knowledge to set up the above mentioned inclusive analysis strategy in chapter 4. This analysis enables us to get information on some generic properties thus being qualified to produce the input for more dedicated analysis at the LHC.

Chapter 3

Deciphering Scaling Properties

3.1 Jet number scaling in SM backgrounds

As explained in section 2.2 jets are one of the very generic features of SUSY models with a dark matter candidate. Usually new physics searches use specific cuts tuned to one of these spectra to reduce the background and enhance the signal as was outlined in section 2.3. The events surviving these cuts mostly lie in very particular phase space regions. A consequence of this is that we are faced with huge uncertainties of the backgrounds in these regions as well as a sculpting of the signal itself. If we like to broaden our search strategies to larger regions in phase space we are faced with overwhelmingly large backgrounds. To extrapolate any new physics signal we have to understand the shape of the backgrounds we are faced with. On the other hand the parameter space and the number of possible spectra is very large. Additional to this there are also other theoretical ideas predicting new particles around the TeV scale together with a dark matter candidate [4]. Therefore we can not hope to pick as a first step just the right benchmark point and use it to tune cuts to discover a new physics signal. We need to find evidence for the new physics through deviations in the backgrounds predicted to be described by the SM. Thus it is very important to understand the jet structure of SM backgrounds.

There are mainly two kinds of structure which we could exploit to understand the structure of the number of jets for a given process. For QED we know that for successive photon radiation we observe Poisson scaling [20]. The Sudakov form factor from section 2.1 suggests the same for a single quark line radiating gluons which do not split any further. Poisson scaling is well known and understood in its probabilistic picture from the p_T ordered re summation of radiated soft photons from charged particles in QED interactions. The probability to radiate n photons is given by [20]

$$\begin{aligned} P(n) &= \frac{\lambda^n}{n!} exp(-\lambda) \\ \text{thus} \quad \langle n \rangle &= \lambda, \end{aligned} \tag{3.1}$$

where λ is obtained from the re summation of virtual and unresolvable real photons below some energy threshold and is the expected number of radiated particles. When we talk from scaling properties we mean the behavior of ratios of cross sections, thus

$$R_{\frac{n+1}{n}} = \frac{\sigma_{n+1}}{\sigma_n} = \frac{P(n+1)}{P(n)} = \frac{\lambda}{n+1}. \tag{3.2}$$

Poisson scaling is present in SM backgrounds for example in Higgs searches after cuts for two tagging jets have been asked for [48]. However, the picture for events involving more QCD jets may be more complicated and cannot easily be described by a single line radiating gluons as those gluons can split again to gluons or quarks spoiling the naive estimate of Poisson scaling. Indeed we observe the so called staircase scaling in W,Z plus jets as well as in pure QCD jet events [16,60], defined as

$$R_0 = R_{\frac{n+1}{n}} = \frac{\sigma_{n+1}}{\sigma_n} \quad \forall\ n. \tag{3.3}$$

The theoretical foundation of staircase scaling is not fully understood. Nonetheless, there is no doubt that this feature exists in data [16], which is, on the other hand, well-reproduced by state of the art Monte Carlo codes, which include matching procedures based on the CKKW [17, 18] or MLM [19] schemes. By construction, Poisson-like jet multiplicities are present for QCD in the abelian limit $C_A \to 0$.

As experiment [16] and Monte Carlo studies [15] tell us that staircase scaling is a matter of fact we study its properties in W,Z plus jets as well as QCD jets under the assumption of some very generic cuts typical for inclusive searches for new physics as described in section 2.3

$$\not{E}_T > 100\ GeV \qquad \text{lepton veto: } p_{T,\ \text{lepton}} > 20\ GeV. \tag{3.4}$$

These cuts reduce the backgrounds to a manageable level without constraining the studied phase space to specific regions as for example the spectrum optimized searches do.

To separate new physics events from a QCD sample after some very basic cuts we have to understand the number of jets and their energy or p_T spectra. Our maximally inclusive approach means that aside from the fiducial volume of the detectors all we fix is the algorithmic jet definition to count a jet toward each of the two measurements. Throughout the rest of this section we define jets using the anti-k_T algorithm [62] in FastJet [45] with a resolution $R_{\text{anti}-k_T} = 0.4$ and then require

$$p_{T,j} > \ p_{T,\min} = 50\ \ \text{GeV} \qquad \text{and} \qquad |y_j| < 4.5\ . \tag{3.5}$$

This defines which jets are counted toward n_{jets} as well as the m_{eff} distribution.

Before we can use the n_{jets} distribution to extract new physics in chapter 4 we need to show that we understand this distribution in detail. Obviously, the overall normalization of this distribution is not critical. For any kind of new physics not completely ruled out by the Tevatron experiments the two jet and three jet bins are practically signal free. So the question becomes: what can we say about the shape of $d\sigma/d\ n_{\text{jets}}$.

For W+jets events this kind of distribution has been studied, even at the LHC [60]. We observe the *staircase scaling* [58, 63], an exponential drop in the inclusive n_{jets} rates with constant ratios $\hat{\sigma}_{n+1}/\hat{\sigma}_n$. The numerical value of this ratio is obviously strongly dependent on $p_{T,\min}$. The original staircase scaling describes inclusive jet rates, i.e. it uses $\hat{\sigma}_n$ including all events with at least n jets fulfilling Eq.(3.5). Here we use exclusive jet rates, i.e. counting only events with exactly n jets fulfilling equation (3.5) toward σ_n. This preserves the normalization of the n_{jets} histogram as $\sigma_{\text{tot}} = \sum_n \sigma_n$ and makes it possible to add the bins in the computation of log-likelihood analysis. It is interesting to note that staircase scaling defined either way implies staircase scaling using the other definition, and that the jet-production ratios of the two approaches are identical. If we define the universal exclusive staircase-scaling factor as

$$R \equiv R_{(n+1)/n} = \frac{\sigma_{n+1}}{\sigma_n}\ , \tag{3.6}$$

we find for the usual inclusive scaling denoted by a hat over all parameters

$$\begin{aligned}
\hat{R} \equiv \frac{\hat{\sigma}_{n+1}}{\hat{\sigma}_n} = \frac{\sum_{j=n+1}\sigma_j}{\sigma_n + \sum_{j=n+1}\sigma_j} &= \frac{(\sigma_{n+1} + \sigma_{n+1}\frac{\sigma_{n+2}}{\sigma_{n+1}} + \ldots)}{\sigma_n + (\sigma_{n+1} + \sigma_{n+1}\frac{\sigma_{n+2}}{\sigma_{n+1}} + \ldots)} \\
&= \frac{\sigma_{n+1}\sum_{j=0}^{\infty} R^j}{\sigma_n + \sigma_{n+1}\sum_{j=0}^{\infty} R^j} = \frac{\dfrac{R\sigma_n}{1-R}}{\sigma_n + \dfrac{R\sigma_n}{1-R}} \\
&= \frac{R\sigma_n}{(1-R)\sigma_n + R\sigma_n} = R\ .
\end{aligned} \tag{3.7}$$

The same relation we find when we include a finite upper limit to the number of jets in the sum over j. Note, however, that this argument only holds for a strict staircase scaling where the ratio $R_{(n+1)/n}$ does not depend on the number of jets n. But in that case it means that the merits of perturbative QCD generalize to a fully jet-exclusive final state with a perturbatively well-defined approach to higher order corrections while lower multiplicities can be utilized to constrain the higher ones in a phenomenological approach once staircase scaling is in place.

In this section we will show that (1) such a scaling exists not only for W/Z+jets but also for pure QCD events and (2) we can reliably estimate the scaling factor and possible deviations from it from theory. A purely data-driven background analysis of this distribution might be possible and should be combined with our results. For example, we can one by one remove the missing energy cut and the lepton veto in Eq.(4.1) which gives us background dominated event samples

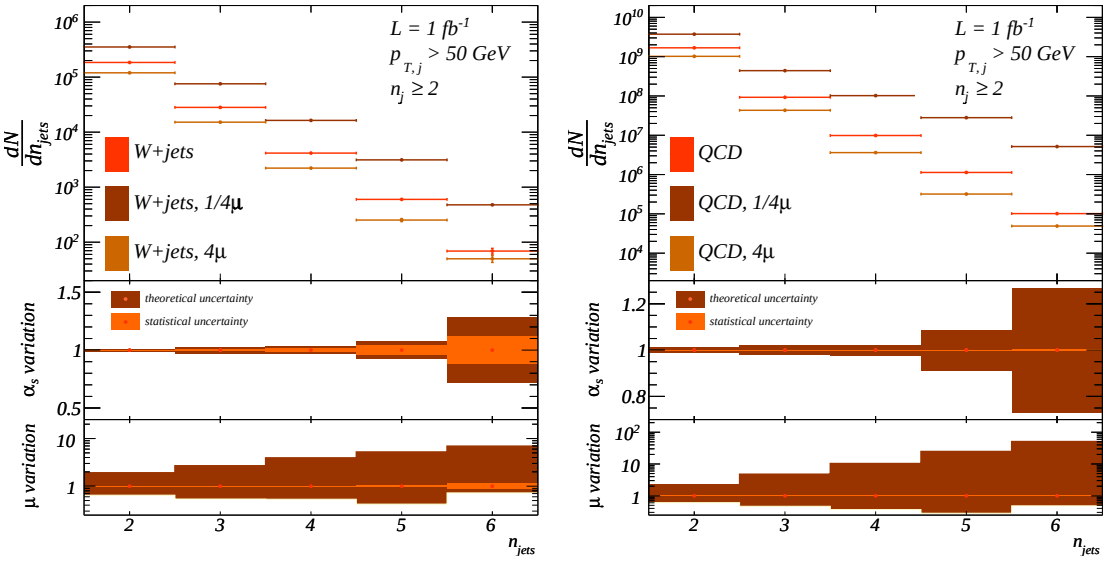

Figure 3.1: Exclusive $d\sigma/d\ n_{\text{jets}}$ distribution for W+jets (left) and QCD jets production at the LHC. Only the jet cuts given in Eq.(3.5) are applied, neither a $\not{E}_T$ cut nor a lepton veto is imposed. The second panel shows the parametric uncertainty due to a consistent change of $\alpha_s(m_Z)$ between 0.114 and 0.122. The third panel shows the reach of a consistent scale factor treatment which can be experimentally determined and should not be considered a theory uncertainty.

to a reasonably large number of hard jets. Adding the background rejection cuts will then have an impact on the scaling, which we can estimate reliably. For the signal hypothesis we have to entirely rely on QCD predictions.

As a starting point we discuss the established staircase scaling in W+jets production. The behavior of Z+jets is exactly the same. For our analysis we produce CKKW-matched [17] background samples for W+jets (to 5 ME jets), Z+jets (to 5 ME jets), $t\bar{t}$+jets (to 2 ME jets), and QCD jets (to 6 ME jets) with SHERPA-1.2.3 [34][1]. Higher order corrections to the inclusive scaling we expect to, if anything, improve the assumption of a constant jet ratio $\hat{R}$ for example in W+jets production [64]. To achieve numerical stable results for the pure QCD case we simulate up to 80M events.

In the left panel of Figure 3.1 we show the exclusive n_{jets} distribution for the LHC running at 7 TeV center of mass energy. To increase our statistics to large enough values of n_{jets} we do not apply the selection cuts Eq.(4.1) in this first step. We already see that we can qualitatively fit a line through the central points on a logarithmic axis for each set of input parameters.

Before we quantitatively evaluate this scaling we need to consider the uncertainties associated with our simulation. This is crucial if we want to use the n_{jets} scaling as a background estimate for new physics searches in QCD final states. There are two distinct sources of uncertainty in our simulation. First, there exists a parametric uncertainty, namely the input value of $\alpha_s(m_Z)$ or some other reference scale. To address this, we consistently evaluate the parton densities around the central NLO value $\alpha_s(m_Z) = 0.118$ inside a window $0.114 - 0.122$ [65] and keep this value for all other appearances of the strong coupling in our matrix-element plus parton-shower Monte-Carlo simulations. In Figure 3.1 we see that the resulting error bar on the $d\sigma/d\ n_{\text{jets}}$ increases with the number of jets, but stays below 30% even for the radiation of six jets. For luminosities around 1 fb^{-1} the error on α_s is roughly of the same order as the experimental statistical error. Systematic errors we do not consider, even though they will at some point dominate over the statistical errors. After any kind of realistic background rejection the combined experimental error will exceed the parametric α_s uncertainty.

The reason why we cannot use staircase scaling in W+jets to measure α_s is a second source of QCD uncertainty: aside from the parametric α_s error band, an actually free parameter in

[1] The number of used matrix elements (ME) in the simulation corresponds to the highest multiplicity treatment mentioned in section 2.1.3.

channel (cuts)	$R_{2/1}$	$R_{3/2}$	$R_{4/3}$	$R_{5/4}$	$R_{6/5}$	$R_{7/6}$	R_0	$\frac{dR}{d\ n_{\text{jets}}}$
	SHERPA simulation						linear fit	
W+jets ($p_{T,j} > 50$ GeV)	0.1931(3)	0.1494(5)	0.157(1)	0.138(3)	0.115(8)	0.09(2)	0.150(1)	−0.001(1)
W+jets (+ lepton veto)	0.2290(4)	0.1494(7)	0.164(2)	0.139(4)	0.12(1)	0.09(2)	0.149(1)	−0.002(1)
W+jets (+ $\not{E}_T > 100$ GeV)	0.252(1)	0.224(2)	0.190(5)	0.16(1)	0.15(2)	0.09(4)	0.239(3)	−0.032(3)
Z+jets ($p_{T,j} > 50$ GeV)	0.1463(2)	0.1504(6)	0.147(1)	0.138(4)	0.123(9)	0.07(2)	0.154(1)	−0.006(1)
Z+jets (+ $\not{E}_T > 100$ GeV)	0.2251(6)	0.185(1)	0.166(3)	0.154(6)	0.14(1)	0.08(3)	0.193(2)	−0.018(2)
QCD jets ($p_{T,j} > 50$ GeV)	—	0.0552(1)	0.1074(5)	0.106(1)	0.125(5)	0.12(1)	0.105(2)	0.001(1)
$(t\bar{t})_{hh}$+jets ($p_{T,j} > 50$ GeV)	3.69(9)	1.26(2)	0.67(1)	0.366(9)	0.24(1)	0.15(5)		
$(t\bar{t})_{\ell\ell/h}$+jets ($p_{T,j} > 50$ GeV)	1.96(2)	0.851(7)	0.465(5)	0.260(5)	0.168(8)	0.12(2)		
$(t\bar{t})_{\ell\ell/h}$+jets (+ lepton veto)	1.75(2)	0.765(10)	0.391(7)	0.228(8)	0.14(1)	0.12(3)		
$(t\bar{t})_{\ell\ell/h}$+jets (+ $\not{E}_T > 100$ GeV)	1.60(5)	0.83(2)	0.49(2)	0.25(2)	0.15(2)	0.19(7)		

Table 3.1: Jet ratios for all Standard Model channels, including (semi-)leptonic and hadronic top pairs for the central scale choice $\mu = \mu_0$. The quoted errors are statistical errors from the Monte Carlo simulation. The numbers correspond to the curves shown in Figures 3.1 and 3.2.

our QCD simulation is a common scaling factor μ/μ_0 in all appearances of the factorization and renormalization scales, including the starting scale of the parton shower. Identifying all scales follows the experimental extraction of the parton densities and α_s in a simultaneous fit. The interpretation of DGLAP splitting in terms of large logarithms tells us that the factorization and renormalization scales have to be identified with the transverse momentum of the radiated jets. By definition, such leading-logarithm considerations leave open the proportionality factor in the relation $\mu \propto |p_{T,j}|$. Any constant factor can be separated from the dangerous logarithm as a non-leading constant value.

Because this constant cannot be derived from first principles we vary it in the range $\mu/\mu_0 = 1/4 - 4$ and show the numerical result in Figure 3.1. As expected, the variation of the jet rates with this scaling parameter is huge — much larger than the experimental uncertainties we expect from the LHC and which we know from the Tevatron. In Figure 3.1 we can first of all check that introducing such a scaling factor does not seriously impact the observed staircase scaling. Counting such a constant toward the theory uncertainty is questionable if we can determine it experimentally. For example for SHERPA we know from Tevatron that the scaling factor should essentially be unity [66], which in the spirit of Monte-Carlo tuning means that for example in SHERPA the naive default parameter choice comes out as correctly describing the data. Of course, this does not have to be true for other simulation tools. An interesting question to ask once we have access to it at the LHC would be if this *per se* free parameter really is the same for different channels, like W/Z+jets and QCD jets.

In the right panel of Figure 3.1 we show the same distributions for pure QCD jet production. Again, not applying the cuts in Eq.(4.1) we observe staircase scaling, however, with some caveats for the two and three jet bins. This is related to the definition of the hard process. The two jet processes is for kinematic reasons always back to back. Thus it passes always the jet criterion for the ME in SHERPA . This might be not the case for a three jet ME. Thus giving the two jet bin a higher rate.

As expected, the scale factor μ/μ_0 has very large impact not on the existence of a staircase scaling but on the jet ratio R. The parametric uncertainty due to the error bar on $\alpha_s(m_Z)$ is again small once we vary the strong coupling consistently everywhere, staying below 30% for up to six jets. The parametric uncertainty for the pure QCD case and the W+jets case is clearly very similar. The scale factor variation $\mu/\mu_0 = 1/4 - 4$ gives an even larger band of possible ratios of cross sections, to be contrasted with a reduced statistical uncertainty compared to the W+jets case. Our argument that this over-all scale factor should be determined experimentally is therefore even more applicable for the QCD case. To date such an analysis does not exist, so while in the following we will use unity as the appropriate scale factor for SHERPA this needs to be verified experimentally. But concerning the comparison with Tevatron [66] we expect it too be a good estimate.

Once we understand the size of theory uncertainties for the exclusive $d\sigma/d\ n_{\text{jets}}$ distribution we need to quantify the quality of the observed staircase scaling. Since the quantitative outcome will depend on the background rejection cuts we apply, we study the scaling without the cuts shown

in Eq.(4.1), after the lepton veto only, and including the lepton veto as well as the missing energy cut. Starting from the individual $R_{(n+1)/n}$ values we fit a line through all relevant data points, as a function of n_{jets}

$$R(\ n_{\text{jets}}) = R_0 + \frac{dR}{d\ n_{\text{jets}}}\ \ n_{\text{jets}}\ , \tag{3.8}$$

and determine the slope to compare it to our prediction $dR/d\ n_{\text{jets}} = 0$.

In Table 3.1 we list the exclusive jet ratios as shown in Figure 3.1. For the W/Z+jets case we see that the radiation of one compared to a second jet off the Drell-Yan process $R_{2/1}$ does not show this scaling. The reason for this specific feature is the definition of the hard core process alluded to before. To generate the relatively hard jets and the large missing energy mimicking the signal events we need to at least consider W/Z+1 jet as the core process. In addition, we do not take into account any separation criterion between the first jet and the gauge boson, which means we treat σ_1 different from all other σ_n. In Table 3.1 we see that we are lucky for the Z+jets case, but we are not for the W+jets case. The tricky definition of the hard process σ_1 as the base of additional jet radiation suggests that we start our staircase scaling analysis with $R_{3/2}$.

The statistical uncertainties which we show in Table 3.1 and which enter the fit of the slope as defined in Eq.(3.8) always increase toward larger jet multiplicity. This is an effect of the way we simulate these events which completely corresponds to an experimental analysis. If we generate (or measure) all n_{jets} bins in parallel the first bin will always have by far the smallest error. Therefore, it determines the constant scaling factor R_0 in our fit as well as in a measurement. For larger values of n_{jets} we become statistics dominated, which means that Monte Carlo simulations can extend the reach of actual measurements at any given point in time toward larger jet multiplicities. This is the phase space region in which we need to provide new physics searches at the LHC with accurate background estimates.

Some of the rows listed in Table 3.1 we also depict in Figure 3.2. For electroweak gauge boson production we see that without any cuts W and Z production show the same scaling parameter R_0 as well as a small negative slope. Within errors the staircase scaling holds to six and possibly seven jets, even though we see a slight slope developing toward larger numbers of jets. This is a phase space effect which is expected once we start probing gluon parton densities and their sharp drop toward larger parton momentum fractions and which is well modeled by our computation.

Adding the lepton veto does not change the staircase scaling at all. This means that forcing the W boson to decay into one fairly soft lepton and a harder neutrino does not affect the behavior of the recoiling jets. Adding a significant $\not{E}_T$ cut, on the other hand, has a measurable effect on the jet ratios as well as on the slope. For experimental applications of this scaling, however, it is important to note that the phase space effects for large n_{jets} as well as the effect of kinematic cuts are completely described by our simulation.

For pure QCD events we find a remarkable agreement with the staircase scaling hypothesis, which seems to be supported by recent LHC analysis [16]. The definition of the hard core process is somewhat problematic since there exists no inherent hard scale in the $2 \to 2$ process and the

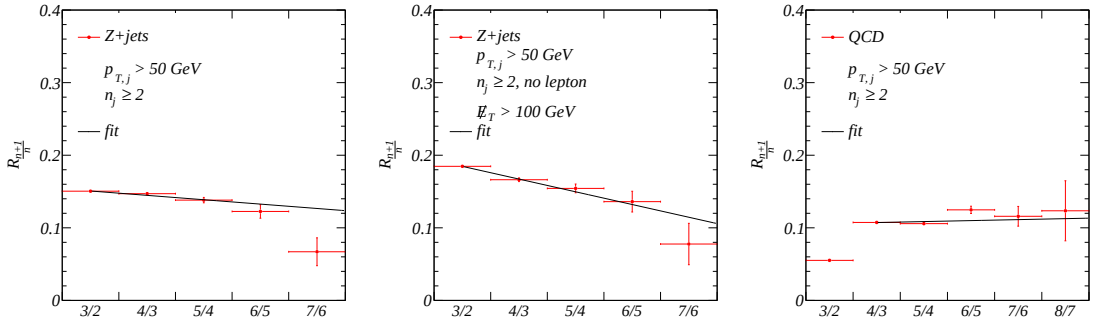

Figure 3.2: Jet ratios for Z+jets production (without and with the $\not{E}_T > 100$ GeV cut) and QCD jets production, corresponding to the numbers listed in Table 3.1. The error bars indicate the remaining Monte Carlo uncertainty in our simulation.

infrared behavior of s-channel and t-channel diagrams is very different. Therefore, we define σ_3 as the starting point of our analysis and $R_{4/3}$ as the first relevant cross section ratio. Table 3.1 and Figure 3.2 show that the ratios $R_{(n+1)/n}$ are essentially constant to eight jets. The slope within statistical uncertainties is, in contrast to W/Z production, fully compatible with zero. The central R_0 values for W/Z+jets and QCD jets production are slightly different, which is expected by the different core processes and by the different background rejection cuts.

3.2 Using photon plus jets as a testing lab

We like to study the staircase scaling in more detail. While we are not able to derive it from first principals we can figure out for which particle configurations we expect staircase scaling and how these differ from the Poisson case.

A prominent channel to test these expectations is photon plus jets production as we put forward in this section. The total cross section which we compute to be $\sigma = 10410.6 \pm 329.152\ pb$ at LO is large enough to already by now have large enough data[2] sets that do not only allow us to perform MC validation, but also put us into a position to experimentally comment on potential staircase scaling in photon plus jets production with a fairly small statistical uncertainty. This way, as we show, we can use different kinematic regimes of the photon to test various theoretical hypotheses of QCD radiation against actual data.

At first glimpse photon plus jets does not posses any particular scaling behavior which falls into either the Poissonian or staircase like category. This is probably also the reason why, to our knowledge, nobody has tried to study a potential staircase behavior in photon plus jets production until now. In section 3.3 we show that staircase scaling is realized if non-photon plus jet like events are singled out from the event sample. This amounts to a situation very similar to the one encountered in case of the production of a massive electroweak gauge boson in association with jets.

For the definition of jets in the following sections we use an anti-k_T algorithm implemented for example in FastJet [45] with a resolution of $R_{\text{resolve}} = 0.4$. When dealing with photons in a QCD environment there arise some subtleties familiar from perturbative calculations [49]. A photon can arise from a non-perturbative fragmentation process whose minimization requires isolation. Naive isolation in terms of a hard cut on, e.g., the jet photon distance in the azimuthal angles pseudo rapidity plane limits the phase space of soft gluon emission and is infrared unsafe. In our approach we use the Frixione isolation criterion [49]. We define such a photon candidate to be identified as a photon when the hadronic energy deposit in a cone of size $R_{\text{separation}} < 0.4$ around the photon is smaller than 10% of the photon candidate's transverse momentum. The separation $R_{\text{separation}}$ we compute with

$$R = \sqrt{\Delta\eta^2 + \Delta\Phi^2} \tag{3.9}$$

from pseudo rapidity η and polar angle Φ. If this criterion is not met the photon candidate is pushed into the jet finding algorithm. We apply photon and jet cuts

$$p_T^\gamma \geq 50\ \text{GeV},\ |\eta_\gamma| \leq 2.5 \qquad p_T^j \geq 50\ \text{GeV},\ |y_j| \leq 4.5\,, \tag{3.10}$$

where y denotes rapidity, respectively. For our computation we take only the hardest produced photon into account. If further separated photons are produced they are ignored[3]. For the simulation underlying this study we use Sherpa v1.3.0 [34] and perform Ckkw matching up to 5 matrix element jets. To achieve accurate enough predictions we produce 130M events.

3.3 Photons and the staircase case

We propose two different cut scenarios to establish staircase scaling in γ+jets. Inspired by the picture of the photon being a massless Z we study a mass criterion to mimic the recoil in weak

[2] By now the Lhc has collected more than 1 fb^{-1} [50]

[3] This process is suppressed by at least an factor of α_{em}.

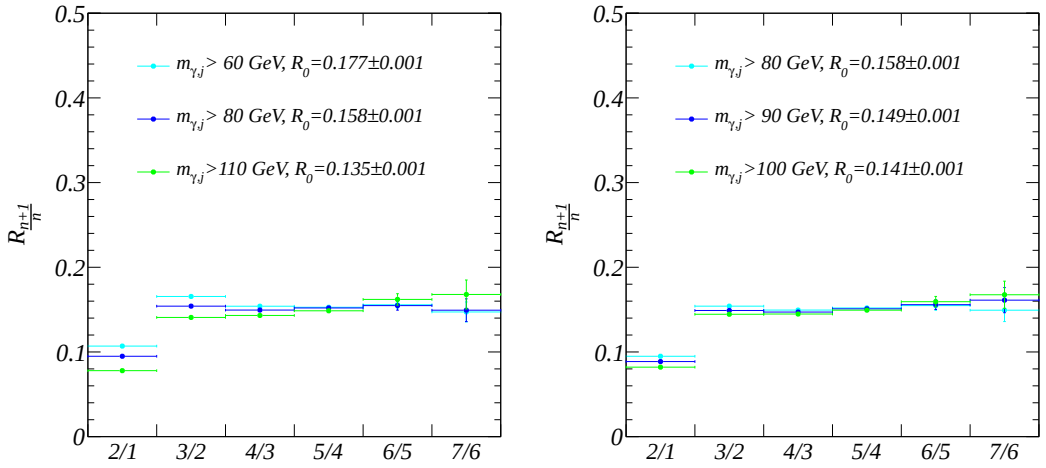

Figure 3.3: Impact of the mass criterion on the scaling properties of γ+jets. Left: Invariant mass criterion between photon and each jet for different masses in the range of $m_{\gamma j} > 60,\ 80$ and 110 GeV narrowing down the phase space region where scaling occurs. Right: Changing the mass criterion enables us to tune to different scaling parameters R_0.

gauge boson production

$$m_{\gamma,\text{jet}} > m_{\text{cut}} \quad \forall \text{ jets}, \tag{3.11}$$

where $m_{\gamma,\text{jet}}$ is the invariant mass obtained from adding the four vectors of the photon and the jet. In figure 3.3 we observe a phase space region between 60 and 110 GeV where the γ+jets sample shows staircase behavior. It is interesting to note that this region falls together with the masses of the weak gauge bosons[4]. We are also able to tune the actual scaling value R_0 within this mass window.

Although the motivation of the mass criterion is the connection of mass and scaling in the weak boson case measuring the invariant masses of jet and γ combinations may be tainted with

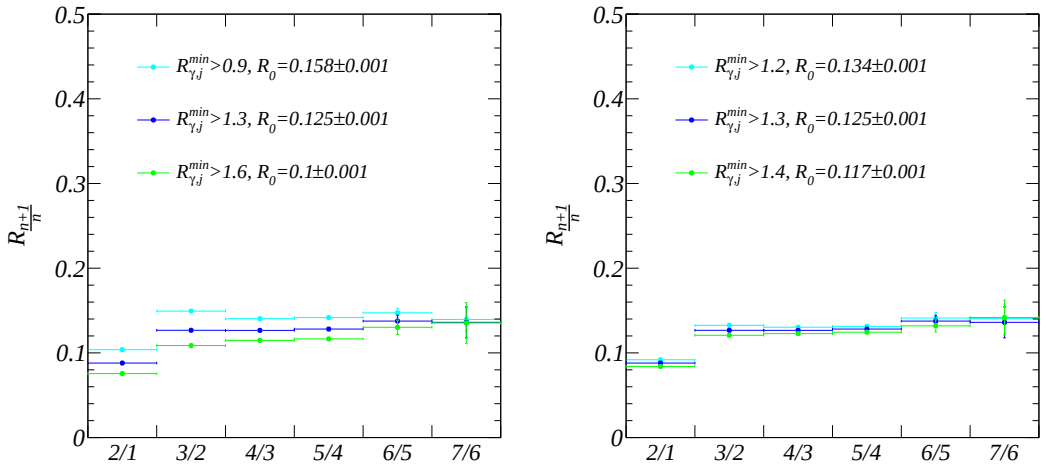

Figure 3.4: Staircase scaling obtained with the minimal separation criterion. Left: Whole phase space region showing staircase scaling. Right: Tuning the scaling parameter R_0 seems to be more stable than with the mass criterion.

[4]If this is by accident or not is to this point not clear as we still do not understand staircase scaling from first principles.

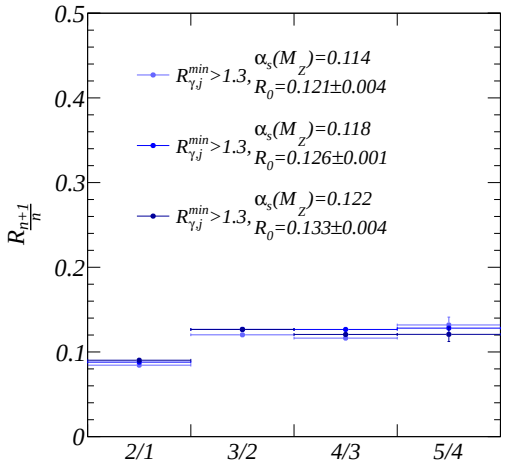

Figure 3.5: Consistent variation of α_s does not spoil staircase scaling. The uncertainties to the central R_0 value are small compared to the range of $R^{\min}$'s where scaling is present.

nasty uncertainties at the LHC due to the jet energy uncertainties. An more intrigue cut scenario uses the minimal separation criterion. Asking the jet and the photon to have some invariant mass forces them to separate, see also figure 3.9, as two massless parallel four vectors square to zero. Therefore we study also

$$R^{\min}_{\gamma,\,\text{jet}} > R_{\text{cut}} \quad \forall \text{ jets}, \tag{3.12}$$

where R is computed with equation (3.9) Again we observe a rather large region of $R^{\min}$ values where staircase scaling is present. A closer look reveals that different $R^{\min}$ values generate different staircase scaling parameters R_0, see figure 3.4.

Before we can make any quantitative remarks about the scaling properties and the fitted R_0's we have to address the uncertainties in our Monte Carlo simulation. There is the uncertainty of $\alpha_s(M_Z)$. We study this uncertainty by varying its NLO value of 0.118 consistently between 0.114 and 0.122 including the appropriate pdf sets. As we are interested in the staircase scaling properties we study the impact of the uncertainties of α_s on the resolution of our separation criterion and the possible deviation from staircase scaling[5].

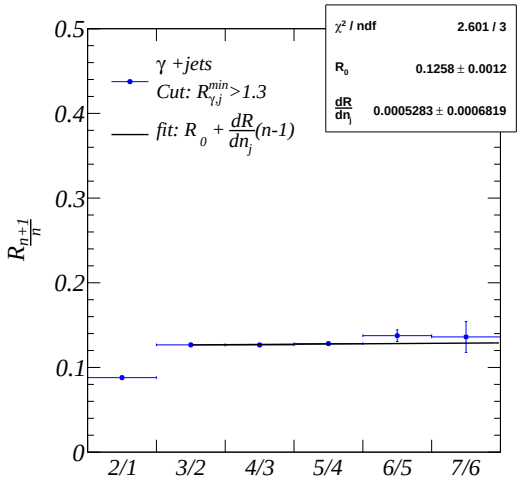

Figure 3.6: Staircase scaling in the phase space region constraint by the minimal separation criterion.

[5]As is also outlined in section 3.1 there is in principal an over all free parameter which can not be computed

We observe as shown in figure 3.5 only slight variations in the scaling behavior due to a change of α_S[6]. More important the changes to R_0 due to uncertainties in α_s are smaller than steps of size 0.1 in our $R^{\min}$ criterion. This means we can scan the different $R^{\min}$'s producing staircase scaling with a reasonable stepping size. Note however that the study presented here is done on parton level. To make reasonable statements about the possible resolution of $R^{\min}$ values in experiment a dedicated detector simulation has to be performed. There is also another uncertainty in our Monte Carlo study. In principle we had to check for the variation of the free parameter μ again, but in the spirit of section 3.1 and reference [15] we handle it as a tuning parameter which we expect to be unity for the SHERPA generator.

The by far best performance we observe for $R^{\min} > 1.3$. Clear staircase properties are present even in the $n_{\text{jets}} = 7$ bin as is shown in figure 3.6.

Kinematics

Now that we have a region in phase space showing pronounced staircase scaling we study the kinematic configuration of those events. If we understand the arrangement between the photon and the jets we may draw conclusions on other cases where staircase scaling occurs. Without any cuts the photon would be most often radiated together with the second hardest jet, as shown in figure 3.7, in a back to back configuration with the hardest jet. We also observe an enhancement of photons at small separations in R with respect to this second hardest jet. These photons come from collinear radiation of quark lines. It is this collinear radiation which spoils our staircase scaling.

The separation and the mass criterion perform both quite similar. We can understand the appearance of staircase scaling in the light of the kinematics in Z+jets where staircase scaling is observed. As the Z is heavy it can only be produced if its recoil is counter balanced which causes

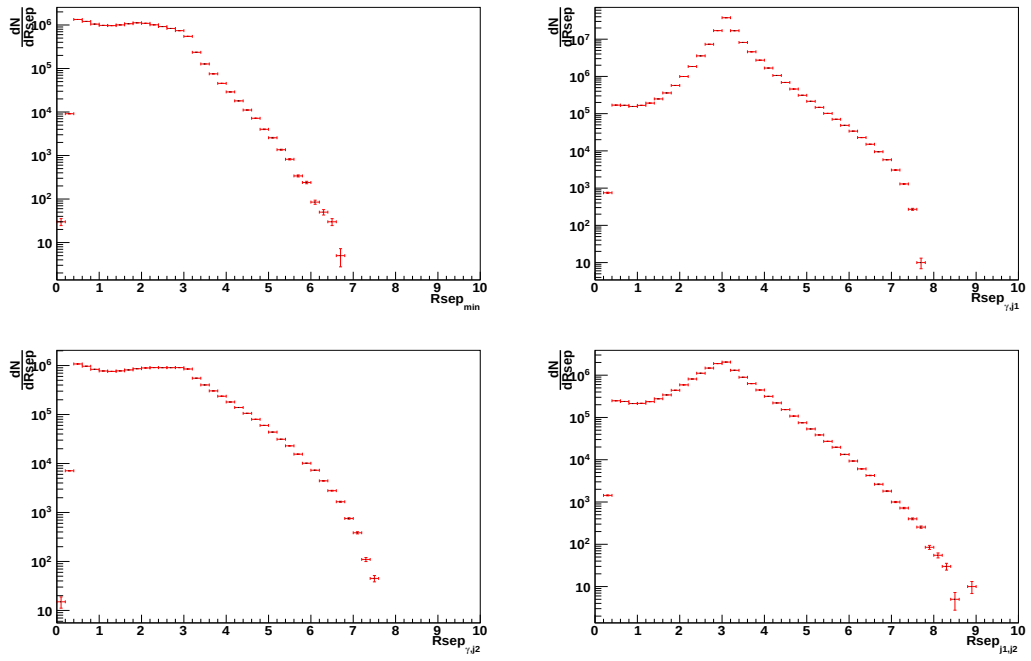

Figure 3.7: Separation between the photon and the two hardest jets in(η, Φ) plane. While all other jets are distributed equally over the whole phase space (upper left) the hardest jet is most often back to back. The second hardest jet however shows enhanced behavior to small R which are cut off by the Frixione criteria for isolated

from first principals. However, in the spirit of ref. [15] we treat this free parameter as tuning factor determined by experiment. For SHERPA we expect it to be close to the default value [66].

[6]The reason why this plot shows not as much multiplicity bins is due to limited simulation statistics for the α_s variations.

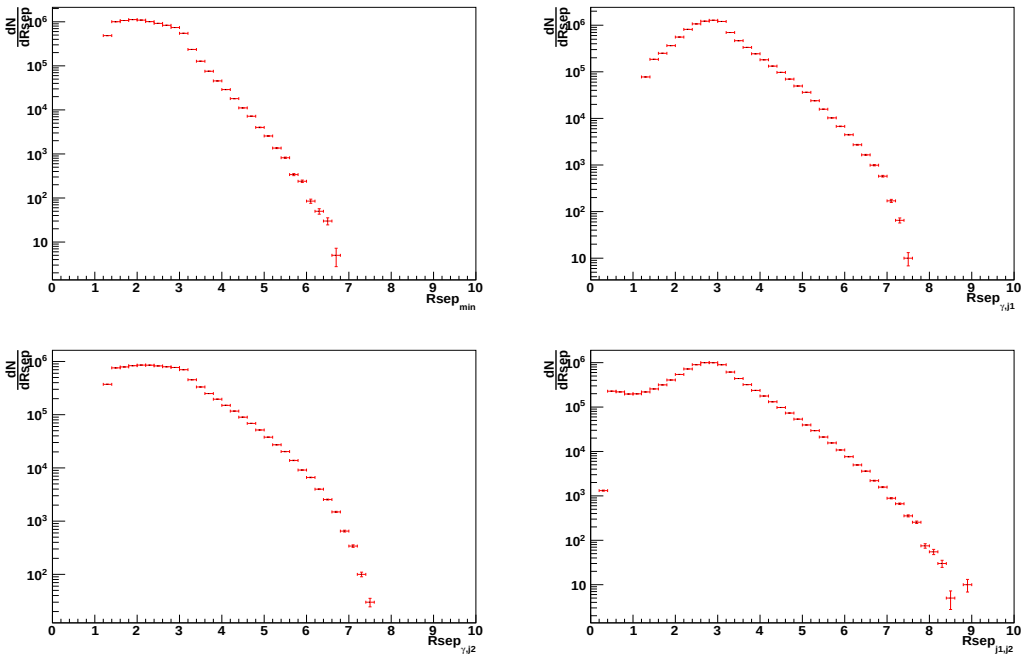

Figure 3.8: Separation between the photon and the two hardest jets in(η, Φ) plane for staircase scaling. All collinear enhanced photons have been removed.

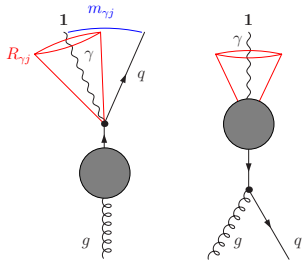

Figure 3.9: Left: Pictorial description of our two cut scenarios. Right: Forcing the photon to be separated suppresses collinear QED radiation. 1 is denoting that the photon p_T is hardest in comparison to those of the jets.

the QCD jets to be mostly separated from the Z. With our cut scenarios we mimic this behavior for the photon plus jets channel and find the same behavior. The reason why this happens not automatically with the γ+jets is the masslessness of the photon. At any point we can radiate a collinear photon which has by no means to be soft in our center of mass system. The photon its self is an abelian particle thus setting an end to further branching which might appear had we radiated an additional gluon and thus spoiling our QCD staircase scaling. Forbidding these event structure by forcing the photon to recoil against the QCD , see figure 3.8 opens again the way for the partons to shower only in a QCD like manner, see also figure 3.9. This means that the origin of the staircase scaling may be found in the ability of the gluon to split to two gluons.

3.4 Photons and the Poisson case

In the derivation of the Poisson scaling for gauge boson radiation of a fermion line leading to equation (3.1) enter two assumptions. The first concerns the used splitting kernels namely that there exists only one. This leads to angle ordered emission of the gauge bosons off the fermion line. Thus avoiding combinatorial factors of $n!$. The other one is about the over counting of the bosonic phase space which leads to the $1/n!$ factor. An example for such a statistical treatment are the

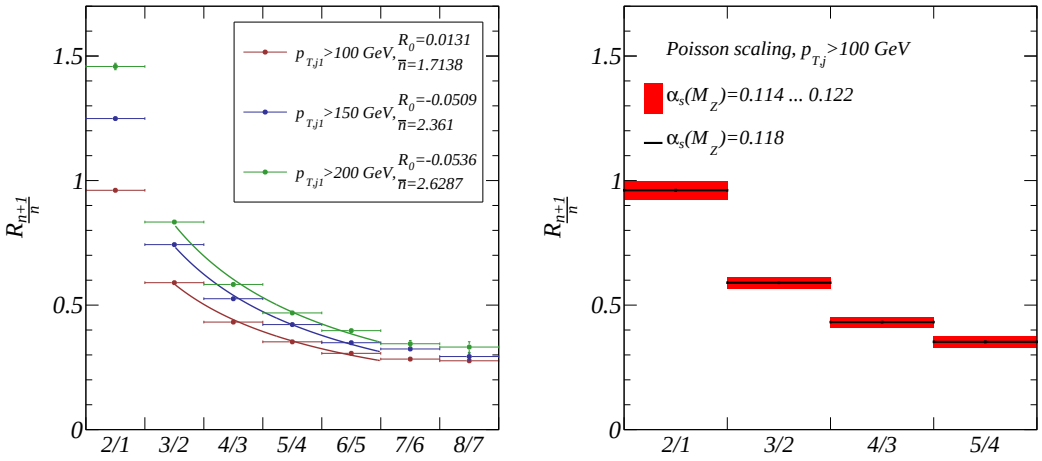

Figure 3.10: Poisson scaling for γ+jets production at the LHC. Left: Different transverse momentum cuts for the leading jet lead to Poisson scaling, all other jets have $p_T > 20\ GeV$. Right: A consistent variation of α_s shows only small effects on the ratios in the Poisson case regime.

Sudakov factors. To achieve $\frac{1}{n+1}$ drop in the n_{jet} ratios we need to induce a large logarithm. This can be done by asking for a large p_T for the first jet. This way we introduce terms of the form

$$log\left(\frac{p_{T,\text{leading jet}}}{p_{T,\text{average}}}\right). \tag{3.13}$$

In this way we get a well defined hard subprocess. From figure 3.3 we could also conclude that a cut of the form m_{γ,j_1} induces a preferred direction which also leads to an enhanced logarithm, but

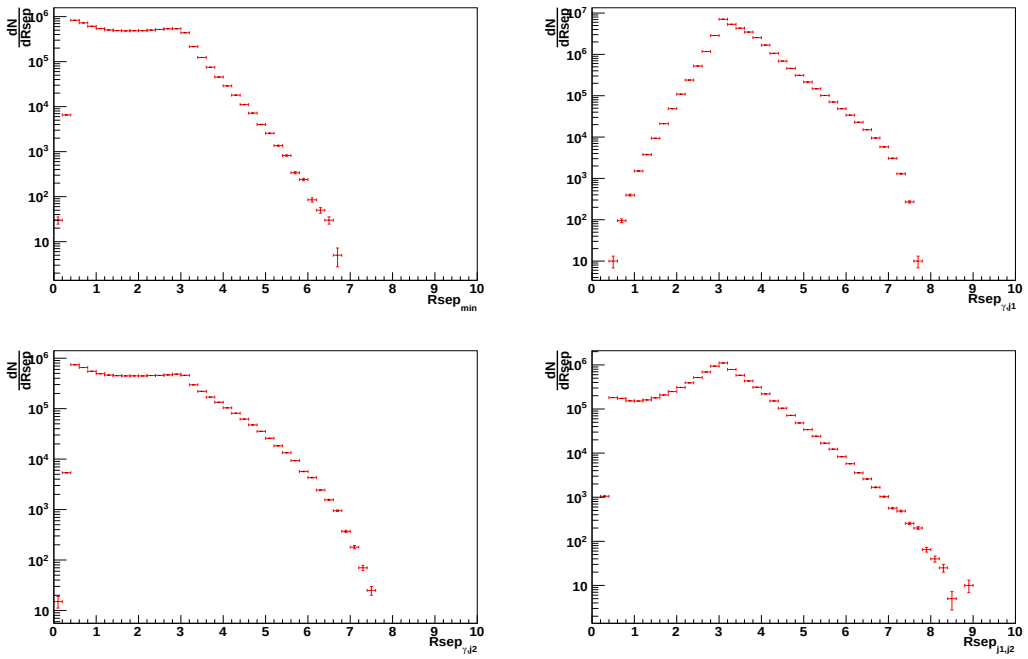

Figure 3.11: Separation between the photon and the two hardest jets in(η, Φ) plane for Poisson scaling. While all other jets are distributed equally over the whole phase space (upper left) the hardest jet is nearly almost back to back. The second hardest jet however shows enhanced behavior to small R which are cut off by the Frixione criteria for isolated photons. Thus collinear photon emission is enhanced in Poisson scaling contrary to the staircase behavior.

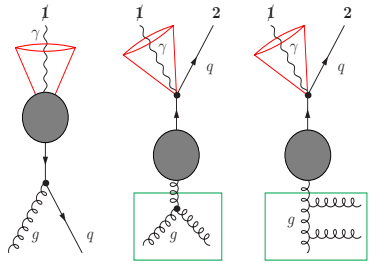

Figure 3.12: Kinematic structure for the Poisson scaling case. Photon radiation is enhanced in the collinear regime and comes mostly from the second hardest jet.

it turns out that we find the cleanest Poisson scaling by requiring

$$p_{T,\gamma} > 20GeV \qquad p_{T,j} > 100, 20, 20, \ldots GeV \qquad |\eta_\gamma| < 2.5, \qquad |y_j| < 4.5, \tag{3.14}$$

instead of equation (3.5). The lower value of 20 GeV for p_T ensures a larger logarithm and higher statistics. To test for Poisson scaling we fit the function

$$R_{\frac{n+1}{n}} = \frac{\bar{n}}{n+1} + R_0. \tag{3.15}$$

Here R_0 checks for remnants of the staircase scaling. $\bar{n}$ is the average number of emitted partons and corresponds to the parameter λ in equation (3.1). From the values in figure 3.10 we see that the larger we force the logarithm to be the higher becomes the expected number of jets. As for the staircase scaling we do not include the one jet bin in our analysis due to the definition of the hard process. Having two jets produces often a photon which is close to the second jet, see figure 3.11. On the other hand forcing the first jet to be very hard enables it to radiate additional not so hard partons, see figure 3.12. Thus a non vanishing value for the expected number of jets occurs.

The large logarithm is induced by forcing the first jet to be very heavy. The larger the jet multiplicity the weaker is the expression of the Poisson scaling. In figure 3.10 we show different cuts for the leading jet as well as the fit values. As we have done for the staircase case we omit the two over one bin. If the fit in figure 3.10 would also include the highest multiplicity bins the fitted value of R_0 would rather be in the range of 0.3 as the effect of the induced log vanishes in the highest multiplicity bins. This shows the impact of the decreased p_T cut when compared to figure 3.3 and 3.4. In addition we show the effect of a consistent change in α_s.

Having only a constraint on the leading jet leads to no further separation criterion between the photon and the other jets. Thus fragmented photon production is not suppressed as strong as for the staircase case. Thus the kinematic configuration in the Poisson case is mostly that leading jet and photon are back to back, while the second jet shows enhancement in the collinear region which is is a remnant of the rather arbitrary selection of the R value for the Frixione photon criterion.

Chapter 4

Using Staircase Scaling for an Autofocus

4.1 Jets with missing energy

Missing transverse energy is a general signature for dark matter related new physics at hadron colliders [8]. It has a long history at the Tevatron and to date gives the strongest bounds on squark and gluino masses in supersymmetric extensions of the Standard Model. At the LHC the first new exclusion limits for squarks and gluinos have recently appeared, in the CMSSM toy model as well as in a more general setup [9–11]. All of these analysis are based on jets plus missing energy including a lepton veto which constitutes the most generic search strategy for strongly interacting new particles decaying into a weakly or super-weakly interacting dark matter candidate [8, 12].

While the first results are based on very inclusive cuts, following the ATLAS [13] and CMS [14] documentations we expect more specific analysis to appear soon. The reason is that in their current form the analysis can and should be optimized for specific new physics mass spectra. More specialized analysis for jets plus missing energy rely on a missing transverse momentum cut and on a certain number of staggered jet transverse momentum cuts [13, 14]. Unfortunately, they are therefore hard to adapt to modified mass spectra and by definition show a poor performance for not optimized model parameters. In addition, they are counting experiments in certain phase-space regions, which means that for any additional information on the physics behind an anomaly we have to wait for a dedicated analysis.

A major problem of searches for new physics in pure QCD plus missing energy final states is the prediction of background distributions. Aside from the improved signal-to-background ratio this is one of the reasons why applying fairly restrictive cuts on the number of jets and on their transverse momentum is a promising strategy. Such cuts relieve us from having to understand the complete p_T spectra [55] of general exclusive or inclusive n_{jets}-jet events at the LHC . Experimentally, however, we should by now be in a position to simulate these distributions using the CKKW [17, 18] or MLM [19] matching methods implemented in SHERPA [34], ALPGEN [56], or MADEVENT [46]. The different approaches have been compared in some detail, for example for W+jets production [39, 57]. What is still missing is a systematic study of theory uncertainties in multi-jet background simulations for top quark analysis and new physics searches, i.e. including large jet multiplicities down to intermediate jet transverse momenta, but reflecting a well defined hard scale given by the signal process. In 4.5 we incorporate a log likelihood analysis to our backgrounds. The log likelihood is an additive quantity for statistical independent bins. For that reason we define all observables as exclusive, specifically in the number of jets.

In the following sections we establish a proper simulation of multi-jet processes and estimate their theory uncertainties, with a focus on the question what actually constitutes the theory error. This way LHC data in control regions can be used to understand very generic scaling features (*staircase scaling*[1]) which have already been observed in data [59, 60] and which we can extend based on appropriate Monte Carlo studies. This staircase scaling we can reproduce and study using QCD Monte Carlo simulations, including different hard processes and the effects of cuts. Combining these simulations with LHC data should give us a quantitative handle on multi-jet rates in many applications.

Moreover, we can use our knowledge about the exclusive n_{jets} distributions to predict other notoriously difficult multi-jet observables. So once we understand the uncertainties on the multi-jet spectra we turn to the effective mass. In its many incarnations it either includes the leading jet or it does not and is either limited to four jets or any other number of jets [61]. Obviously, any specific definition of this mass variable increases its sensitivity to theory uncertainties. We study the most

[1] Staircase scaling for jet rates is often referred to as Berends scaling. However, to our best knowledge it was first introduced and discussed by the authors of Ref. [58].

generic definition of the effective mass including *all jets* visible above a transverse momentum threshold. As we add up jets the uncertainties of this observable are closely linked to those of the jet-multiplicity distribution. Using the scaling properties of the exclusive jet multiplicities we can strongly reduce the theory uncertainty in the effective-mass spectrum in a consistent manner. The same should be true for other multi-jet observables which we can use to extract new physics from jet dominated backgrounds.

Similar questions are currently being asked to control regions in a purely data-driven approach. However, the conversion from background regions into the signal region either by shifting the kinematic regime or by changing the hard core processes off which we radiate jets requires a good understanding for example of the effects of background rejection cuts and of background sculpting features in the definition of these observables. These effects we can reliably estimate in an appropriate Monte Carlo study and then combine for example with an over-all normalization from data.

Finally, we suggest an analysis strategy which on the one hand makes maximum use of the jet patterns and on the other hand does not require any tuning of cuts. The only ingredient of our analysis which does not involve jets is a missing transverse energy cut to reduce pure QCD backgrounds and an isolated lepton veto against W+jets and semi leptonic tops backgrounds. To reduce them to a manageable level we require

$$\not{E}_T > 100 \text{ GeV} \qquad \text{and a lepton veto if} \quad p_{T,\ell} > 20 \text{ GeV}, \; |y_\ell| < 2.5 \tag{4.1}$$

as the basic and only electroweak cuts to reduce the QCD background. The exact numbers are not very dependent on the details of the model as long as the new physics sector provides a WIMP dark matter candidate. To account for fake missing energy from QCD jets we apply an additional factor of $1/500$ for pure QCD and hadronic top-quark final states. This rough fake rate we estimate from Ref. [9]. It provides us with a rather conservative estimate compared e.g. to Ref. [14].

After these very generic acceptance cuts a two-dimensional correlation of the effective mass vs the exclusive jet multiplicity is the appropriate distribution to extract limits on strongly interacting new physics or in the case of an excess study the mass scale as well as the color charge of the new states. Because all our observables are defined jet-exclusively we can to a good approximation study this two-dimensional distribution using a log-likelihood shape analysis. The contributions of different regions in the n_{jets}- m_{eff} space to the binned log-likelihood automatically focus on the correct phase-space region and are readily available for improved analysis as well as theoretical interpretation.

4.2 Decay jets vs jet radiation

In contrast to the QCD and gauge-boson background n_{jets} distributions from heavy particles decaying to jets include two sources of jets: first, there are decay jets, which dependent on the spectrum might or might not be hard enough to stick out. Second, there is QCD jet radiation, which for heavy states will generically be relatively hard and dominated by collinear splitting in the initial state [67, 70], leading to a non-zero maximum value of the number of expected initial-state radiation jets [8, 69]. Due to the hard scale of new-physics processes on the one hand and because we need to simulate supersymmetric decays inclusively we best generate the new-physics events with Herwig++-v2.4.2 [71] and normalize the cross sections with Prospino2.1 [33]. All supersymmetric mass spectra we generate with SoftSusy [72] using the SLHA output format [73] and use Sdecay [74] to calculate the leading-order branching ratios. We check the jet-radiation results from the Herwig++ shower with Mlm merging up to two additional jets implemented in MadEvent [70], using Pythia [75] for parton showering and hadronization as shown in fig. 4.1.

For the case of Susy we are actually able to stick out the expected number of decay jets from the spectrum. In table 4.1 all the masses for the SPS1a spectrum generated with SoftSusy [72] are listed. All these particles can decay to a Sm particle and a lighter Susy particle except for the $\tilde{\chi}_1^0$ as it is protected by R-parity. Into which particular particles a heavy Susy state decays is described by its branching ratios. From the color structure of the sparticels our naive estimate would be mostly one decay jet for color triplets like squarks and one additional decay jet for color octets like gluinos as they have to decay to a squark first to get rid of their color charge. In table 4.2 we collect the largest branching ratios for the gluino generated with Sdecay [74] and

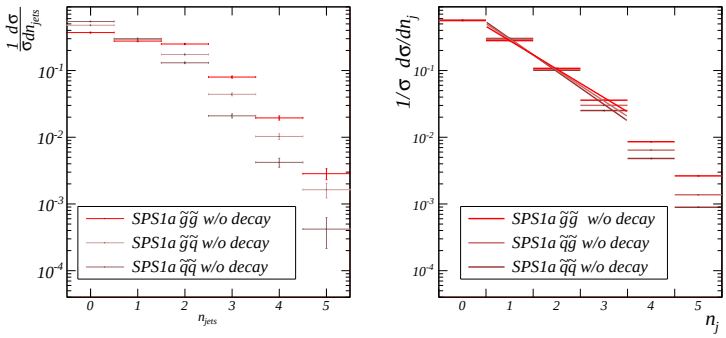

Figure 4.1: Normalized exclusive $d\sigma/d\ n_{\text{jets}}$ distributions for supersymmetric particle production. QCD jet radiation only for the MADEVENT sample (left) as well as for the HERWIG++ sample (right). Jets are counted once they fulfill Eq.(3.5).

Particle	Mass[GeV]	Particle	Mass[GeV]	Particle	Mass[GeV]
$\tilde{g}$	604	$\tilde{b}_2$	548	$\tilde{\nu}_{\mu,L}$	186
$\tilde{t}_2$	586	$\tilde{b}_1$	515	$\tilde{\nu}_{\tau,L}$	185
$\tilde{s}_L$	571	$\tilde{t}_1$	401	$\tilde{\chi}_2^0$	181
$\tilde{d}_L$	571	$\tilde{\chi}_2^+$	382	$\tilde{\chi}_1^+$	180
$\tilde{c}_L$	565	$\tilde{\chi}_4^0$	381	$\tilde{e}_R^-$	144
$\tilde{u}_L$	565	$\tilde{\chi}_3^0$	364	$\tilde{\mu}_R^-$	144
$\tilde{u}_R$	548	$\tilde{\tau}_2^-$	206	$\tilde{\tau}_1^-$	134
$\tilde{c}_R$	548	$\tilde{\mu}_L^-$	202	$\tilde{\chi}_1^0$	97
$\tilde{d}_R$	548	$\tilde{e}_L^-$	202		
$\tilde{s}_R$	548	$\tilde{\nu}_{e,L}$	186		

Table 4.1: SUSY particles for the SPS1a benchmark point sorted by their mass. The $\tilde{\chi}_1^0$ is the only stable particle. All others decay via decay chains into $\tilde{\chi}_1^0$.

possible decay chains for this heavy colored states in SPS1a. From those numbers we can compute the expected number of decay jets for gluinos[2]

$$\langle \tilde{g}_{\text{decays}} \rangle \approx 2.5. \tag{4.2}$$

The reason for the difference to our naive guess is that the gluino decays only in 40% of the cases to a $\tilde{q}_R$ which gives us the expected two decay jets. All the other decay chains produce mostly three or even more decay jets. We see this feature also in section 4.5 in fig. 4.6. The exact number and the possible decay chains rely heavily on the selected spectrum. This is one of the reasons why we propose a spectrum independent search strategy. As we will see in section 4.5 the proposed search strategy allows to get information about this avarge number thus providing us with a hint for what kind of spectrum we have to search.

$\tilde{g}$ decay	possible decay chains	# decay jets	BR
$\tilde{g} \underset{(56GeV)}{\overset{(40\%)}{\longrightarrow}} \tilde{q}_R$	$\tilde{q}_R \underset{(452GeV)}{\overset{(98\%)}{\longrightarrow}} \tilde{\chi}_1^0$	2	0.390

[2]Due to simplicity we only show 82.5% of the gluino decays. The weighted sum from table 4.2 is actually $2.1 \approx 82.5\% \times 2.5$.

$\tilde{g} \underset{(89GeV)}{\overset{(22.5\%)}{\longrightarrow}} \tilde{b}_1$	$\tilde{b}_1 \underset{(335GeV)}{\overset{(45\%)}{\longrightarrow}} \tilde{\chi}_1^-$	$\tilde{\chi}_1^- \underset{(46GeV)}{\overset{(95\%)}{\longrightarrow}} \tilde{\tau}_1$	$\tilde{\tau}_1 \underset{(37GeV)}{\overset{(100\%)}{\longrightarrow}} \tilde{\chi}_1^0$		4	0.096
		$\tilde{\chi}_1^- \underset{(83GeV)}{\overset{(4\%)}{\longrightarrow}} \tilde{\chi}_1^0$			3	0.004
	$\tilde{b}_1 \underset{(334GeV)}{\overset{(35\%)}{\longrightarrow}} \tilde{\chi}_2^0$	$\tilde{\chi}_2^0 \underset{(47GeV)}{\overset{(87\%)}{\longrightarrow}} \tilde{\tau}_1$	$\tilde{\tau}_1 \underset{(37GeV)}{\overset{(100\%)}{\longrightarrow}} \tilde{\chi}_1^0$		4	0.069
		$\tilde{\chi}_2^0 \underset{(37GeV)}{\overset{(6\%)}{\longrightarrow}} \tilde{e}_R$	$\tilde{e}_R \underset{(47GeV)}{\overset{(100\%)}{\longrightarrow}} \tilde{\chi}_1^0$		4	0.005
		$\tilde{\chi}_2^0 \underset{(37GeV)}{\overset{(6\%)}{\longrightarrow}} \tilde{\mu}_R$	$\tilde{\mu}_R \underset{(47GeV)}{\overset{(100\%)}{\longrightarrow}} \tilde{\chi}_1^0$		4	0.005
	$\tilde{b}_1 \underset{(114GeV)}{\overset{(14\%)}{\longrightarrow}} \tilde{t}_1$	$\tilde{t}_1 \underset{(221GeV)}{\overset{(67\%)}{\longrightarrow}} \tilde{\chi}_1^+$	$\tilde{\chi}_1^+ \underset{(46GeV)}{\overset{(95\%)}{\longrightarrow}} \tilde{\tau}_1$	$\tilde{\tau}_1 \underset{(37GeV)}{\overset{(100\%)}{\longrightarrow}} \tilde{\chi}_1^0$	5	0.016
			$\tilde{\chi}_1^+ \underset{(83GeV)}{\overset{(4\%)}{\longrightarrow}} \tilde{\chi}_1^0$		4	0.001
		$\tilde{t}_1 \underset{(304GeV)}{\overset{(19\%)}{\longrightarrow}} \tilde{\chi}_1^0$			3	0.006
		$\tilde{t}_1 \underset{(220GeV)}{\overset{(12\%)}{\longrightarrow}} \tilde{\chi}_2^0$	$\tilde{\chi}_2^0 \underset{(47GeV)}{\overset{(87\%)}{\longrightarrow}} \tilde{\tau}_1$	$\tilde{\tau}_1 \underset{(37GeV)}{\overset{(100\%)}{\longrightarrow}} \tilde{\chi}_1^0$	5	0.003
			$\tilde{\chi}_2^0 \underset{(37GeV)}{\overset{(6\%)}{\longrightarrow}} \tilde{e}_R$	$\tilde{e}_R \underset{(47GeV)}{\overset{(100\%)}{\longrightarrow}} \tilde{\chi}_1^0$	5	0.001
			$\tilde{\chi}_2^0 \underset{(37GeV)}{\overset{(6\%)}{\longrightarrow}} \tilde{\mu}_R$	$\tilde{\mu}_R \underset{(47GeV)}{\overset{(100\%)}{\longrightarrow}} \tilde{\chi}_1^0$	5	0.001
$\tilde{g} \underset{(56GeV)}{\overset{(10\%)}{\longrightarrow}} \tilde{b}_2$	$\tilde{b}_2 \underset{(452GeV)}{\overset{(32\%)}{\longrightarrow}} \tilde{\chi}_1^0$				2	0.032
	$\tilde{b}_2 \underset{(147GeV)}{\overset{(25\%)}{\longrightarrow}} \tilde{t}_1$	$\tilde{t}_1 \underset{(221GeV)}{\overset{(67\%)}{\longrightarrow}} \tilde{\chi}_1^+$	$\tilde{\chi}_1^+ \underset{(46GeV)}{\overset{(95\%)}{\longrightarrow}} \tilde{\tau}_1$	$\tilde{\tau}_1 \underset{(37GeV)}{\overset{(100\%)}{\longrightarrow}} \tilde{\chi}_1^0$	5	0.016
			$\tilde{\chi}_1^+ \underset{(83GeV)}{\overset{(4\%)}{\longrightarrow}} \tilde{\chi}_1^0$		4	0.001
		$\tilde{t}_1 \underset{(304GeV)}{\overset{(19\%)}{\longrightarrow}} \tilde{\chi}_1^0$			3	0.005
		$\tilde{t}_1 \underset{(220GeV)}{\overset{(12\%)}{\longrightarrow}} \tilde{\chi}_2^0$	$\tilde{\chi}_2^0 \underset{(47GeV)}{\overset{(87\%)}{\longrightarrow}} \tilde{\tau}_1$	$\tilde{\tau}_1 \underset{(37GeV)}{\overset{(100\%)}{\longrightarrow}} \tilde{\chi}_1^0$	5	0.003
			$\tilde{\chi}_2^0 \underset{(37GeV)}{\overset{(6\%)}{\longrightarrow}} \tilde{e}_R$	$\tilde{e}_R \underset{(47GeV)}{\overset{(100\%)}{\longrightarrow}} \tilde{\chi}_1^0$	5	0.001
			$\tilde{\chi}_2^0 \underset{(37GeV)}{\overset{(6\%)}{\longrightarrow}} \tilde{\mu}_R$	$\tilde{\mu}_R \underset{(47GeV)}{\overset{(100\%)}{\longrightarrow}} \tilde{\chi}_1^0$	5	0.001
	$\tilde{b}_2 \underset{(368GeV)}{\overset{(15\%)}{\longrightarrow}} \tilde{\chi}_1^+$	$\tilde{\chi}_1^+ \underset{(46GeV)}{\overset{(95\%)}{\longrightarrow}} \tilde{\tau}_1$	$\tilde{\tau}_1 \underset{(GeV)}{\overset{(100\%)}{\longrightarrow}} \tilde{\chi}_1^0$		4	0.014
		$\tilde{\chi}_1^- \underset{(GeV)}{\overset{(4\%)}{\longrightarrow}} \tilde{\chi}_1^0$			3	0.001
	$\tilde{b}_2 \underset{(367GeV)}{\overset{(12\%)}{\longrightarrow}} \tilde{\chi}_2^0$	$\tilde{\chi}_2^0 \underset{(47GeV)}{\overset{(87\%)}{\longrightarrow}} \tilde{\tau}_1$	$\tilde{\tau}_1 \underset{(37GeV)}{\overset{(100\%)}{\longrightarrow}} \tilde{\chi}_1^0$		4	0.012
		$\tilde{\chi}_2^0 \underset{(37GeV)}{\overset{(6\%)}{\longrightarrow}} \tilde{e}_R$	$\tilde{e}_R \underset{(47GeV)}{\overset{(6\%)}{\longrightarrow}} \tilde{\chi}_1^0$		4	0.001
		$\tilde{\chi}_2^0 \underset{(37GeV)}{\overset{(6\%)}{\longrightarrow}} \tilde{\mu}_R$	$\tilde{\mu}_R \underset{(47GeV)}{\overset{(100\%)}{\longrightarrow}} \tilde{\chi}_1^0$		4	0.001
$\tilde{g} \underset{(56GeV)}{\overset{(10\%)}{\longrightarrow}} \tilde{t}_1$	$\tilde{t}_1 \underset{(221GeV)}{\overset{(67\%)}{\longrightarrow}} \tilde{\chi}_1^+$	$\tilde{\chi}_1^+ \underset{(46GeV)}{\overset{(95\%)}{\longrightarrow}} \tilde{\tau}_1$	$\tilde{\tau}_1 \underset{(37GeV)}{\overset{(100\%)}{\longrightarrow}} \tilde{\chi}_1^0$		5	0.016

	$\tilde{\chi}_1^+ \xrightarrow[(83GeV)]{(4\%)} \tilde{\chi}_1^0$	4	0.001

Table 4.2: $\tilde{g}$ decay chains for the SPS1a benchmark point and their probability to occur. The direct decay to $\tilde{q}_R$ is the most probable causing two decay jets, but there exist also other decay chains producing more decay jets.

The question for heavy-particle production is how universal its n_{jets} distributions are when we consider Standard Model as well as new-physics particles with different masses and color charges, like top quarks, squarks and gluinos. In Figure 4.2 we first show the n_{jets} distributions for (semi-)leptonic and hadronic top-pair production. We see how all unsubtracted distributions show maxima away from $n_{\text{jets}} = 0$, driven by the presence of decay jets plus relatively hard jet radiation. In addition, they do not show a staircase scaling at large jet multiplicities. Because the particles produced in the hard process have non-negligible masses even compared to the hadronic center-of-mass energy the phase-space suppression for example due to rapidly dropping gluon densities kicks in immediately and bends the otherwise exponential fall-off.

In the Standard Model we can fit the (semi-)leptonic and purely hadronic top-pair distributions for all jets fulfilling Eq.(3.5) to the function

$$\frac{d \log \sigma(\ n_{\text{jets}})}{d\ n_{\text{jets}}} = -b\, \frac{n_{\text{jets}}^2 - a_1\ n_{\text{jets}} + a_0^2}{n_{\text{jets}}}\ . \tag{4.3}$$

The two relevant fit parameters for the normalized distributions shown in Figure 4.2 correspond to the maximum at $n_{\text{jets}} = a_0$, and the (staircase) scaling parameter for QCD jet radiation at large n_{jets} given by $R = \exp(-b)$. Because we do not include higher suppression terms toward large n_{jets} we stop the fit at the endpoints of the curves shown in Figure 4.2. With this fit the mentioned face space suppression becomes obvious as we can observe the deviation for high multiplicities.

In Table 4.3 we list the best fit values for these parameters for both top decays. We immediately see more quantitatively than in Figure 4.2 that for example hadronically decaying top pairs on average include not even one more jet than the (semi-)leptonic sample. Typically only one of two jets from the W decay is accounted for because of the cutoff at $p_{T,\text{min}} = 50$ GeV. Comparing this value to the W mass it is likely that one of the two W decay jets gets boosted above $p_{T,\text{min}}$, but the other one stays below. In contrast, the Jacobian peak of the b-quark energy from the top decay lies above $p_{T,\text{min}}$. Going back to Table 4.3 this means that for top pairs the most likely number of radiated jets is zero, closely followed by one jet emission [69].

For squarks and gluinos the features we see in top-pair production become more pronounced and the average jet multiplicity reflects the color charge of the produced particles. As a reference point in supersymmetric parameter space we consider reasonably low mass gluinos and squarks in the SPS1a benchmark scenario [76], with $m_{\tilde{g}} = 608$ GeV and typical light-flavor squarks around

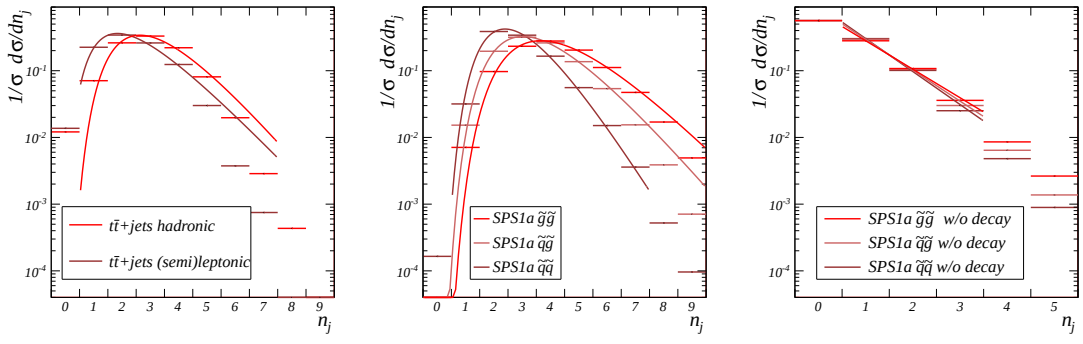

Figure 4.2: Normalized exclusive $d\sigma/d\ n_{\text{jets}}$ distributions for top pairs (left) and supersymmetric particle production. For the latter we show all decay jets plus QCD jet radiation (center) as well as QCD jet radiation only (right). Jets are counted once they fulfill Eq.(3.5).

	$(t\bar{t})_{hh}$	$(t\bar{t})_{\ell\ell/h}$	$\tilde{q}\tilde{q}$	$\tilde{q}\tilde{g}$	$\tilde{g}\tilde{g}$	SUSY	$\tilde{q}\tilde{q}$	$\tilde{q}\tilde{g}$	$\tilde{g}\tilde{g}$
	full		full				jet radiation		
a_0	3.13	2.34	2.89	3.53	4.16	3.15	n.a.	n.a.	n.a
a_1	5.41	3.73	5.28	6.16	7.15	5.48	0.45	0.36	0.21
b	1.25	1.07	1.71	1.25	1.09	1.27	1.14	1.07	0.98

Table 4.3: Parameters defined in Eq.(4.3) and extracted from the unsubtracted distributions shown in Figure 4.2. The parameter a_0 corresponds to the position of the maximum while b captures the approximate scaling at larger n_{jets}. The combined supersymmetric result is based on the appropriately weighted event samples for squarks and gluinos.

$m_{\tilde{q}} \sim 558$ GeV. The new LHC exclusion limits are right at the edge of excluding this standard parameter choice[3]. Because the gluino cannot decay to a gluon it requires two quarks to get rid of its color charge. Squark pairs, including squark-antisquark production, predict two hard decay jets plus some QCD radiation and sub-leading decay jets. In Table 4.3 we see that for this production channel the maximum of a continuous n_{jets} distribution indeed resides almost at $n_{\text{jets}} = 3$. For associated squark-gluino and gluino-pair production the number of jets increases by almost one, corresponding to the second gluino-decay jet which not in all cases is hard enough to appear after requiring $p_{T,\text{min}} = 50$ GeV. The jet multiplicity of the entire supersymmetric sample is close to the average for squark pair production and squark-gluino production which reflects the hierarchy in cross sections of the three processes [33].

Breaking down the supersymmetric signal into individual production processes we can examine the distinct radiation patterns. Gluino pairs radiate significantly more than associated production or squark pairs, which is reflected in the right columns of Table 4.3: $b(\tilde{g}\tilde{g}) < b(\tilde{q}\tilde{g}) < b(\tilde{q}\tilde{q})$. The scaling parameter $R = \exp(-b)$ is consistently larger than for the background samples in Table 3.1. For example for the jet radiation off squark pair production we find $R \approx 0.32$. Moreover, in Figure 4.2 we see that the jet rates for QCD radiation drop off even faster for large multiplicities. This means that there definitely does not exist any staircase scaling behavior for heavy particle pair production above a threshold of 1 TeV at the LHC with a hadronic center-of-mass energy of 7 TeV. This phase space argument should not be mixed with the fact that the hard scale of such processes and with it the logarithmic enhancement for collinear radiation is large, i.e. the validity of the collinear approximation extends to larger values of $p_{T,j}$.

4.3 The number of jets

Now we have everthing together to use the n_{jets}-observable as an appropriate discriminator. In section 3.1 we compute the theoretical uncertainties for our simulation noting that the free factor in our Monte Carlo is rather a tuning parameter which has to be examined by experiment and that the uncertainties due to variation of α_s and the pdf's is well under controll. We are able to reproduce the observed staircase scaling and extrapolate it into even higher jet multiplicities. In section 4.2 we adress the characteristics of jets coming from decaying particles and how those processes differ from the staircase scaling behavior of chapter 3.

Finally, in Figure 4.3 we show the n_{jets} distribution for the supersymmetric signal assuming the SPS1a parameter point and the various Standard Model backgrounds. We apply the background rejection cuts specified in Eqs.(4.1) and (3.5). The variation in shape when including the signal events is statistically significant and appears as an excess of high jet-multiplicity events for $n_{\text{jets}} > 5$. While for lower multiplicities the cross section for our Susy signal is to low to make any difference, we observe for high multiplicities how the deviation from staircase scaling becomes more significant. The associated statistical significance we compute in Section 4.5.

[3]Due to the presentation of the LHC results in the m_0 vs $m_{1/2}$ plane it is also not possible to precisely read off the actual limits in terms of physics mass parameters. Moreover, since squark and gluino masses are both mostly driven by $m_{1/2}$, there does not exist a mapping of the m_0-$m_{1/2}$ plane into the squark-gluino mass plane. Models with significantly heavier gluinos than quarks are excluded in CMSSM searches.

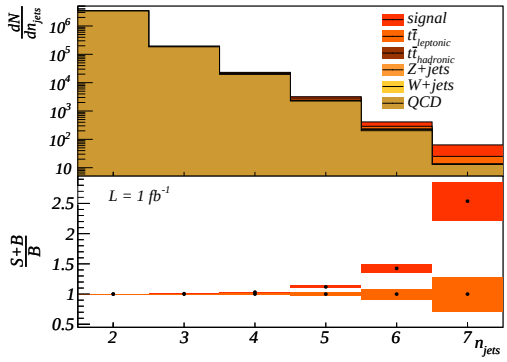

Figure 4.3: Exclusive n_{jets} distribution for all considered Standard-Model backgrounds and the SPS1a signal for supersymmetry. We present the results for an LHC center-of-mass energy of 7 TeV with an integrated luminosity of 1 fb^{-1} and after the cuts specified in Eqs. (4.1) and (3.5). The height of the bands in the lower panel correspond to the predicted statistical error for 1 fb^{-1}.

4.4 The effective mass

Before we turn to exploit the number of jets to extract a new physics signal at the LHC an obvious question is if we can make use of our understanding of the n_{jets} distribution looking at other observables in multi-jet final states. More specifically, we will use the measured scale parameter μ/μ_0 shown in Figure 3.1 to reliably predict observables, which, based on traditional QCD simulations, show an overwhelming theory uncertainty. A classic observable in this respect is the effective mass [61], which for exclusive jet multiplicities we define as

$$m_{\text{eff}} = \not{E}_T + \sum_{\text{all jets}} p_{T,j} \; , \tag{4.4}$$

including all jets fulfilling Eq.(3.5). This definition is neither optimized to take into account a correlation between hard jets and the missing-energy vector nor to remove hard initial-state radiation. Instead, Eq.(4.4) makes a minimal set of assumptions to avoid sculpting the background distribution.

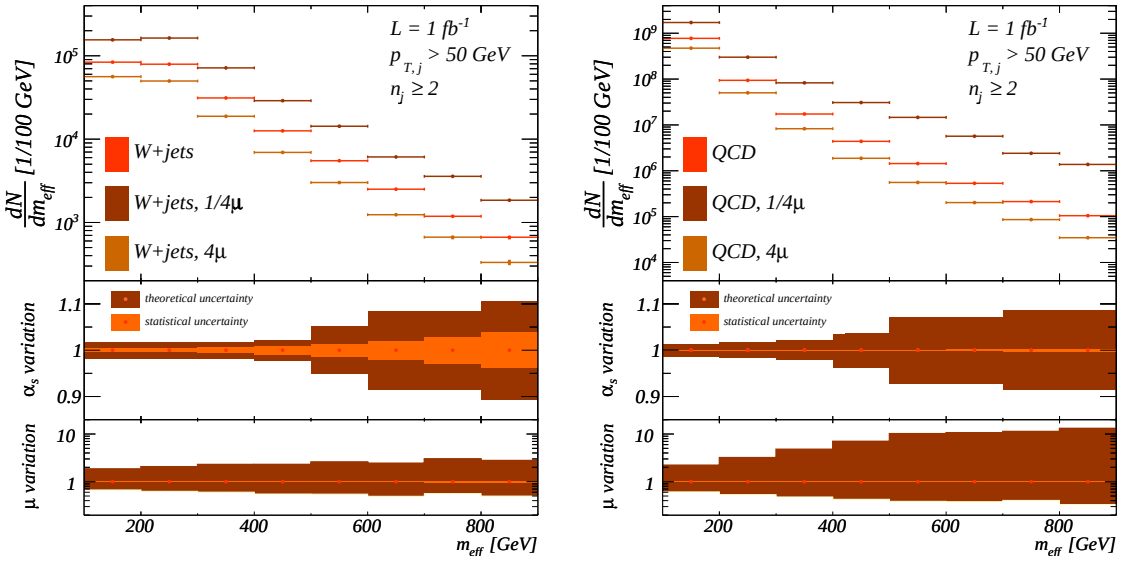

Figure 4.4: Effective mass distribution for W+jets and QCD jets production. Only the jet cuts given in Eq.(3.5) are applied. The second panels show the parametric uncertainty due to a consistent change of $\alpha_s(m_Z)$ between 0.114 and 0.122. The third panels show a consistent scale factor variation which can be experimentally constrained and should not be considered a theory uncertainty.

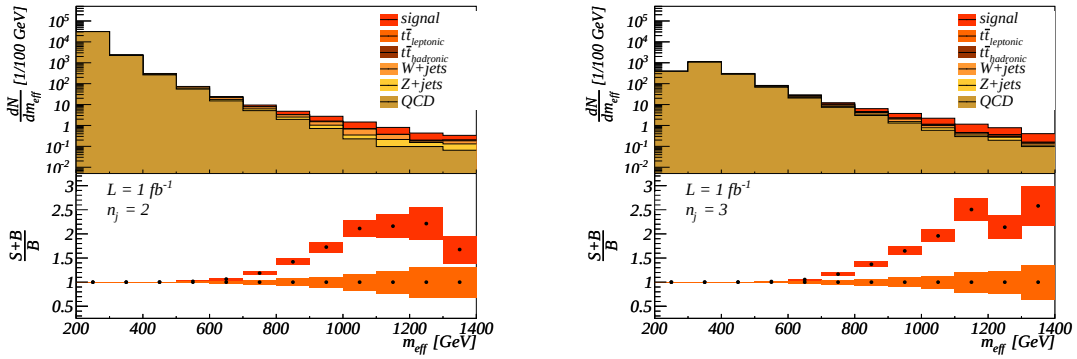

Figure 4.5: Effective mass distribution for exclusive 2-jet and 3-jet events for Standard-Model backgrounds and the supersymmetric signal using the SPS1a parameter point. We assume a center-of-mass energy of 7 TeV with an integrated luminosity of 1 fb^{-1} and apply all cuts in Eqs.(4.1) and (3.5).

Just like the n_{jets} distribution m_{eff} in the Standard Model cannot be reliably predicted by parton-shower Monte Carlos. Jets entering the sum in Eq.(4.4) we have to understand over their entire transverse-momentum spectrum. CKKW [17,18] or MLM [19] matching is therefore the most adequate approach for simulating m_{eff}.

Exactly following the treatment of the n_{jets} distribution in Section **??** we estimate two sources of theory uncertainties, the parametric error from varying the strong coupling and the scale-variation systematics. To not be limited by statistics of our background samples we for now discard the missing energy cut and the lepton veto and instead study the fully inclusive processes. In Figure 4.4 we present the m_{eff} distribution for W+jets and the QCD jets production with $n_{\text{jets}} \geq 2$. The same way as in Figure 3.1 we show the relative impact of the two sources of uncertainty in the lower panels. The parametric error from $\alpha_s(m_Z)$ ranges well below 20% even towards large values of m_{eff}. For the electroweak process this is of similar size to the expected statistical error for an integrated luminosity of 1 fb^{-1}. As expected, towards large m_{eff} the error band increases, but not dramatically.

In contrast, the scale-factor variation $\mu/\mu_0 = 1/4 - 4$ has a huge effect on the m_{eff} simulation, essentially rendering it unpredictive. For values above $m_{\text{eff}} = 500$ GeV the error bands become large enough to make it impossible to extract new physics from this observable, were we to consider the scale variation a proper theory error. However, measurements of multi-jet rates and other jet observables at Tevatron and LHC indicate that for the case of SHERPA this scaling factor is approximately one [66]. Measuring the staircase-scaling factors even more precisely with the 2011 LHC data will further constrain the scale ambiguities underlying our QCD simulations – allowing us to make reliable predictions for e.g. the m_{eff} observable.

To see the impact of m_{eff} in searches for supersymmetry we show the m_{eff} distribution for exclusive 2-jet and 3-jet events in Figure 4.5. It includes Standard-Model backgrounds as well as the supersymmetric signal. All jet-selection and background-rejection cuts specified in Eqs.(4.1) and (3.5) are applied. As mentioned before, QCD jets are the by far dominant channel. Only for $m_{\text{eff}} > 800$ GeV the signal starts overcoming the backgrounds. The statistical uncertainty for 1 fb^{-1} we indicate by the shaded regions in the lower panels. It is worth noticing that the signal+background sample when compared to the pure background sample exhibits a maximum at around $m_{\text{eff}} \sim 1.1$ TeV. This scale corresponds to the squark and gluino masses which for pair production add to 1100 to 1200 GeV. This means that the m_{eff} distribution for exclusive jet multiplicities can serve as background rejection as well as a measure for the mass scale of the new heavy colored states. It is also noteworthy to observe that we actually are able to do conclusions about new physics particle properties in the low multiplicity region. This means that the n_{jets} and m_{eff} observables are perpendicular in their discriminative power verifying our choice to use them as discriminators for a loglikelihood analysis in section 4.5.

4.5 Autofocusing

Following our results in the previous sections we should be able to use the shapes of the n_{jets} and m_{eff} distributions to extract a supersymmetric signal from the now quantitatively understood Standard Model backgrounds. Given that the two distributions are affected independently by the color structure of the new physics sector and by its mass scale(s) we will assess the power of the two-dimensional n_{jets} vs m_{eff} correlations in extracting a discovery or an exclusion. Such a two-dimensional shape analysis is the natural second step after the first completely inclusive searches based on counting events. According to Sections **??**-4.4 systematic experimental uncertainties will start dominating for luminosities around $\mathcal{O}(1 \text{ fb}^{-1})$. Since those are subject to continuous refinement during data taking and need to be addressed within a full detector simulation study we limit ourselves to statistical uncertainties for a given luminosity. While this means that we will not obtain reliable estimates for the discovery reach, we will see that it allows us to discuss the main benefits and limits of the proposed analysis.

As supersymmetric reference models we choose the benchmark point SPS1a, two variations of it, and SPS4. Again, we only apply the cuts given in Eqs.(4.1) and (3.5) and use the exclusive definition of n_{jets} and m_{eff}. For the m_{eff} distribution we choose a binning of 100 GeV, which approximately reflects the experimental resolution towards large m_{eff}.

For given background and signal+background hypotheses we use a binned log-likelihood ratio to compute statistical significances assuming statistically uncorrelated bins

$$\log Q = \sum_{\text{bins}} \left[n_i \log \left(1 + \frac{s_i}{b_i} \right) - s_i \right] . \tag{4.5}$$

It includes the luminosity via the signal and background event numbers s_i and b_i in each bin. While it avoids the limitations of $S/\sqrt{B}$ in regions requiring Poisson statistics it approaches a Gaussian limit for each individual channel when the bin content becomes large. Some features of this well established approach we summarize in Appendix B. Applying a "simple hypothesis test" tells us how likely it is that the background-only hypothesis fakes the predicted signal+background distributions as a statistical fluctuation, i.e. we define the p-value as the SPS1a likelihood ratio's median. The likelihood ratio given in Eq.(4.5) we compute for the exclusive n_{jets}, m_{eff}, and two-dimensional (n_{jets}, m_{eff}) distributions. In this two-dimensional plane the definition of m_{eff}, following Eq.(4.4), only includes exactly n_{jets} jets. With this completely exclusive definition of n_{jets} and m_{eff} we ensure that the sum over all bins in the (n_{jets}, m_{eff}) reproduces the total cross section.

Considering this correlation is similar in spirit to the ($\not{E}_T, H_T$) analysis proposed in Ref. [51]. However, first we focus on the n_{jets} and m_{eff} distributions because in Sections **??**-4.4 we have shown that we can quantitatively understand the staircase scaling behavior of the Standard Model backgrounds and translate its precision into other variables. In addition, as we will see in this section these two variables play a special role, as they not only distinguish signals from backgrounds, but also contain information on the structure of the underlying new-physics model. As mentioned above, for the sake of a proof of concept we ignore all uncertainties except for statistical experimental errors, to avoid correlations in the definition of the log-likelihood.

We can expect from Figures 4.3 and 4.5 that the rate in each individual n_{jets} bin is dominated by Standard-Model processes at low m_{eff}. Most likely, this region will be the control region to normalize the QCD and W/Z+jets backgrounds. With the exception of hadronically decaying top pairs all Standard-Model channels will then show a simple decrease in both directions of the two-dimensional (n_{jets}, m_{eff}) plane which we can predict following the arguments in Sections **??**-4.4. The signal contribution will become visible only once m_{eff} reaches the mass range of the particles produced.

In Table 4.4 we compare the statistical significances for the supersymmetric SPS1a parameter point at 7 TeV center-of-mass energy for the various analysis strategies: first, we show the results based on the total production rates after the inclusive cuts of Eqs.(4.1) and (3.5). As expected, including the signal events leaves us completely consistent with the background-only hypothesis. Next, the likelihood ratio computed from the n_{jets} distribution gives rise to sizable deviations

	signal significance for 35 pb^{-1}
inclusive	$0.2\,\sigma$
n_{jets} (1D)	$1.6\,\sigma$
m_{eff} (1D)	$3.3\,\sigma$
$(n_{\text{jets}}, m_{\text{eff}})$ (2D)	$4.6\,\sigma$

Table 4.4: Confidence levels for the signal plus background sample ruling out the background-only hypothesis based on one and two dimensional log-likelihood distributions. The supersymmetric mass spectrum is given by SPS1a.

from the background for integrated luminosities as small as 35 pb^{-1}. The one-dimensional m_{eff} distribution turns out to be an even better discriminator. It gives us more than twice the n_{jets} significance, namely $3.3\,\sigma$ for $\mathcal{L} = 35\ \text{pb}^{-1}$. The highest significant discriminative power we obtain for the two-dimensional binned (n_{jets}, m_{eff}) case. This is a direct consequence of the additive binned log-likelihood given in Eq.(4.5).

Beyond the relevance of the (n_{jets}, m_{eff}) distributions to extract new particles from backgrounds, we can utilize it to study signal properties. Above, we argue that new physics contributions to n_{jets} will only appear once m_{eff} reaches the mass scale of the sum of both heavy particles produced. However, this only happens if the exclusive n_{jets} value allows us to include the decay jets contributing to m_{eff}. Hence, the new physics contributions to the two observables will show a correlation based on the mass and decay channels of the new particles produced. The decay channels can typically be linked to the color charge of the new particles if we assume that the missing energy particle cannot carry color charge. Color triplets will tend to decay to one hard quark jet while color octets with their diagonal coupling to gluons will radiate two quark jets. This means breaking down the binned log-likelihood ratio over the fully exclusive (n_{jets}, m_{eff}) plane and keeping track of the individual contribution of each bin will automatically focus our search on the appropriate properties of the particles we are looking for.

This statement is not limited to supersymmetry, the SPS1a parameter point or any other assumption about the signal. It can be applied to general physics beyond the Standard Model with strongly interacting new particles and a stable dark matter candidate. In Figure 4.6 we show the contributions of the individual bins to the summed log-likelihood ratio for all signal events combined and split into three production processes. The maximum significance automatically reflects SPS1a's decay paradigm $\tilde{q}\tilde{q}^{(*)} \to 2$ jets and $\tilde{q}^{(*)}\tilde{g} \to 3$ jets, and $\tilde{g}\tilde{g} \to 4$ jets, know already from Figure 4.2. The first two channels we can study using an integrated luminosity of 1 fb^{-1}. Squark pair production is dominant because at the LHC it includes a quark-quark initial state. Associated production, which often is the dominant channel at the LHC, has a comparable statistical yield and features a slightly higher m_{eff} range. Both channels combined define the

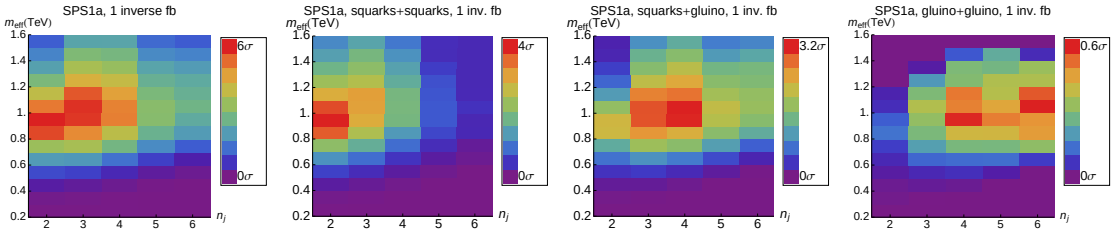

Figure 4.6: Log-likelihood contributions over the (n_{jets}, m_{eff}) plane for the supersymmetric signal using the SPS1a spectrum. The color code is normalized to different maximum significances. In the right image we recognice the two possible decay mechanisms of the gluino due to its color charge. The two maxima nicely reproduce or computation of equation 4.2 with an average of 2.5.

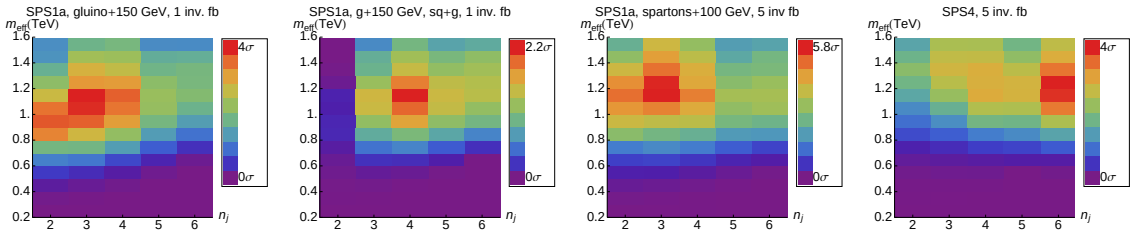

Figure 4.7: Log-likelihood distributions over the ($n_{\rm jets}$, $m_{\rm eff}$) plane for the different supersymmetric spectra. Due to the smaller signal rates we present results for an integrated luminosity of 5 fb^{-1}.

diagonal correlation we see for the combined signal events.

Gluino pair production has the smallest production rate and therefore becomes subleading in the combined supersymmetry sample. However, for this channel we can best follow the imprint of higher jet multiplicities. Due to its large mass and its color charge gluino pairs produce significantly more jet radiation which we can resolve for a sufficiently low $p_{T,\rm min}$ threshold. For $p_{T,\rm min} = 50$ GeV we might just capture the first decay jet from the gluino cascade, reflecting the mass hierarchy $m_{\tilde{g}} - m_{\tilde{q}} \sim 60$ GeV. The peak in the log-likelihood plane around $n_{\rm jets} = 4$ results from the maximum in the $\tilde{g}\tilde{g}$ production cross section. For $n_{\rm jets} = 5$ the background is still large compared to the signal, but dropping at an exponential rate it gets surpassed for $n_{\rm jets} = 6$, explaining the structure we observe in Figure 4.6.

Finally, we can study how changes to the new physics spectrum are reflected in the significances computed from the binned log-likelihood $Q(n_{\rm jets}, m_{\rm eff})$. We investigate three different supersymmetric mass spectra : first, we increase only the gluino mass by 150 GeV with respect to SPS1a ($\sigma^{\rm NLO}_{\rm SUSY} = 2.69$ pb according to Prospino2.1 [33]); second, we increase all colored-sparticle masses by 100 GeV with respect to SPS1a ($\sigma^{\rm NLO}_{\rm SUSY} = 1.63$ pb); third, we consider the SPS4 benchmark [76] with an inverted mass hierarchy $m_{\tilde{q}} \sim 750$ GeV $> m_{\tilde{g}} \sim 730$ GeV ($\sigma^{\rm NLO}_{\rm SUSY} = 0.83$ pb). All of these cross sections are significantly smaller than for SPS1a with its $\sigma^{\rm NLO}_{\rm SUSY} = 4.68$ pb, which means we increase our nominal luminosity to $\mathcal{L} = 5$ fb^{-1}.

In Figure 4.7 we clearly see the effect of the increased gluino mass. The $m_{\rm eff}$ peak for associated squark-gluino production moves to larger values, as does the $n_{\rm jets}$ maximum. However, because the balance between squark pair production and associated squark-gluino production shifts into the direction of the squark pairs, this effect is not quite as pronounced. The second scenario with increased squark and gluino masses leads to a pronounced maximum at larger $m_{\rm eff}$. Due to the smaller signal cross section the sensitivity in particular in the $n_{\rm jets} = 2$ bins gets considerably diminished, appearing as a shift towards higher $n_{\rm jets}$ values. For the all-hadronic search in the SPS4 parameter point longer decay chains for gluinos through bottom squarks appear in the high $n_{\rm jets}$ bins only.

The SPS4 case illustrates that $n_{\rm jets} = 6$ does not have to be the maximum jet multiplicity we need to consider. Once we rely on a combination of data and Monte Carlo methods to describe the $n_{\rm jets}$ staircase scaling for background processes we can extend our analyses to very large jet multiplicities. On the other hand, Figure 4.6 also clearly indicates that for example in the SPS1a parameter point the optimal signal extraction strategy by no means requires us to go to very large jet multiplicities. For the SPS1a parameter point the two-jet bins are leading contributions to the total significance.

Chapter 5
Outlook

We have studied the properties of staircase scaling for various SM backgrounds as well as the emergence of staircase and Poisson scaling in photon plus jets. While at first sight there is no reason to observe one of both cases we are able to identify two phase space regions where staircase scaling respectively Poisson scaling is present. We found:

1. While we cannot derive the staircase scaling of the n_{jets} distribution from first principles we can reproduce it using the appropriate Monte Carlo tools. This includes the scaling feature itself, a careful error analysis, and the scaling violation effects towards large values of n_{jets} due to phase space restrictions.

2. The theory uncertainty on the staircase scaling consists of tunable parameters like over all free factors in the factorization and renormalization scales and on parametric errors like the dependence on α_s. The latter are small. The scale factor hugely overestimates the error and should be thought of as a tuning parameter for the different jet merging implementations. For SHERPA it comes out close to unity.

3. The scaling parameter $R_0 = \sigma_{n+1}/\sigma_n$ depends on the hard process and on kinematic cuts. Both effects we can reliably predict using Monte Carlos, as we have shown for the W/Z+jets and pure jets cases as well as in the photon plus jets channel.

4. These simulations of the staircase scaling in multi-jet processes can be easily combined with data driven techniques, giving us the over-all normalization and a cross check for the first n_{jets} bins. Statistically limited regions of phase space will become accessible via simulations, including a reliable error estimate.

5. Studying the kinematics of the both cases enables us to understand the different particle configurations leading to staircase and Poisson scaling. For staircase scaling soft radiation of the photon must be suppressed while Poisson scaling is more pronounced the more we can increase the collinear radiation.

6. Staircase scaling is a unique QCD feature thus only visible if we separate the photon from the QCD part.

7. To observe Poisson scaling we have to induce a large logarithm thus enhancing the two jet bin the most. Also collinear photon radition is present in these kind of scaling.

The difference between QCD and QED is the self interaction of the gluon. Collinear splitting of partons is ok while colinear splitting of photons spoils the staircase scaling feature. This is a hint that we might find a solution by understanding the same arguments which lead to Poisson scaling in the QED case for pure Yang-Mills theory.

In the second part we applied the properties of staircase scaling to a new physics search. Using the staircase scaling we are able to constrain the uncertainties on otherwise hard to predict multi-jet observables as the n_{jets} distribution, its link to other multi-jet observables, and the application of jet-exclusive observables to new physics searches and found:

1. While we cannot derive the staircase scaling of the n_{jets} distribution from first principles we can reproduce it using the appropriate Monte Carlo tools. This includes the scaling feature itself, a careful error analysis, and the scaling violation effects towards large values of n_{jets} due to phase space restrictions.

2. The theory uncertainty on the staircase scaling consists of tunable parameters like over all free factors in the factorization and renormalization scales and on parametric errors like the dependence on α_s. The latter are small. The scale factor hugely overestimates the error and should be thought of as a tuning parameter for the different jet merging implementations. For SHERPA it comes out close to unity.

3. The scaling parameter $R_0 = \sigma_{n+1}/\sigma_n$ depends on the hard process and on kinematic cuts. Both effects we can reliably predict using Monte Carlos, as we have shown for the W/Z+jets and pure jets cases as well as in the photon plus jets channel.

4. These simulations of the staircase scaling in multi-jet processes can be easily combined with data driven techniques, giving us the over-all normalization and a cross check for the first n_{jets} bins. Statistically limited regions of phase space will become accessible via simulations, including a reliable error estimate.

5. Understanding staircase scaling of multi-jet processes allows us to predict other multi-jet variables, like the effective mass m_{eff}. Again, this includes a proper treatment of theory uncertainties. In addition, the completely inclusive definition of m_{eff} removes dangerous artifacts due to the usual truncations.

6. Based on for example the n_{jets} vs m_{eff} correlation for a fixed $p_{T,\text{min}}$ we can define a likelihood-based analysis avoiding model or spectrum specific background rejection cuts. Such shape analysis in multi-jet search channels are the natural extension of the early inclusive ATLAS and CMS searches.

Of course this simple first approximation to the exclusive zero-lepton search for jets plus missing energy is not the only application of such methods. Searches including leptons, b tags, or hard photons will benefit from the same treatment, as long as they include non-negligible numbers of jets. The same is true for hadronically decaying top quarks in the Standard Model.

Acknowledgments

My first thanks to Tilman who gave me the great opportunity to work on this exciting physics project for his advise. I also would like to thank my other collaborators Christoph and Steffen. I had a great time working with you guys and my motivation to do physics is now even higher than when I started. As the latter two are leaving Heidelberg this autumn I wish the very best for you, your families and your future science. But I also have to mention Dorival, David, Michi and Bob. Thanks for your advise and help and all the nice barbecues at the Neckarwiese. Maybe this is a good place to mention that all my studies would not have been possible without the Bafög program. Warm thanks to my friend and flatmate Vanessa with whom living was a pleasure although my urge to do research may have reduced my actual fraction of the household chores. And of course Jann and Anna for saving stress full days with a Feierabendbier ☺.

Appendix A
External gluons and ghosts

In section 2.1 we mentioned the complicated form of the gluon propagator due to the gauge fixing. This leads to the introduction of ghost terms [20, 26]. To explore their meaning it is instructive to remember the photon from QED . To make the photon a physical quantity we have to impose polarization vectors allowing the photon only transverse polarizations. In the computation of squared matrix elements this leads to the so called polarization sum

$$\sum_{\text{polarizations}} \epsilon(k)_\mu \epsilon(k)^*_\nu = -\eta_{\mu\nu}. \tag{A.1}$$

As gluons are mass less gauge bosons as are photons the same argument applies about their polarization being physical. Again we have to introduce polarization vectors to make the gluons physical. As it turns out the polarization sum from Eq. A.1 is not the correct way for gluons [26]. The reason for that is the gluon self interaction. The triple gluon vertex is in its structure mimicked by the gluon ghost vertex. This is the meaning behind the ghosts. They cancel the unphysical degrees of freedom if gluons are involved. If we use also ghosts in our Feynman diagrams the unphysical degrees of freedom are removed correctly and we can safely use Eq. A.1 again[1]. As ghosts are scalars the question arises how to incorporate them correctly in the computation of an spin/polarization and color averaged squared matrix element. In many text books this question is only touched vaguely [26, 77] and to our knowledge sometimes outlined miss guiding. As ghosts are meant to cancel the unphysical degrees of freedom they can not be applied after averaging over polarizations, but only before.

To achieve a systematic understanding of how to use unphysical ghosts as external entities in our computation, we start with the cases involving no external gluons, namely scattering of quarks[2]. As no external gluons are present we have no trouble with any polarization sums and can use the Feynman rules from fig. 2.2 and 2.3. Due to symmetry reasons the squared matrix elements of the processes $qq' \to qq'$, $q\bar{q'} \to q\bar{q'}$ and $q\bar{q} \to q'\bar{q'}$ are equal under appropriate exchange

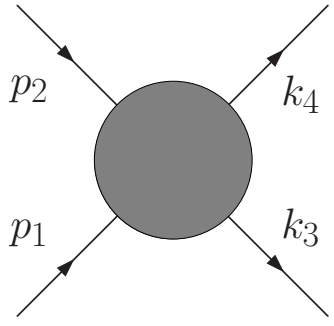

Figure A.1: Labeling of the momentum of the incoming (p) and outgoing (k) partons. The counting index runs from 1 to 4.

[1] There is also the possibility to work in a so called physical gauge where no ghosts appear in the Feynman rules [26]. However, this not only complicates the gluon propagator even more, but also complicates the polarization sum introducing a new four vector n into the computation. This vector is again unphysical and has to drop out of the computation.

[2] To keep the computations simple we only consider $2 \to 2$ processes in this chapter

of the three Mandelstam variables given by

$$\begin{aligned} s = (p_1 + p_2)^2 &\approx 2p_1p_2 \\ t = (p_1 - k_3)^2 &\approx -2p_1k_3 \\ u = (p_1 - k_4)^2 &\approx -2p_1k_4 \\ \text{with } s + t + u = 0, & \end{aligned} \tag{A.2}$$

where the momentum labels are given by the configuration in fig. A.1. The $\approx$ in Eq. A.2 gets an equal for massless particles as in our case. We only have to consider one Feynman diagram depicted in fig. A.2.

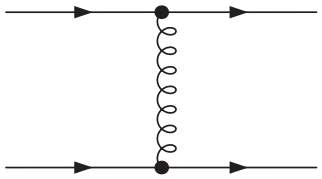

$$= \frac{ig_s^2}{t}\overline{u}(k_3)T^a\gamma^\mu u(p1)\overline{u}(k_4)T^a\gamma_\mu u(p_2) \tag{A.3}$$

Figure A.2: Feynman graph and matrix element for qq' scattering.

Squaring Eq. A.3 and computing all the Dirac traces we get

$$|M^2| = 16\frac{s^2 + u^2}{t^2}. \tag{A.4}$$

From this we can get for example to the $q\overline{q}$ process by interchanging s and t. Now we have to average over the initial state spins and colors. For the three mentioned processes we get

$$\begin{aligned} qq' \to qq' \qquad & g_s^4\frac{4}{9}\frac{s^2 + u^2}{t^2} \\ q\overline{q'} \to q\overline{q'} \qquad & g_s^4\frac{4}{9}\frac{s^2 + u^2}{t^2} \\ q\overline{q} \to q'\overline{q'} \qquad & g_s^4\frac{4}{9}\frac{t^2 + u^2}{s^2}. \end{aligned} \tag{A.5}$$

For the other two remaining processes with no external gluons we can do the same computation involving one additional diagram to get

$$\begin{aligned} qq \to qq \qquad & g_s^4\frac{4}{9}\left(\frac{s^2 + u^2}{t^2} + \frac{s^2 + t^2}{u^2}\right) - \frac{8}{27}\frac{s^2}{ut} \\ q\overline{q} \to q\overline{q} \qquad & g_s^4\frac{4}{9}\left(\frac{s^2 + u^2}{t^2} + \frac{t^2 + u^2}{s^2}\right) - \frac{8}{27}\frac{u^2}{st}. \end{aligned} \tag{A.6}$$

There are three QCD processes involving two external gluons $q\bar{q} \to gg$, $gg \to q\bar{q}$ and $gq \to gq$. Due to symmetry we have to compute only one of those. We chose to compute $q\bar{q} \to gg$. Two of the diagrams we have to consider are similar to those of $e^+e^- \to \gamma\gamma$, see fig. A.3, but there is one additional diagram involving the gluon triple vertex. To correct for the extra degrees of freedom in that diagram we have to take into account a diagram describing a $q\bar{q} \to$ ghost ghost process, see fig. A.4. But how do we figure out the correct assignment of signs and relative weights? We could guess that the ghosts have to come along with a minus sign, however we have not to rely

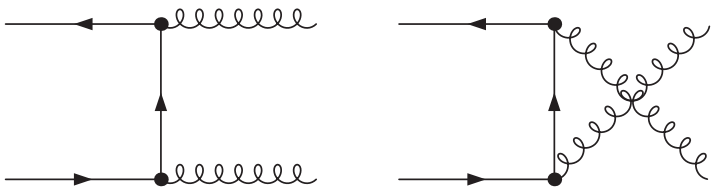

$$= -ig_s^2 v(p_2)\left[T^a T^b \gamma^\mu \frac{\not{p}_1 - \not{k}_3}{t}\gamma^\nu + T^b T^a \gamma^\nu \frac{\not{p}_1 - \not{k}_4}{u}\gamma^\mu\right] u(p_1) \tag{A.8}$$

Figure A.3: Feynman graph and matrix element for $q\bar{q}$ to gg process similar to the QED case.

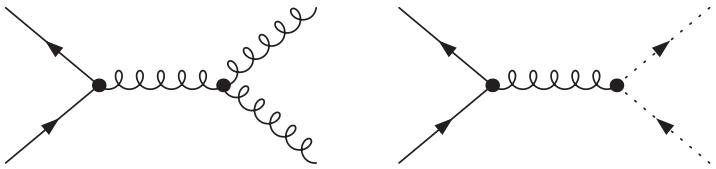

$$\begin{aligned} M_{\text{3gluon}} &= \frac{-g_s^2}{s} f_{abe} T^e v(p_2)\gamma^\sigma u(p_1)\left(\eta_{\sigma\mu}(-2k_4 - k_3)_\nu + \eta_{\mu\nu}(k_4 - k_3)_\sigma + \eta_{\nu\sigma}(2k_3 + k_4)_\mu\right) \\ M_{\text{ghost}} &= \frac{g_s^2}{s} f_{abe} T^e v(p_2)\gamma^\sigma u(p_1) k_{4,\sigma} \end{aligned} \tag{A.9}$$

Figure A.4: Feynman graph and matrix element for $q\bar{q}$ to gg process due to the gluon triple vertex and corresponding ghost diagram to counter balance the too many degrees of freedom.

on guessing. The optical theorem [20] is the answer to that question. In fig. A.5 we can see how diagrams with loops are connected to absolute squared matrix elements. We find that we have to include a factor of $1/2$ for the gluon loop and a factor -1 for the ghost loop. But this gives us together with the factor of 2 from the optical theorem an overall relation between the squared gluon matrix element and the squared ghost matrix element of the form

$$|M_{\text{total}}|^2 = |M_{\text{gluon}}|^2 - 2 * |M_{\text{ghost}}|^2. \tag{A.7}$$

With that information we can now compute the squared matrix elements. For the gluon and ghost parts we get

$$\begin{aligned} |M_{\text{gluon}}|^2 &= -\frac{416}{3} - 240\frac{u^2}{s^2} - 240\frac{u}{s} + \frac{128}{3}\frac{u}{t} - \frac{128}{3}\frac{s}{u} \\ |M_{\text{ghost}}|^2 &= -24\frac{u^2}{s^2} - 24\frac{u}{s}. \\ \Rightarrow |M_{\text{total}}|^2 &= -\frac{416}{3} - 192\frac{u^2}{s^2} - 192\frac{u}{s} + \frac{128}{3}\frac{u}{t} - \frac{128}{3}\frac{s}{u}. \end{aligned} \tag{A.10}$$

Including the right averaging factors and interchanging the Mandelstam variables appropriately

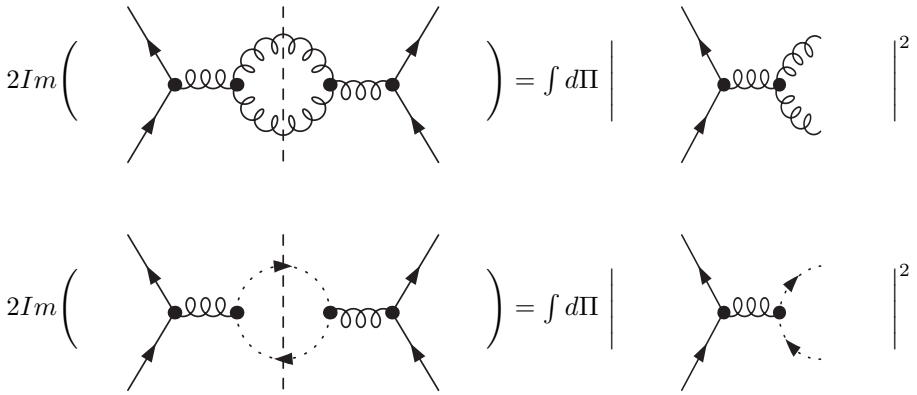

Figure A.5: The optical theorem in the language of Feynman graphs involving the gluon triple vertex (top) and the ghosts (bottom). The cutting causes the loop to collapse to a phase-space integral denoted by $\int d\Pi$. The gluon loop comes with an additional factor of $1/2$ while the ghost loop gets a factor of -1.

we get for all three possible processes

$$\begin{aligned} q\overline{q} \to gg \qquad & g_s^4 \left(\frac{32}{27} \frac{t^2+u^2}{tu} - \frac{8}{3} \frac{t^2+u^2}{s^2} \right) \\ gg \to q\overline{q} \qquad & g_s^4 \left(\frac{1}{6} \frac{t^2+u^2}{tu} - \frac{3}{8} \frac{t^2+u^2}{s^2} \right) \\ gq \to gq \qquad & g_s^4 \left(-\frac{4}{9} \frac{s^2+u^2}{su} + \frac{s^2+u^2}{t^2} \right). \end{aligned} \tag{A.11}$$

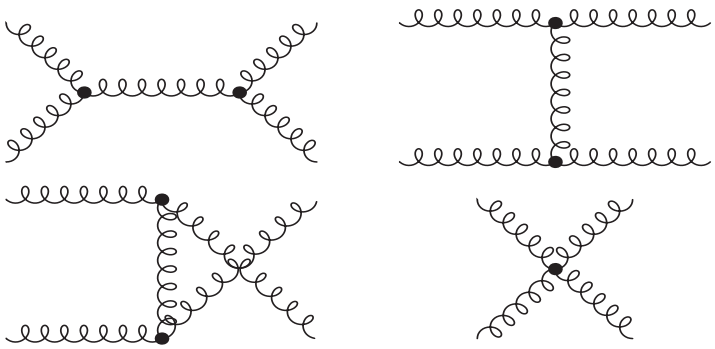

Figure A.6: Diagrams for pure gluon scattering without ghosts.

If we use equation. A.7 in a more complicated environment namely pure gluon scattering the number of terms we have to include gets large. In this case we have four diagrams involving only gluons depicted in figure A.6. The number of ghost diagrams gets huge displaying that this technique might be very interesting from a QFT point of view but is very unpractical. Nevertheless

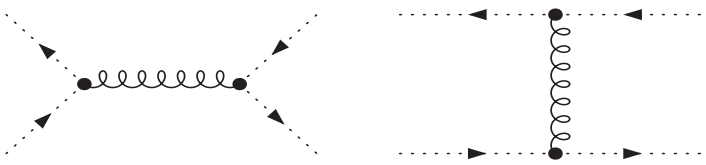

Figure A.7: All external states are ghosts.

we state the ghost diagrams which should be included in the figures A.8 to A.7. The squared matrix element for this process is

$$gg \to gg \qquad g_s^4 \frac{9}{2}\left(3 - \frac{tu}{s^2} - \frac{su}{t^2} - \frac{st}{u^2}\right). \tag{A.12}$$

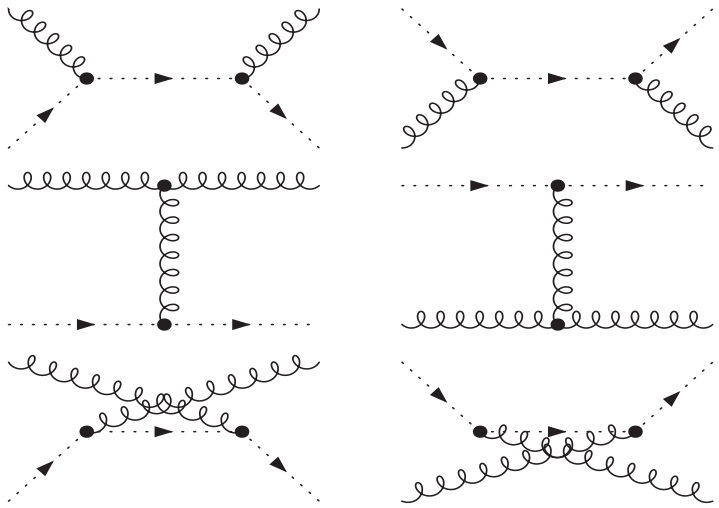

Figure A.8: First set of ghost diagrams with one ghost in the incoming state and one in the outgoing.

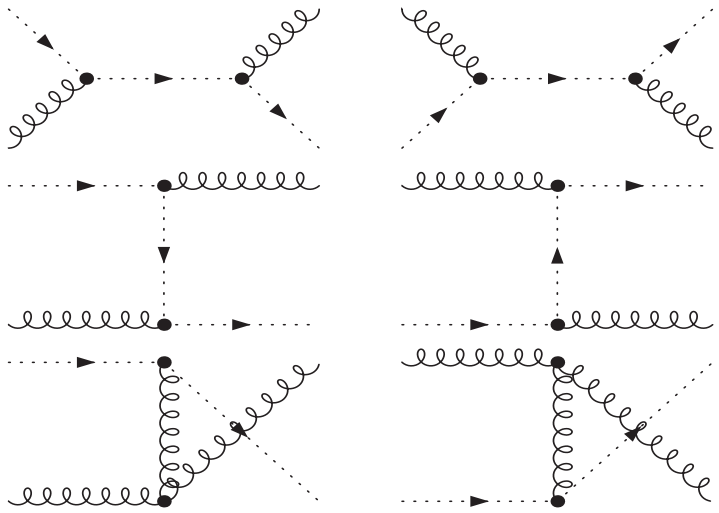

Figure A.9: Second set of ghost diagrams with one ghost in the incoming state and one in the outgoing.

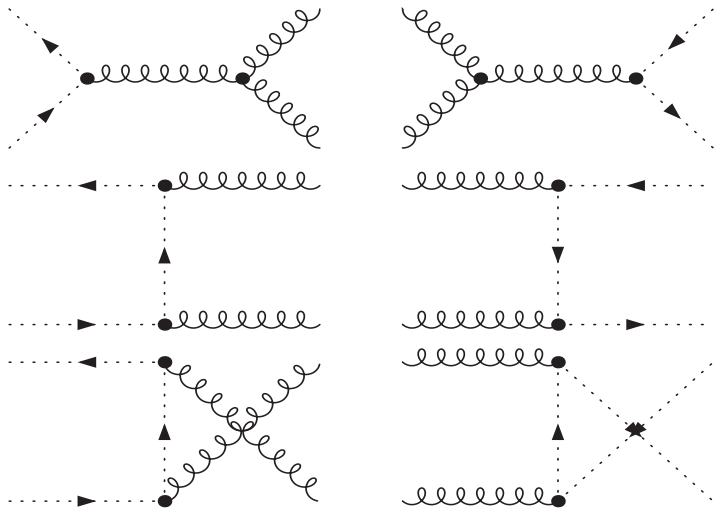

Figure A.10: Left: Two ghosts in the incoming and gluons in the outgoing state. Right: Gluons in the incoming and two ghosts in the outgoing state.

Appendix B

Hypothesis Test

In this section we briefly review the binned log-likelihood ratio hypothesis tests which we apply in Section 4.5. It discriminates between two specific hypotheses and has been used for the combined LEP-Higgs limits [52], Tevatron analyses [53], and in various contexts of LHC Higgs phenomenology [54]. According to the Neyman–Pearson lemma [78] the likelihood ratio is the most powerful test statistic (e.g. signal+background vs background-only). We compute the (binned) log-likelihood ratio

$$\begin{aligned} \mathcal{Q} = -2 \log Q &= -2 \log \frac{L(\text{data} \,|\, \mathcal{S}+\mathcal{B})}{L(\text{data} \,|\, \mathcal{B})} \\ &= 2 \left[s - n \log \left(1 + \frac{s}{b} \right) \right] \stackrel{\text{binned}}{=} 2 \sum_{i \in \text{bins}} \left[s_i - n_i \log \left(1 + \frac{s_i}{b_i} \right) \right] , \end{aligned} \tag{B.1}$$

where s and b denote the signal $\mathcal{S}$ and background $\mathcal{B}$ event numbers for a given luminosity, split into the bins i. The probabilities to observe n events given the expected numbers s and b in Eq.(B.1) are determined by Poisson distributions

$$L(\text{data} \,|\, \mathcal{S}+\mathcal{B}) = \frac{(b+s)^n e^{-(s+b)}}{n!} \qquad\qquad L(\text{data} \,|\, \mathcal{B}) = \frac{b^n e^{-b}}{n!} . \tag{B.2}$$

The sum in Eq.(B.1) extends over all contributing channels. The likelihood distributions we generate as pseudo-data around each hypothesis' central value, which means that in principle we can include any kind of correlation. In this work we limit ourselves to statistically independent bins i of the n_{jets} and m_{eff} distributions. The set of entries in each bin $\{n_i\}$ we simulate numerically and histogram them as a function of $\mathcal{Q}$, following the Neyman-Pearson lemma. To simulate the log-likelihood distributions we need to specify which hypothesis the bin entries $\{n_i\}$ should follow, i.e. we can compute $\mathcal{Q}_{\mathcal{S}+\mathcal{B}}$ or $\mathcal{Q}_{\mathcal{B}}$. In Figure B.1 we show both $\mathcal{Q}$ distributions for the binned one-dimensional n_{jets} distribution studied in our paper.

In our analysis we are interested in the probability that the background alone fakes the expected signal+background distributions. This confidence level is given by the integral of the background distribution $\mathcal{Q}_{\mathcal{B}}$over the signal+background range, indicated by the red-shaded region in Figure

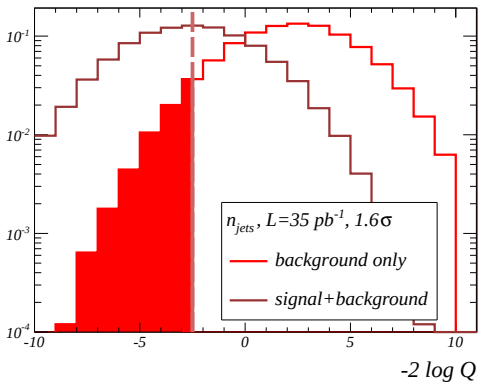

Figure B.1: Log-likelihood ratio distributions based on the n_{jets} discriminator for a luminosity of 35 pb^{-1}. The confidence level is computed by evaluating the overlap of the background-only distribution with the signal+background maximum.

B.1. This signal+background range is defined as all likelihood values above the median of the likelihood distribution assuming the signal+background hypothesis

$$\mathrm{CL}_{\mathcal{B}} = \int_{-\infty}^{\langle \mathcal{Q}_{\mathcal{S}+\mathcal{B}} \rangle} \mathrm{d}\mathcal{Q}\, \mathcal{Q}_{\mathcal{B}} = \mathrm{erfc}\left(\frac{Z}{\sqrt{2}}\right) , \tag{B.3}$$

where for illustration purposes we convert the confidence levels into the Gaussian number of standard deviations Z via the inverse error function.

Bibliography

[1] WMAP-collobaration,
SEVEN-YEAR WILKINSON MICROWAVE ANISOTROPY PROBE (WMAP1) OBSERVATIONS:COSMOLOGICAL INTERPRETATION;
arXiv:1001.4538v3 [astro-ph.CO].

[2] M. Trodden,
Electroweak Baryogenesis;
arXiv:9803479v2 [hep-ph]

[3] S. Martin,
A Supersymmetry Primer;
arXiv:9709356v5 [hep-ph].

[4] E. Witten,
Search for a realistic Kaluza-Klein theory;
Nuclear Physics B Volume 186, Issue 3, 10 August 1981, Pages 412-428.

[5] N. Arkani-Hamed, A. Cohen, E. Katz and A. Nelson,
The Littlest Higgs;
arXiv:0206021v2 [hep-ph].

[6] Steven Weinberg,
Implications of dynamical symmetry breaking;
Physical Review D, Band 13, 1976, S. 974–996.

[7] M. Battaglia, I. Hinchliffe and D. Tovey,
Cold Dark Matter and the LH;
arXiv:0406147 [hep-ph].

[8] D. E. Morrissey, T. Plehn and T. M. P. Tait,
New Physics at the LHC;
arXiv:0912.3259 [hep-ph].

[9] ATLAS Collaboration,
ATLAS-CONF-2010-065.

[10] CMS Collaboration,
Search for Supersymmetry in pp Collisions at 7 TeV in Events with Jets and Missing Transverse Energy;
arXiv:1101.1628 [hep-ex].

[11] D. S. M. Alves, E. Izaguirre and J. G. Wacker,
It's On: Early Interpretations of ATLAS Results in Jets and Missing Energy Searches;
arXiv:1008.0407 [hep-ph].

[12] H. Baer, C. Chen, F. Paige *et al.*,
Signals for minimal supergravity at the CERN large hadron collider: Multi - jet plus missing energy channel;
Phys. Rev. **D52** (1995) 2746-2759.
I. Hinchliffe, F. E. Paige, M. D. Shapiro *et al.*,
Precision SUSY measurements at CERN LHC;
Phys. Rev. **D55** (1997) 5520-5540.
L. Randall, D. Tucker-Smith,
Dijet Searches for Supersymmetry at the LHC;
Phys. Rev. Lett. **101** (2008) 221803.
A. J. Barr, C. Gwenlan,
The Race for supersymmetry: Using m(T2) for discovery;
Phys. Rev. **D80** (2009) 074007.

[13] G. Aad *et al.* [ATLAS Collaboration],
The ATLAS Experiment at the CERN Large Hadron Collider;
JINST **3** (2008) S08003.

[14] G. L. Bayatian *et al.* [CMS Collaboration],
CMS technical design report, volume II: Physics performance;
J. Phys. G **34** (2007) 995.

[15] C. Englert, T. Plehn, P. Schichtel and S. Schumann,
Jets plus Missing Energy with an Autofocus;
arXiv:1102.4615 [hep-ph].

[16] ATLAS Collaboration,
ATLAS-CONF-2010-084.

[17] S. Höche, F. Krauss, S. Schumann and F. Siegert,
QCD matrix elements and truncated showers;
JHEP **0905** (2009) 053.

[18] S. Catani, F. Krauss, R. Kuhn *et al.*,
QCD matrix elements + parton showers;
JHEP **0111** (2001) 063.
F. Krauss,
Matrix elements and parton showers in hadronic interactions;
JHEP **0208** (2002) 015.

[19] M. L. Mangano, M. Moretti and R. Pittau,
Multijet matrix elements and shower evolution in hadronic collisions: W b bbar + n jets as a case study;
Nucl. Phys. B **632** (2002) 343 .

[20] M. E. Peskin and D. V. Schroeder,
An Introduction to Quantum Field Theory;
Westview Press.

[21] C. Englert, T. Plehn, P. Schichtel, and S. Schumann,
Establishing Jet Scaling Patterns with a Photon;
arXiv:1108.5473v1 [hep-ph].

[22] Fermilab;
http://vms-db-srv.fnal.gov/fmi/xsl/VMS_Site_2/000Return/photography/r_online_mrdetail.xsl?-db=VMS_Frames\&-lay=WWWBrowse\&-recid=87595\&-find=.

[23] J. Alcaraz *et al*,
The LEP electroweak working group http://lepewwg.web.cern.ch/LEPEWWG/.

[24] Particle Data Group;
http://pdg.lbl.gov/2011/tables/rpp2011-sum-leptons.pdf.

[25] R. K. Ellis, W. J. Stirling and B. R. Webber,
QCD and Collider Physics;
Cambridge University Press.

[26] G. Dissertori, I. Knowles and M. Schmelling,
Quantum Chromodynamics;
Oxford Science Publications.

[27] G. Salam,
Towards Jetography;
arXiv:0906.1833v2 [hep-ph].

[28] T. Plehn,
LHC Lecture Notes;
http://www.thphys.uni-heidelberg.de/~plehn/lhc.pdf.

[29] LHAPDF Group,
http://projects.hepforge.org/lhapdf/.

[30] M. Shiozawa *et al*,
Search for proton decay via $p \to e^+ pi^0$ in a large water Cherenkov detector;
Phys. Rev. Lett. 81, 3319-3323 (1998).

[31] T. Lia *et al*,
Elements of F-ast Proton Decay;
arxive:1003.2570 [hep-ph].

[32] T. Figy *et al*,
Higgs Production via Weak Boson Fusion in the Standard Model and the MSSM;
arXiv:1012.4789v2 [hep-ph].

[33] W. Beenakker, R. Höpker, M. Spira and P. M. Zerwas,
Squark and gluino production at hadron colliders;
Nucl. Phys. B **492** (1997) 51.
T. Plehn,
Production of supersymmetric particles at high-energy colliders;
arXiv:hep-ph/9809319
www.thphys.uni-heidelberg.de/~tplehn/prospino.

[34] T. Gleisberg, S. Höche, F. Krauss, M. Schönherr, S. Schumann, F. Siegert and J. Winter,
Event generation with SHERPA 1.1;
JHEP **0902** (2009) 007.

[35] G. Blazeya*et al*,
Run II Jet Physics;
arXiv:0005012v2 [hep-ph].

[36] P. Nason,
A new method for combining NLO QCD with shower Monte Carlo algorithms;
arXiv:0409146 [hep-ph].

[37] F. Maltoni*et al*,
Color-flow decomposition of QCD amplitudes;
arXiv:0209271v2 [hep-ph]

[38] Homepage of the Sherpa Event Generator;
`http://www.sherpa-mc.de/`.

[39] A. Buckley, J. Butterworth, S. Gieseke *et al.*,
General-purpose event generators for LHC physics;
arXiv:1101.2599 [hep-ph].

[40] NASA,
What is the Universe Made Of?;
`http://map.gsfc.nasa.gov/universe/uni_matter.html`.

[41] D. Morrissey, T. Plehn, and T. Tait,
Physics searches at the LHC;
`http://www.thphys.uni-heidelberg.de/~plehn/review.pdf`.

[42] P. Sheerwood et al.,
Atlfast;
`http://www.hep.ucl.ac.uk/atlas/atlfast/`.

[43] M. Bahr et al.,
Herwig++ Physics and Manual;
arXiv:0803.0883v3 [hep-ph].

[44] HepMC a C++ Event Record for Monte Carlo Generators;
`http://lcgapp.cern.ch/project/simu/HepMC/`.

[45] M. Cacciari and G. P. Salam,
Dispelling the N^3 myth for the k_t jet-finder;
Phys. Lett. B **641** (2006) 57.
M. Cacciari, G. P. Salam and G. Soyez, `http://fastjet.fr`.

[46] J. Alwall, P. Demin, S. de Visscher *et al.*,
MadGraph/MadEvent v4: The New Web Generation;
JHEP **0709** (2007) 028.

[47] B. Allanach et al.,
The Snowmass Points and Slopes: Benchmarks for SUSY Searches;
arXiv:0202233v1 [hep-ph].

[48] E. Gerwick, T. Plehn and S. Schumann,
Understanding Jet Scaling and Jet Vetos in Higgs Searches;
arXive:1108.3335v1 [hep-ph].

[49] S. Frixione, Phys. Lett. B **429** (1998) 369; S. Hoeche, S. Schumann and F. Siegert, Phys. Rev. D **81** (2010) 034026; F. Campanario, C. Englert and M. Spannowsky, Phys. Rev. D **83** (2011) 074009.

[50] ATLAS Colaboration,
Annual Charts of Luminosity;
`https://twiki.cern.ch/twiki/bin/view/AtlasPublic/LuminosityPublicResults`.

[51] J. Alwall, M. -P. Le, M. Lisanti, J. G. Wacker,
Model-Independent Jets plus Missing Energy Searches;
Phys. Rev. **D79** (2009) 015005.

[52] R. Barate *et al.* [LEP Working Group for Higgs boson searches],
Search for the standard model Higgs boson at LEP;
Phys. Lett. B **565** (2003) 61.

[53] T. Junk,
Confidence Level Computation for Combining Searches with Small Statistics;
Nucl. Instrum. Meth. A **434** (1999) 435,
CDF Note 8128 [cdf/doc/statistics/public/8128],
CDF Note 7904 [cdf/doc/statistics/public/7904].

[54] H. Hu and J. Nielsen,
in '1st Workshop on Confidence Limits',
CERN 2000-005 (2000)
arXiv:9906010.
K. Cranmer and T. Plehn,
Maximum significance at the LHC and Higgs decays to muons; Eur. Phys. J. C **51** (2007) 415.
A. De Rujula, J. Lykken, M. Pierini *et al.*,
Higgs look-alikes at the LHC;
Phys. Rev. **D82** (2010) 013003.
Y. Gao, A. V. Gritsan, Z. Guo *et al.*,
Spin determination of single-produced resonances at hadron colliders;
Phys. Rev. **D81** (2010) 075022.
D. E. Soper and M. Spannowsky,
Combining subjet algorithms to enhance ZH detection at the LHC;
JHEP **1008** (2010) 029.

[55] for an early correct description of one jet over its entire p_T range see:
M. Bengtsson and T. Sjostrand,
Coherent Parton Showers Versus Matrix Elements: Implications Of Petra - Pep Phys. Lett. B **185** (1987) 435.
M. Bengtsson and T. Sjostrand,
A Comparative Study of Coherent and Noncoherent Parton Shower Evolution;
Nucl. Phys. B **289** (1987) 810.
G. Miu and T. Sjostrand,
W production in an improved parton shower approach;
Phys. Lett. B **449** (1999) 313.
E. Norrbin and T. Sjostrand,
QCD radiation off heavy particles;

Nucl. Phys. B **603** (2001) 297.
M. H. Seymour,
A Simple prescription for first order corrections to quark scattering and annihilation processes;
Nucl. Phys. **B436** (1995) 443-460.
M. H. Seymour,
Matrix element corrections to parton shower algorithms;
Comput. Phys. Commun. **90** (1995) 95-101.
G. Corcella, M. H. Seymour,
Initial state radiation in simulations of vector boson production at hadroncolliders;
Nucl. Phys. **B565** (2000) 227-244.

[56] M. L. Mangano, M. Moretti, F. Piccinini *et al.*,
ALPGEN, a generator for hard multiparton processes in hadronic collisions;
JHEP **0307** (2003) 001.

[57] J. Alwall, S. Höche, F. Krauss *et al.*,
Comparative study of various algorithms for the merging of parton showers and matrix elements in hadronic collisions;
Eur. Phys. J. **C53** (2008) 473-500.

[58] S. D. Ellis, R. Kleiss, W. J. Stirling,
W's, Z's and Jets;
Phys. Lett. **B154** (1985) 435.

[59] V. M. Abazov *et al.* [D0 Collaboration],
Measurement of the ratios of the Z/gamma* + ¿= n jet production cross sections to the total inclusive Z/gamma* cross section in p anti-p collisions at s**(1/2) = 1.96-TeV;
Phys. Lett. **B658** (2008) 112-119.
T. Aaltonen *et al.* [CDF - Run II Collaboration],
Measurement of inclusive jet cross-sections in Z/gamma*(—¿ e+ e-) + jets production in p anti-p collisions at s**(1/2) = 1.96-TeV;
Phys. Rev. Lett. **100** (2008) 102001.

[60] ATLAS Collaboration,
Measurement of the production cross section for W-bosons in association with jets in pp collisions at sqrt(s) = 7 TeV with the ATLAS detector;
arXiv:1012.5382 [hep-ex].

[61] for a review see e.g.
A. J. Barr, C. G. Lester,
A Review of the Mass Measurement Techniques proposed for the Large Hadron Collider;
J. Phys. G **G37** (2010) 123001.

[62] M. Cacciari, G. P. Salam, G. Soyez,
The Anti-k(t) jet clustering algorithm;
JHEP **0804** (2008) 063.

[63] F. A. Berends, W. T. Giele, H. Kuijf, R. Kleiss and W. J. Stirling,
Multi - Jet Production In W, Z Events At P Anti-P Colliders;
Phys. Lett. B **224** (1989) 237.
F. A. Berends, H. Kuijf, B. Tausk *et al.*,

On the production of a W and jets at hadron colliders;
Nucl. Phys. **B357** (1991) 32.

[64] C. F. Berger, Z. Bern, L. J. Dixon *et al.*,
Precise Predictions for W + 4 Jet Production at the Large Hadron Collider;
arXiv:1009.2338 [hep-ph].

[65] H. L. Lai, M. Guzzi, J. Huston, Z. Li, P. M. Nadolsky, J. Pumplin and C. P. Yuan,
New parton distributions for collider physics;
Phys. Rev. D **82** (2010) 074024.

[66] F. Krauss, A. Schälicke, S. Schumann *et al.*,
Simulating W / Z + jets production at the Tevatron;
Phys. Rev. **D70** (2004) 114009.
V. M. Abazov *et al.* [DØ Collaboration],
Measurement of the normalized $Z/\gamma^* - > \mu^+\mu^-$ transverse momentum distribution in $p\bar{p}$ collisions at $\sqrt{s} = 1.96$ TeV;
Phys. Lett. **B693** (2010) 522-530.
S. Höche, S. Schumann, F. Siegert,
Hard photon production and matrix-element parton-shower merging;
Phys. Rev. **D81** (2010) 034026.
G. Aad *et al.* [ATLAS Collaboration],
Measurement of the production cross section for W-bosons in association with jets in pp collisions at sqrt(s) = 7 TeV with the ATLAS detector;
arXiv:1012.5382 [hep-ex].
DØ Collaboration,
Note 6032-CONF. F. A. Dias, E. Nurse and G. Hesketh,
LO vs NLO comparisons for Z + jets: MC as a tool for background determination for NP searches at LHC;
arXiv:1102.0917 [hep-ph]. ATLAS Collaboration,
Measurement of Dijet Azimuthal Decorrelations in pp Collisions at sqrt(s)=7 TeV;
arXiv:1102.2696 [hep-ex].

[67] T. Plehn, D. Rainwater, P. Z. Skands,
Squark and gluino production with jets;
Phys. Lett. **B645** (2007) 217-221.

[68] J. Alwall, S. de Visscher, F. Maltoni,
QCD radiation in the production of heavy colored particles at the LHC;
JHEP **0902** (2009) 017.

[69] T. Plehn and T. M. P. Tait,
Seeking Sgluons;
J. Phys. G **36** (2009) 075001.

[70] J. Alwall, S. de Visscher, F. Maltoni,
QCD radiation in the production of heavy colored particles at the LHC;
JHEP **0902** (2009) 017.

[71] M. Bahr, S. Gieseke, M. A. Gigg *et al.*,
Herwig++ Physics and Manual;
Eur. Phys. J. **C58** (2008) 639-707.

[72] B. C. Allanach,
SOFTSUSY: a program for calculating supersymmetric spectra;
Comput. Phys. Commun. **143** (2002) 305-331.

[73] P. Z. Skands, B. C. Allanach, H. Baer *et al.*,
SUSY Les Houches accord: Interfacing SUSY spectrum calculators, decay packages, and event generators;
JHEP **0407** (2004) 036.

[74] M. Mühlleitner, A. Djouadi, Y. Mambrini,
SDECAY: A Fortran code for the decays of the supersymmetric particles in the MSSM;
Comput. Phys. Commun. **168** (2005) 46-70.

[75] T. Sjostrand, S. Mrenna, P. Z. Skands,
PYTHIA 6.4 Physics and Manual;
JHEP **0605** (2006) 026.

[76] B. C. Allanach *et al.*,
The Snowmass points and slopes: Benchmarks for SUSY searches, in Proc. of the APS/DPF/DPB Summer Study on the Future of Particle Physics (Snowmass 2001);
Eur. Phys. J. C **25** (2002) 113.

[77] R. Field,
Applications of perturbative QCD;
Addison-Wesley.

[78] J. Neyman and E. S. Pearson,
Philosophical Transactions;
of the Royal Society of London. Series A Vol. 231, (1933); pp. 289-337.

Statement of Authorship

Ich versichere, dass ich diese Arbeit selbstständig verfasst habe und keine anderen als die angegebenen Quellen und Hilfsmittel benutzt habe.

Heidelberg, den

Peter Schichtel